

This discussion paper is/has been under review for the journal Atmospheric Chemistry and Physics (ACP). Please refer to the corresponding final paper in ACP if available.

# Heterogeneous ice nucleation on atmospheric aerosols: a review of results from laboratory experiments

C. Hoose and O. Möhler

Institute for Meteorology and Climate Research – Atmospheric Aerosol Research,  
Karlsruhe Institute of Technology, Karlsruhe, Germany

Received: 9 April 2012 – Accepted: 2 May 2012 – Published: 16 May 2012

Correspondence to: C. Hoose (corinna.hoose@kit.edu)

Published by Copernicus Publications on behalf of the European Geosciences Union.

## Laboratory ice nucleation experiments

C. Hoose and O. Möhler

[Title Page](#)

[Abstract](#)

[Introduction](#)

[Conclusions](#)

[References](#)

[Tables](#)

[Figures](#)

◀

▶

◀

▶

[Back](#)

[Close](#)

[Full Screen / Esc](#)

[Printer-friendly Version](#)

[Interactive Discussion](#)



## Abstract

A small subset of the atmospheric aerosol population has the ability to induce ice formation at conditions under which ice would not form without them (heterogeneous ice nucleation). While no closed theoretical description of this process and the requirements for good ice nuclei is available, numerous studies have attempted to quantify the ice nucleation ability of different particles empirically in laboratory experiments. In this article, an overview of these results is provided. Ice nucleation onset conditions for various mineral dust, soot, biological, organic and ammonium sulphate particles are summarized. Typical temperature-supersaturation regions can be identified for the onset of ice nucleation of these different particle types, but the various particle sizes and activated fractions reported in different studies have to be taken into account when comparing results obtained with different methodologies. When intercomparing only data obtained under the same conditions, it is found that dust mineralogy is not a consistent predictor of higher or lower ice nucleation ability. However, the broad majority of studies agrees on a reduction of deposition nucleation by various coatings on mineral dust. The ice nucleation active surface site (INAS) density is discussed as a normalized measure for ice nucleation activity. For most immersion and condensation freezing measurements on mineral dust, estimates of the temperature-dependent INAS density agree within about two orders of magnitude. For deposition nucleation on dust, the spread is significantly larger, but a general trend of increasing INAS densities with increasing supersaturation is found. For soot, the presently available results are divergent. Estimated average INAS densities are high for ice-nucleation active bacteria at high subzero temperatures. At the same time, it is shown that some other biological aerosols, like certain pollen grains and fungal spores, are not intrinsically better ice nuclei than dust, but owe their high ice nucleation onsets to their large sizes. Surface-area-dependent parameterizations of heterogeneous ice nucleation are discussed. For immersion freezing on mineral dust, fitted INAS densities are available, but should not be used outside the temperature interval of the data they were based on. Classical

## Laboratory ice nucleation experiments

C. Hoose and O. Möhler

[Title Page](#)

[Abstract](#)

[Introduction](#)

[Conclusions](#)

[References](#)

[Tables](#)

[Figures](#)

◀

▶

◀

▶

[Back](#)

[Close](#)

[Full Screen / Esc](#)

[Printer-friendly Version](#)

[Interactive Discussion](#)



nucleation theory, if employed with one fitted contact angle, does not reproduce the observed temperature dependence for immersion nucleation, temperature and super-saturation dependence for deposition nucleation, and time dependence.

## 1 Introduction

- 5 Ice crystals in the atmosphere have important impacts on radiative transfer, precipitation formation, and the microphysical and optical properties of clouds. Therefore, their formation has been studied both in the field and under controlled conditions in laboratory experiments since many years (e.g., Dufour, 1861; Schaefer, 1949; Georgii and Kleinjung, 1967; DeMott et al., 2011). It is known that water droplets in the atmosphere  
10 do not freeze instantaneously at 0 °C. Their freezing can either be triggered by aerosol particles acting as a so-called ice nuclei (IN), or occur homogeneously (without IN) at about –38 °C (Pruppacher and Klett, 1997). The goal of many laboratory studies was and is to assess the ice nucleation ability of selected aerosol particles of a specific composition (e.g., Pruppacher and Saenger, 1955; Isono et al., 1959a). While earlier  
15 parameterizations of heterogeneous ice nucleation (Young, 1974; Meyers et al., 1992) did not include any aerosol-specific dependencies, the results of such experiments and their parametrical descriptions are nowadays frequently used in atmospheric models on different scales, from cloud resolving models to global climate models (e.g., Kärcher and Lohmann, 2003; Liu and Penner, 2005; Lohmann and Diehl, 2006; Grützun et al.,  
20 2008; Phillips et al., 2009; Eidhammer et al., 2010; Hoose et al., 2010a,b; Storelvmo et al., 2011), and enter the calculations of aerosol indirect effects in mixed-phase and cirrus clouds.

In this article, we will provide a summary and overview of historical and recent ice nucleation experiments. Results for a wide range of different aerosol types, sizes, obtained with different instruments and experimental boundary conditions are intercompared. In individual studies, where the focus is often on instrument development and/or process studies, such comparisons to results with other instruments are often selective  
25

12, 12531–12621, 2012

ACPD

[Title Page](#)

[Abstract](#)

[Introduction](#)

[Conclusions](#)

[References](#)

[Tables](#)

[Figures](#)

◀

▶

◀

▶

[Back](#)

[Close](#)

[Full Screen / Esc](#)

[Printer-friendly Version](#)

[Interactive Discussion](#)



or omitted, with the exception of a few coordinated instrument intercomparison exercises (Langer, 1973; DeMott et al., 2011). Here, we try to set the individual studies and their results into a larger context. The parameters which possibly influence results from different instruments will be discussed one for one, and consistent tendencies will be identified. In addition, we will discuss to what degree parametrical descriptions agree with these general features of the data. However, within this study, we will not attempt to provide quality classifications of methods or individual studies, or new unified parameterizations.

It is also an aim of this article to make the results of laboratory experiments more accessible to potential users within the modelling community. Furthermore, we will scrutinize some common assumptions in models, e.g. fixed thresholds for nucleation onset (e.g., Hendricks et al., 2011), the higher ice nucleation efficiency of certain mineral phases (e.g., Lohmann and Diehl, 2006), the assignment of nucleation modes to certain temperature intervals (e.g., Ervens et al., 2011) and the applicability of classical nucleation theory (e.g., Khvorostyanov and Curry, 2005; Liu and Penner, 2005; Hoose et al., 2010b).

Finally, we will identify open questions and give recommendations for future studies.

## 2 Onset conditions for heterogeneous ice nucleation

Temperature ( $T$ ) and saturation ratio with respect to ice ( $S_i$ ) are the main environmental factors which determine ice nucleation. Laboratory ice nucleation experiments aim at the determination of the aerosol-specific ice nucleation properties under controlled environmental conditions. Early results have often been reported as “onset” temperatures and saturation ratios, i.e. the highest temperatures and lowest saturation ratios for which a certain amount of ice formation is observed. This “onset” either corresponds to a detection limit or to a chosen activated fraction.

In both experiments and in the atmosphere, aerosols can experience a variety of different trajectories in the  $T$ - $S_i$  space, as shown in Fig. 1. Above  $S_i = 1$ , the dashed

## Laboratory ice nucleation experiments

C. Hoose and O. Möhler

[Title Page](#)

[Abstract](#)

[Introduction](#)

[Conclusions](#)

[References](#)

[Tables](#)

[Figures](#)

◀

▶

◀

▶

[Back](#)

[Close](#)

[Full Screen / Esc](#)

[Printer-friendly Version](#)

[Interactive Discussion](#)



horizontal line in Fig. 1, ice is the stable phase. Supercooled liquid water is in equilibrium with the vapour phase along the solid diagonal line, which represents the ice saturation ratio at liquid water saturation. Concentrated solution droplets are in thermodynamic equilibrium at lower relative humidities with respect to water according the water activity of the solutes. At temperatures below about  $-38^{\circ}\text{C}$ , water and solution droplets freeze homogeneously. The homogeneous nucleation rate of solutes can be formulated as a function of the water activity  $a_w$  (Koop et al., 2000). In Fig. 1 and the following diagrams, the isoline for a homogeneous nucleation rate coefficient of  $5 \times 10^{14} \text{ m}^{-3} \text{ s}^{-1}$  is indicated for reference.

Figure 2 summarizes ice nucleation onset data from a large number of studies with atmospherically relevant aerosol particles. The data shown here correspond not only to different particle species and nucleation modes, as indicated by the colors and symbols, but also to different experimental methods, particles sizes, sample preparation, activated fraction and more. This complicates the comparison of results from different studies, in some cases making it even impossible. Therefore we will focus in the following on relative and normalized efficiencies, expressed by different metrics, and search for recurring patterns and parametrical dependencies in different experiments.

In the following, the data shown in the overview plot of Fig. 2 will be analysed in more detail. In particular, the following factors are thought to be relevant for onset supersaturation/temperature of ice nucleation: the chemical composition (discussed in Sect. 3.1), for mineral dust its mineralogy (discussed in Sect. 3.2), coatings (discussed in Sect. 3.4), the activated fraction for which the “onset” is reported in conjunction with the particle surface area (discussed in Sect. 4.1), and time (discussed in Sect. 4.2). Before that, we will give a brief overview of atmospheric conditions which are relevant to heterogeneous ice nucleation.

## Typical ice nucleation onset in the atmosphere

The ice nucleation onset conditions measured for different aerosol particles can be compared to typical ice onsets in the atmosphere. For mixed-phase clouds, a number

## Laboratory ice nucleation experiments

C. Hoose and O. Möhler

[Title Page](#)

[Abstract](#)

[Introduction](#)

[Conclusions](#)

[References](#)

[Tables](#)

[Figures](#)

◀

▶

◀

▶

[Back](#)

[Close](#)

[Full Screen / Esc](#)

[Printer-friendly Version](#)

[Interactive Discussion](#)



of in-situ and remote sensing observations are available which quantified typical water to ice transition temperatures (Korolev et al., 2003; Field et al., 2004; Kanitz et al., 2011). These indicate that, depending on the measurement location, more than half of the clouds at temperatures lower than  $-15$  to  $-20^{\circ}\text{C}$  contain ice, while at higher temperatures, clouds are more often purely liquid (within the detection limit of the instrument). These transition temperatures coincide with immersion freezing onset temperatures of some mineral dusts and biological particles. If seeding from upper levels can be excluded for the investigated cases, it can be inferred that such particles have to be present in the atmosphere to explain the observed cloud phase distribution. This inference is supported by a shift of the liquid-to-ice-transition to higher temperatures for dusty conditions (Seifert et al., 2010).

For cirrus clouds, the frequency of occurrence of ice-supersaturations (Haag et al., 2003; Krämer et al., 2009) gives some indications on the availability of IN. Both in clear air and in cirrus clouds, ice saturation ratios up to about 130 % are not uncommon, which lets us presume that particles nucleating ice at lower saturation ratios (e.g., large mineral dusts or specific crystalline organic acids) are not ubiquitous in the upper troposphere. However, as supersaturations can persist in the presence of crystals due sustained cooling or suppressed growth (Peter et al., 2006), no further conclusions can be drawn about the maximum or minimum efficiency of IN required to explain the observed humidity distribution (Spichtinger and Gierens, 2009).

### 3 Qualitative influence of composition on ice nucleation properties

#### 3.1 Main groups of atmospherically relevant IN

IN are generally solid, water-insoluble particles (Pruppacher and Klett, 1997). The crystallographic structure of surfaces seems to have some influence on their ice nucleation abilities (Mason, 1971). In addition, so-called active sites, i.e. localized topographic features like cracks or chemical impurities, can determine a particle's ice nucleation

[Title Page](#)[Abstract](#)[Introduction](#)[Conclusions](#)[References](#)[Tables](#)[Figures](#)[|◀](#)[▶|](#)[◀](#)[▶|](#)[Back](#)[Close](#)[Full Screen / Esc](#)[Printer-friendly Version](#)[Interactive Discussion](#)

behaviour (Pruppacher and Klett, 1997). However, so far, predictions of a material's ice nucleation ability based on its chemical or physical properties are impossible. The following sections provide an overview of the ice nucleation abilities of mineral dust particles, soot, bioaerosols (bacteria, fungal spores and pollen), solid ammonium sulphate, organic acids and humic-like substances. Nucleation onset conditions from numerous experiments are shown separately for these particle types in Figs. 3–5. Details about the data sources are listed in Tables 1–6. It should be noted that these "onset" data cover a wide range of ice-active particles fractions, as indicated in Tables 1–5 wherever available. The experiments are conducted with many different instruments and experimental setups, which are listed in Table A2. For details about instrumentation and measurement principles, we refer the reader to the original works and to the overviews given by DeMott (2002) and DeMott et al. (2011).

### 3.1.1 Mineral dust

Because of the large number of experiments with mineral dust, these are separated into four graphs (Fig. 3), Fig. 3a, b including only results with mainly submicron particles (either monodisperse or size distributions with a mode diameter smaller than  $1\text{ }\mu\text{m}$ ) and Fig. 3c, d including experiments with larger particles. More detailed size specifications for the mineral dust samples are given in Table 1. Comparing Fig. 3a, b with c, d, it is obvious that larger particles tend to nucleate ice at lower supersaturations and higher temperatures. The data are colour-coded with respect to the mineralogical composition of the samples. Black symbols represent natural desert dust samples collected in different regions of the world. Green symbols represent Arizona test dust (ATD), a commercial product of milled soil dust available from Powder Technology, Inc. Blue, red and yellow symbols represent kaolinite, montmorillonite, and illite, respectively, which are common clay minerals. For submicron particles, there seems to be a tendency of natural desert dusts to require the highest ice-supersaturations for activation, i.e. to be worse IN than kaolinite, montmorillonite and ATD in the deposition nucleation mode. This will be further investigated below. Otherwise, it is remarkable that

[Title Page](#)[Abstract](#)[Introduction](#)[Conclusions](#)[References](#)[Tables](#)[Figures](#)[◀](#)[▶](#)[◀](#)[▶](#)[Back](#)[Close](#)[Full Screen / Esc](#)[Printer-friendly Version](#)[Interactive Discussion](#)

the observations of ice nucleation on dust span the full range of water-subsaturated and water-saturated conditions below  $-10^{\circ}\text{C}$ . Some data are also measured in significantly water-supersaturated conditions (e.g., Koehler et al., 2010).

### 3.1.2 Soot

- For soot, fewer experiments are available, and those available show little overlap in the reported ice nucleation onset conditions (Fig. 4a and Table 2). In addition to these results, it should be noted that several studies report negative results (no ice nucleation within the instrument's detection limit) under certain investigated conditions. These are presented in Fig. 4b: at  $-40^{\circ}\text{C}$ , Kanji and Abbatt (2006) observed onset relative humidities for deposition ice nucleation in experiments with n-hexane soot deposited on a substrate, which were not statistically different from those for the blank substrate. Dymarska et al. (2006) observed droplet formation before ice formation (occurring also on the bare substrate) for almost all experiments at temperatures between  $-15$  and  $-30^{\circ}\text{C}$ ; Friedman et al. (2011) did not observe ice formation below water saturation for temperatures of  $-20$  and  $-30^{\circ}\text{C}$ , and only droplet formation above water saturation. Furthermore, at  $-40^{\circ}\text{C}$ , only homogeneous freezing was observed, similar to Koehler et al. (2009) (also at  $-40^{\circ}\text{C}$ ). The negative results are in disagreement with a number of experiments (DeMott, 1990; Diehl and Mitra, 1998; Gorbunov et al., 2001; Popovicheva et al., 2008; Kireeva et al., 2009; Fornea et al., 2009) which observed ice nucleation on soot particles already at temperatures above  $-30^{\circ}\text{C}$ . However, the latter were conducted in other nucleation modes (see Table 2) and partly with large particles or unknown particle concentrations per droplet (see also the discussion in Kärcher et al., 2007).

Also soot particles vary in composition, e.g. with respect to their organic carbon content, depending on the combustible and the combustion technique. Möhler et al. (2005b) and Crawford et al. (2011) found a significant decrease in ice nucleation activity with increasing organic carbon content at temperatures around  $-65^{\circ}\text{C}$  and  $-47^{\circ}\text{C}$ , respectively. However, no systematic trends related to the soot type are seen from the

## Laboratory ice nucleation experiments

C. Hoose and O. Möhler

[Title Page](#)

[Abstract](#)

[Introduction](#)

[Conclusions](#)

[References](#)

[Tables](#)

[Figures](#)

◀

▶

◀

▶

[Back](#)

[Close](#)

[Full Screen / Esc](#)

[Printer-friendly Version](#)

[Interactive Discussion](#)



experiments at higher temperatures. Despite the large spread in the results, it can be confirmed from this qualitative overview that soot is a generally worse ice nucleus than mineral dust, nucleating at higher ice-supersaturations for deposition nucleation and at lower temperatures for immersion freezing.

### 5 3.1.3 Primary biological aerosol particles

Figure 5a displays selected ice nucleation results for potentially airborne primary biological particles. Among bioaerosols, in particular bacteria, the ability to nucleate ice is a selective property. Only a small number of bacterial strains and fungal species has been identified as ice nucleation active at high subzero temperatures, and even 10 among these, only a small fraction of all cells actually nucleates ice at temperatures roughly higher than  $-10^{\circ}\text{C}$  (Hirano and Upper, 1995). Most experiments with biological particles are conducted as so-called droplet-freezing assays (Vali, 1971; Vali et al., 1976), i.e. testing for immersion freezing. Most of the data points in Fig. 5a therefore lie on the water saturation line. For Snomax<sup>TM</sup>, an artificial snow inducer consisting 15 of proteins derived from *Pseudomonas syringae* bacteria, deposition nucleation has been observed (Chernoff and Bertram, 2010; DeMott et al., 2011). These data are not included in Fig. 5a because Snomax<sup>TM</sup> particles don't occur in the natural atmosphere.

More results on freezing experiments with biological particles, also from other habitats, are discussed in Després et al. (2012).

### 20 3.1.4 Solid ammonium sulphate

At conditions relevant for cirrus clouds in the upper troposphere and lower stratosphere, crystalline ammonium sulphate particles have been observed to nucleate ice efficiently at water-subsaturated conditions, both as deposition nuclei and as immersion nuclei in solution droplets (Fig. 5b).

## Laboratory ice nucleation experiments

C. Hoose and O. Möhler

[Title Page](#)

[Abstract](#)

[Introduction](#)

[Conclusions](#)

[References](#)

[Tables](#)

[Figures](#)

◀

▶

◀

▶

[Back](#)

[Close](#)

[Full Screen / Esc](#)

[Printer-friendly Version](#)

[Interactive Discussion](#)



### 3.1.5 Organic acids and humic-like substances

Also some organic acids in crystalline form have been observed to nucleate ice under cirrus conditions (Fig. 5c), most notably oxalic acid (Zobrist et al., 2006; Wagner et al., 2010) and malonic acid (Shilling et al., 2006). At temperatures below  $-65^{\circ}\text{C}$ , citric acid aerosol particles in a glassy state have been observed to nucleate ice at  $S_i > 1.2$  (Murray et al., 2010b). Other organic substances, such as dicarboxylic acids (Prenni et al., 2001) or secondary organic products of the ozonolysis of various precursors (Prenni et al., 2009), were shown not to nucleate ice heterogeneously. Furthermore, Fig. 5c includes results for humic acids (produced by the degradation of dead organic matter) and biomass burning aerosols (tested solely at  $-30^{\circ}\text{C}$ , Petters et al., 2009).

### 3.1.6 Others

In addition, a number of other components of the atmospheric aerosol are occasionally found to act as IN. Among these are volcanic ash particles (Durant et al., 2008; Hoyle et al., 2011; Steinke et al., 2011) and sea salt (Wise et al., 2012). No onset nucleation plots are shown for these particle types because of the limited number of measurements. Furthermore, artificial particles which usually do not occur in the atmosphere (e.g. silver iodide, metaldehyde, metal oxides), some of them being very efficient IN (Vonnegut, 1947; Fukuta, 1963), are excluded from this overview.

### 3.2 Comparison of different minerals

20 Natural mineral dust particles are usually internal mixtures of different clay minerals, quartz and other components. Laboratory studies have therefore often reverted to the use of pure minerals, in order to reduce the complexity encountered in natural dusts. For pure minerals, the chemical composition and the crystalline structure can be determined more accurately. For example, Mason (1960) tried to relate the ice nucleation abilities of different minerals to their lattice structure. Previous modelling studies have

# Laboratory ice nucleation experiments

C. Hoose and O. Möhler

Title Page

## Abstract

## Introduction

## Conclusion

## References

Tables

Figure

Back

**Close**

Full Screen / Esc

[Printer-friendly Version](#)

## Interactive Discussion



used measurements of ice nucleation of pure minerals as a basis for parametrizations, and have assumed for sensitivity experiments that montmorillonite is a better ice nucleus than kaolinite (Diehl et al., 2006; Lohmann and Diehl, 2006; Hoose et al., 2008; Storelvmo et al., 2008). Ideally, the ice nucleation properties of a complex natural dust particle can be inferred if the composition of the particle and the ice nucleation properties of all components are known. The most abundant minerals in the clay size fraction of mineral dust are kaolinite, illite and montmorillonite (Mason, 1960; Zimmermann et al., 2008). Their relative ice nucleation abilities are compared in the following, including only studies which examined kaolinite, montmorillonite and/or illite with the same methods and under comparable experimental conditions.

Figure 6a compares temperatures for the freezing onset or a specific active fraction of kaolinite and montmorillonite particles at otherwise comparable conditions (i.e. the same weight percent in Murray et al. (2010a), the same particle sizes in Welti et al., 2009). In the experiments by Mason and Maybank (1958), Mason (1960), Hoffer (1961) and Pitter and Pruppacher (1973), the particle sizes and active fractions are not well constrained, but are assumed to be similar for the kaolinite and montmorillonite experiments. Zimmermann et al. (2008) reported onset temperatures corresponding to a larger active fraction for kaolinite than for montmorillonite (2–3 % versus 1%).

As visible in Fig. 6a, no systematic difference between the ice nucleation temperatures of montmorillonite and kaolinite is found. The immersion freezing experiments with particle suspensions (Hoffer, 1961; Pitter and Pruppacher, 1973; Murray et al., 2010a) and the contact freezing experiments (Pitter and Pruppacher, 1973) show higher freezing temperatures for montmorillonite, while the other experiments (for which the nucleation modes are not unambiguously determined) found higher freezing temperatures for kaolinite (Mason and Maybank, 1958; Mason, 1960; Roberts and Hallett, 1968; Zimmermann et al., 2008). Zuberi et al. (2002) found no significant difference between kaolinite and montmorillonite as immersion ice nucleus in aqueous ammonium sulphate droplets.

## Laboratory ice nucleation experiments

C. Hoose and O. Möhler

[Title Page](#)

[Abstract](#)

[Introduction](#)

[Conclusions](#)

[References](#)

[Tables](#)

[Figures](#)

◀

▶

◀

▶

[Back](#)

[Close](#)

[Full Screen / Esc](#)

[Printer-friendly Version](#)

[Interactive Discussion](#)



Also in deposition nucleation experiments, reported as supersaturation thresholds at fixed temperatures (Fig. 6b), the comparison of kaolinite versus montmorillonite remains inconclusive. Both a higher efficiency of kaolinite (Zimmermann et al., 2008; Eastwood et al., 2008; Chernoff and Bertram, 2010) and a higher efficiency of montmorillonite (Salam et al., 2007; Welti et al., 2009) are found.

Fewer studies have compared the ice nucleation ability of illite to that of kaolinite (Mason, 1960; Hoffer, 1961; Zimmermann et al., 2008; Bundke et al., 2008; Welti et al., 2009; Chernoff and Bertram, 2010). The results are summarized in Fig. 7. The data shown here are selected in the same way as for the comparison in Fig. 6. Similar to the kaolinite-montmorillonite comparison, no definite conclusions can be drawn about the nucleation ability of illite compared to kaolinite, because different experiments come to opposite results both expressed as onset temperatures or as onset saturation ratios.

The reason for the heterogeneity of these results may lie in the different origin and the purity of the samples which are used. Isono and Ibeke (1960) and Pinti et al. (2012) show that kaolinites, montmorillonites and illites from different sources can have different physical and chemical properties. Zimmermann et al. (2008) point out that the chemical composition of minerals, in particular of montmorillonite and illite, can be highly variable. Murray et al. (2010a) mention that the commercially available minerals, which are used in some of the above studies, were acid washed or chemically treated. This may have affected their nucleation abilities. For deposition nucleation experiments, the dispersion method (wet or dry) may have influenced the results, because it may have a substantial impact on the hygroscopicity of the minerals (Herich et al., 2009). Furthermore, Mason and Maybank (1958) and Roberts and Hallett (1968) found that preactivation could reduce or even invert the differences in freezing onset between kaolinite and montmorillonite.

Based on the data summarized here, the validity of the common model assumption of the superior ice nucleation ability of montmorillonite compared to kaolinite has to be questioned.

<a href="#">Title Page</a>	
<a href="#">Abstract</a>	<a href="#">Introduction</a>
<a href="#">Conclusions</a>	<a href="#">References</a>
<a href="#">Tables</a>	<a href="#">Figures</a>
<a href="#"></a>	<a href="#"></a>
<a href="#"></a>	<a href="#"></a>
<a href="#">Back</a>	<a href="#">Close</a>
<a href="#">Full Screen / Esc</a>	
<a href="#">Printer-friendly Version</a>	
<a href="#">Interactive Discussion</a>	

### 3.3 Natural dusts compared to dust surrogates

Frequently, the commercially available Arizona Test Dust (ATD) is used in laboratory experiments as a surrogate for desert dusts (e.g., Knopf and Koop, 2006; Marcolli et al., 2007). ATD is milled, washed and heated in order to provide enough material of the desired size (Möhler et al., 2006). Alternatively, surface soil samples (e.g., Field et al., 2006; Kulkarni and Dobbie, 2010) or sedimented dust storm particles (e.g., Isono et al., 1959a; Niemand et al., 2012) have been studied. Ideally, these samples are only sieved to retrieve the small size fraction, but have not undergone any milling or further processing. It has been speculated that ATD could be more active than so-called natural (unprocessed) soil samples, either due enhanced roughness resulting from the milling or due to a different mineralogical composition (Möhler et al., 2006). In Fig. 8, results from deposition nucleation experiments which tested both ATD and natural desert dusts under comparable conditions are summarized. Only a limited number of studies fulfills this requirement and allows such a direct comparison. In most experiments, natural desert dusts required higher supersaturations over ice for a comparable activation, provided that the data are compared with the same instrument, for the same active fraction, at similar temperatures and form the similar particle sizes. An exception to this observation are Kanji et al. (2008) and Möhler et al. (2006)'s data at low temperatures ( $< -60^{\circ}\text{C}$ ).

Contrary to the above finding that natural desert dust samples might be relatively inefficient IN due to lower surface roughness and atmospheric aging, Conen et al. (2011) provide evidence for enhanced ice nucleation activity of agricultural soil samples compared to pure montmorillonite due to biological residues in the soil.

### 3.4 Influence of coatings

A number of experiments has investigated the effect of surface reactions and coatings on mineral dust particles on their ice nucleation efficiency. These studies are of high relevance, because atmospheric dust particles frequently undergo processing by trace

### Laboratory ice nucleation experiments

C. Hoose and O. Möhler

[Title Page](#)

[Abstract](#)

[Introduction](#)

[Conclusions](#)

[References](#)

[Tables](#)

[Figures](#)

◀

▶

◀

▶

[Back](#)

[Close](#)

[Full Screen / Esc](#)

[Printer-friendly Version](#)

[Interactive Discussion](#)



gases or in clouds. Table 6 lists pertinent experiments. Most studies focussed on the treatment of mineral dust with sulfuric acid, but also ammonium sulfate, nitric acid, secondary organic aerosol (SOA), ammonia and ozone were used. In Fig. 9, results from deposition and condensation nucleation experiments with coated and uncoated mineral dust particles are summarized. The saturation ratios for activation of a specific fraction of particles at otherwise similar conditions (temperature, particle size) are reported. Most measurements shown here report higher saturation ratios for coated particles than for uncoated ones, i.e. a deactivation of mineral dust by surface treatments. The largest changes in saturation ratio are found for coatings by SOA (Möhler et al., 2008a; Koehler et al., 2010). Also sulfuric acid and ammonium sulfate treatments generally increased the saturation ratio by up to 0.3, with three exceptions: Cziczo et al. (2009a) observed nearly identical nucleation onset saturation ratios for uncoated, sulfuric acid coated and ammonium sulfate coated illite particles (but slightly lower temperatures for the coated particles, not shown). Sullivan et al. (2010a) found a variable effect of nitric acid coatings on the nucleation ability of ATD particles, which under some conditions even nucleated more ice than uncoated particles. At one out of five investigated temperatures, also Knopf and Koop (2006) observed an increase in the nucleation ability of sulfuric acid coated ATD particles. Salam et al. (2007) observed an increase of the ice nucleation efficiency of montmorillonite particles after ammonia gas exposure.

Regarding the transferability of these results to atmospheric conditions, the coating mechanism (in some cases involving heating of the sample), the trace gas concentrations and the actual fraction of coated particles in the cited studies have to be critically evaluated.

## Laboratory ice nucleation experiments

C. Hoose and O. Möhler

[Title Page](#)

[Abstract](#)

[Introduction](#)

[Conclusions](#)

[References](#)

[Tables](#)

[Figures](#)

◀

▶

◀

▶

[Back](#)

[Close](#)

[Full Screen / Esc](#)

[Printer-friendly Version](#)

[Interactive Discussion](#)



## 4 Determining factors of ice nucleation efficiency

### 4.1 Surface area dependence

It was shown in the previous section that supermicron dust particles tend to nucleate ice at higher temperatures and lower supersaturations over ice than smaller ones. This  
5 effect will be investigated and quantified in this section.

Heterogeneous ice nucleation is occurring at the surface of solid aerosol particles. Although the exact mechanism is still obscure, several surface-related requirements have been suggested for efficient IN: the chemical bond requirement, the crystallographic requirement, and the active-site requirement (Pruppacher and Klett, 1997). The larger  
10 the surface area of an aerosol particle, the higher is the probability that some part of its (in reality always) non-uniform surface area fulfils the necessary requirement for nucleation. Also in classical nucleation theory, which in its simplest form assumes uniform surfaces, the nucleation rate is proportional to the surface area, because nucleation is assumed to occur stochastically with the same probability everywhere on the uniform  
15 surface (Fletcher, 1958).

As a simplified quantification of the aerosol size effect on the observed IN fractions and nucleation onsets, the metric of “ice nucleation active surface site (INAS) densities” is employed in the following (DeMott, 1995; Connolly et al., 2009). The INAS density describes the number of ice-nucleation active sites at a certain temperature and supersaturation, normalized by the aerosol surface area. The approach is based on the assumption that the investigated aerosol sample is of uniform composition. Time dependence is not taken into account. In the following, the INAS density  $n_s$  (averaged over the investigated sample) is calculated from the following equation:  
20

$$n_s(T, S_i) = -1/A_{\text{aer}} * \ln(1 - f_{\text{IN}}(T, S_i)) \quad (1)$$

25

$$\approx f_{\text{IN}}(T, S_i)/A_{\text{aer}}$$

In this expression,  $f_{\text{IN}}$  is the ice nucleation active fraction under the considered conditions, and  $A_{\text{aer}}$  is the aerosol surface per particle. The approximation is valid for small

[Title Page](#)

[Abstract](#)

[Introduction](#)

[Conclusions](#)

[References](#)

[Tables](#)

[Figures](#)

◀

▶

◀

▶

[Back](#)

[Close](#)

[Full Screen / Esc](#)

[Printer-friendly Version](#)

[Interactive Discussion](#)



values of  $f_{IN}$ . Under the assumption of a constant INAS density independent of size, Eq. (1) can also be applied to polydisperse particles, with  $A_{aer}$  obtained from the total aerosol surface area concentration divided by the total aerosol number concentration.

$n_s$  has previously been used to quantify the nucleation ability of mineral dusts (Connolly et al., 2009; Niedermeier et al., 2010; Broadley et al., 2012; Niemand et al., 2012), volcanic ash (Bingemer et al., 2011; Steinke et al., 2011), and marine diatoms (Alpert et al., 2011). Fig. 10 illustrates the corresponding ice nucleation active fractions for a given INAS density and particle size.

In the following, Eq. (1) is applied to the previously discussed ice nucleation data (where possible). The data shown here are calculated based on the information available in the cited publications, except for cases in which  $n_s$  was provided directly (Connolly et al., 2009; Niedermeier et al., 2010; Murray et al., 2011; Broadley et al., 2012; Niemand et al., 2012). Where the ice nucleation active fraction  $f_{IN}$  was given as a range of values (e.g. an onset corresponding to 0.1 to 1 %), this range is converted into a range of  $n_s$ . In the case of Pinti et al. (2012), frozen fractions of 0.1 % to 2.6 % (V. Pinti, personal communication, 2012) were assumed for the freezing onset in the emulsion experiments, and a frozen fraction of 1 for the bulk experiments. For the aerosol surface area  $A_{aer}$ , an estimate based on the information given in the original publication is associated with large uncertainties, in particular for polydisperse particles. In most cases, we had to estimate  $A_{aer}$  from the reported average size  $d$  by  $A_{aer} = \pi d^2$ . This approach neglects any deviations when the reported size is the mobility diameter instead of the geometric diameter (Welti et al., 2009; Koehler et al., 2010) or when the distribution has a large spread (Wang and Knopf, 2011). Where a range of sizes is given instead of an average size (Knopf and Koop, 2006; Zimmermann et al., 2008), we proceed as with the case of a range of  $f_{IN}$  values.

#### 4.1.1 Immersion/condensation freezing

Figures 11 to 13 display  $n_s$  for immersion/condensation freezing. ATD, desert dusts, three clay minerals, soot and bioaerosol data are examined separately. The data stem

## Laboratory ice nucleation experiments

C. Hoose and O. Möhler

[Title Page](#)

[Abstract](#)

[Introduction](#)

[Conclusions](#)

[References](#)

[Tables](#)

[Figures](#)

◀

▶

◀

▶

[Back](#)

[Close](#)

[Full Screen / Esc](#)

[Printer-friendly Version](#)

[Interactive Discussion](#)



## Laboratory ice nucleation experiments

C. Hoose and O. Möhler

[Title Page](#)

[Abstract](#)

[Introduction](#)

[Conclusions](#)

[References](#)

[Tables](#)

[Figures](#)

◀

▶

◀

▶

[Back](#)

[Close](#)

[Full Screen / Esc](#)

[Printer-friendly Version](#)

[Interactive Discussion](#)



of  $n_s$ . It should be noted that Murray et al. (2011), Broadley et al. (2012) and Pinti et al. (2012) used values of the specific surface area determined by BET (Brunauer, Emmett and Teller gas adsorption technique, Brunauer et al., 1938). This method is expected to yield higher surface areas than our simplified assumption of spherical dust particles, because surface irregularities, cracks, etc. contribute to the surface area measured by BET, which then results in a lower value of  $n_s$ .

For soot (Fig. 12a), there is a vast disparity between the INAS densities derived from different experiments. The only true immersion freezing experiment with soot (DeMott, 1990) yields values of  $n_s$  comparable to mineral dust, and similar results are found by Kanji et al. (2011) above water saturation. By contrast, on the one hand, the INAS density calculated from values given in Dymarska et al. (2006) for one experiment in which ice formation was observed above water saturation, but without indication of liquid droplet formation prior to ice nucleation, are significantly lower. On the other hand, Gorbunov et al. (2001) measured relatively high activated fractions for soot particles already at  $-20^\circ\text{C}$  which translate into INAS densities higher than those for mineral dust. It should also be noted that soot particles are often fractal-like agglomerates for which the simple assumption of spherical particles may lead to a large error in the calculated INAS density.

The results for bioaerosols (Fig. 12b) are particularly interesting, because the ice nucleation onset is often reported for a very small activated fraction  $f_{\text{IN}}$ , e.g.  $10^{-6}$  (see overview in Després et al., 2012). In addition, most primary biological particles belong to the coarse mode aerosol. For the calculation of  $n_s$ , generic values for the particle diameters were assumed in the absence of better information: 1  $\mu\text{m}$  for bacteria, 5  $\mu\text{m}$  for fungal spores, and 20  $\mu\text{m}$  for pollen grains. Due to the small activated fractions and rather larger particle diameters, for a number of experiments with ice nucleation onsets above  $-5^\circ\text{C}$ , very small values of  $n_s$  ( $10^4$  to  $10^6 \text{ m}^{-2}$ ) are estimated. For pollen and fungal spores,  $n_s$  remains smaller than  $10^{10} \text{ m}^{-2}$  even at the lowest investigated temperatures. We will refer to these particles as “biological aerosols with intermediate ice nucleation activity” in the following.

## Laboratory ice nucleation experiments

C. Hoose and O. Möhler

[Title Page](#)

[Abstract](#)

[Introduction](#)

[Conclusions](#)

[References](#)

[Tables](#)

[Figures](#)

◀

▶

◀

▶

[Back](#)

[Close](#)

[Full Screen / Esc](#)

[Printer-friendly Version](#)

[Interactive Discussion](#)



A second group of data points for bacterial immersion freezing indicates significantly higher INAS densities than the other investigated particle types. In particular, for some bacteria (e.g. Jayaweera and Flanagan, 1982), INAS densities  $> 10^{10} \text{ m}^{-2}$  are reached already at temperatures above  $-10^\circ\text{C}$ . For mineral dust, these values are typically reached only below  $-20^\circ\text{C}$ . These biological particles will be referred to as having a "high ice nucleation activity".

Taking all immersion/condensation freezing INAS densities together (Fig. 13), a typical range of values for average mineral dust particles can be identified (indicated by the blue line in the plot). These range from  $10^6$ – $10^8 \text{ m}^{-2}$  at  $-10^\circ\text{C}$  to  $10^{10}$ – $10^{12} \text{ m}^{-2}$  close to  $-35^\circ\text{C}$ , i.e. roughly increasing by one order of magnitude per cooling of 5 K. Also some of the intermediately ice nucleation active biological particles exhibit INAS densities in this range. The much steeper increase of INAS densities at higher temperatures for highly ice nucleation active biological particles is indicated with the green dashed line.

It can not be determined with certainty whether  $n_s(T)$  for dust and biological particles retains this steady increase at decreasing temperatures (although a number of experiments with one aerosol type found similar exponential temperature dependencies of  $n_s$ , Niedermeier et al., 2010; Murray et al., 2011). E.g., it is thinkable that  $n_s(T)$  for biological particles might level off at temperatures lower than  $-20^\circ\text{C}$ . Furthermore, it should be noted that several measurements show large deviations from the average values of  $n_s(T)$ , and that a difference by one or two orders of magnitudes has a large impact if applied for the calculation of atmospheric IN concentrations.

#### 4.1.2 Deposition nucleation

Similar to the above analysis for immersion/condensation freezing, we apply the calculation of  $n_s$  to deposition nucleation experiments in the following. For deposition nucleation,  $n_s$  depends on both  $S_i$  and (though weaker) on  $T$ . Here, the data are binned into intervals of 10 K and shown as a function of  $S_i$  (Figs. 14 and 15). Due to a limited number of experiments which provide the necessary information, this could only be

## Laboratory ice nucleation experiments

C. Hoose and O. Möhler

[Title Page](#)

[Abstract](#)

[Introduction](#)

[Conclusions](#)

[References](#)

[Tables](#)

[Figures](#)

◀

▶

◀

▶

[Back](#)

[Close](#)

[Full Screen / Esc](#)

[Printer-friendly Version](#)

[Interactive Discussion](#)



## Laboratory ice nucleation experiments

C. Hoose and O. Möhler

[Title Page](#)

[Abstract](#)

[Introduction](#)

[Conclusions](#)

[References](#)

[Tables](#)

[Figures](#)

◀

▶

◀

▶

[Back](#)

[Close](#)

[Full Screen / Esc](#)

[Printer-friendly Version](#)

[Interactive Discussion](#)



done for ATD, kaolinite and desert dusts. Again, the normalization of the ice nucleation onsets by the activated fraction and surface area tends to reveal a better agreement between different experiments than the nucleation onset data, but the spread remains large. Within each temperature bin,  $n_s$  increases steeply with increasing  $S_i$ . In Fig. 14, where all estimates of  $n_s$  for the different minerals are shown together, no clear differences between the three mineral dusts are visible. The absolute values of  $n_s$  range mostly between  $10^6$ – $10^{12} \text{ m}^{-2}$ , i.e. similar to those for immersion freezing. In Fig. 15, the four selected temperature intervals are plotted together. The expected signal of increasing  $n_s$  with decreasing  $T$  at a given supersaturation is not visible in this representation. Instead, this figure clearly illustrates the vast spread of INAS densities at low supersaturations, which is larger than the experimental uncertainties and probably related to systematic differences between different methods, and/or to individual particle or material characteristics.

## 4.2 Observed time dependence

With the description of ice nucleation as a stochastic process, an increase of the activated particle fraction with longer measurement times is expected. This time dependence can only be resolved if a large number of particles within the sample exhibits the same ice nucleation probability at a given  $T$  and  $S_i$ . For the CFDC-type and mixing cloud chamber experiments listed in Tables 1 to 6, which all operate at fixed temperature and relative humidity, the residence time varies between 1.6 s and 120 s. Similarly, in the experiments with decreasing temperatures and/or increasing relative humidities during the measurement, the inverse cooling rates vary from 6 s to 600 s per K and/or per % increase in relative humidity.

The time dependence in the analysis of literature data (comparable to Sect. 4.1), can be investigated for experiments at constant conditions via an estimation of the

nucleation rate coefficient:

$$j_{\text{het}}(T, S_i) \approx \frac{f_{\text{IN}}(T, S_i)}{A_{\text{aer}} \Delta t} \quad (2)$$

$\Delta t$  is the time for which the aerosol is exposed to the temperature  $T$  and the supersaturation  $S_i$ . For experiments at water saturation with a constant cooling, the nucleation rate coefficient can be determined incrementally from

$$\begin{aligned} f_{\text{IN}}(T) &\approx A_{\text{aer}} \int j_{\text{het}}(T(t)) dt \\ &= A_{\text{aer}} \int j_{\text{het}}(T(t)) \left( \frac{dT}{dt} \right)^{-1} dT \end{aligned} \quad (3)$$

This leads to

$$j_{\text{het}}(T) \approx \frac{1}{A_{\text{aer}}} \frac{df_{\text{IN}}}{dT} \frac{dT}{dt} \quad (4)$$

- For the immersion freezing data in Fig. 13, such an analysis did not yield a better agreement between different experiments (not shown). For example, for ATD,  $\Delta t$  is similar for Kanji et al. (2011) and Hoyle et al. (2011), but both  $j_{\text{het}}$  and  $n_s$  differ by more than a factor of 10.

A more in-depth analysis of the influence of time on the activated fraction was conducted by Murray et al. (2011) and Broadley et al. (2012). In their experiments, the cooling rate could be varied by more than a factor of 10, and additional isothermal experiments with residence times up to 4000 s were conducted. Their results are summarized in Fig. 16, along with two experiments by Niedermeier et al. (2011b) and DeMott (1990). While Murray et al. (2011)'s results indicate significantly more ice nucleation in experiments with slower cooling rates, the other studies do not confirm this behaviour and instead show sometimes more, sometimes less ice nucleation when more time is available for freezing. It should also be noted that the spread in the data entering these

## Laboratory ice nucleation experiments

C. Hoose and O. Möhler

[Title Page](#)

[Abstract](#)

[Introduction](#)

[Conclusions](#)

[References](#)

[Tables](#)

[Figures](#)

◀

▶

◀

▶

[Back](#)

[Close](#)

[Full Screen / Esc](#)

[Printer-friendly Version](#)

[Interactive Discussion](#)



calculations is large. For none of the experiments, the ratio of ice fraction or INAS densities in the slow versus fast experiments converges towards the ratio of the cooling rates or residence times, as would be expected if nucleation was described well by a temperature-dependent nucleation rate with one value for all particles. Nevertheless,

- 5 Murray et al. (2011) found that such a single component stochastic model fits their data best, in particular if constant-temperature experiments are considered. It is still unclear why other aerosol particles behave differently.

## 5 Parametrical descriptions

In this section, we attempt to present various ice nucleation parameterizations using  
10 similar metrics as the measurements, in order to allow a direct comparison.

### 5.1 Immersion freezing parameterizations: temperature and surface area dependence

As discussed in Sect. 4.1, it is a well-established idea that ice nucleation probability is related to the surface area of the nucleus. Most parameterizations which link  
15 heterogeneous ice nucleation to aerosol properties assume proportionality to aerosol surface area. Three classes of these surface-related parameterizations for immersion freezing will be discussed in more detail below: empirical fits of INAS densities, parameterizations derived from ambient IN measurements, and parameterizations based on classical nucleation theory. A few other parameterizations assume proportionality  
20 to drop volume instead to aerosol surface area (Bigg, 1953; Diehl and Wurzler, 2004). It can be assumed that this apparent volume dependence reflects the fact that in the experiments which they are based on, the investigated droplets contained more than one aerosol particle, and thus the larger the droplets the larger the aerosol surface area included in them (Murray et al., 2011).

[Title Page](#)[Abstract](#)[Introduction](#)[Conclusions](#)[References](#)[Tables](#)[Figures](#)[Back](#)[Close](#)[Full Screen / Esc](#)[Printer-friendly Version](#)[Interactive Discussion](#)

## 5.1.1 Parameterizations of INAS densities

Recently, empirical parameterizations for the INAS density  $n_s(T)$  for immersion freezing have been derived from laboratory experiments (Connolly et al., 2009; Niedermeier et al., 2010; Lüönd et al., 2010; Steinke et al., 2011; Broadley et al., 2012; Niemand et al., 2012). These formulations are fits to measured data for a specific aerosol type, and are a function of the temperature only (Fig. 17a). Different functional forms with two to four fit parameters have been applied, yielding varying slopes of the temperature dependence. The parameterizations by Connolly et al. (2009), Niedermeier et al. (2010) and Lüönd et al. (2010) fall off steeply at high subzero temperatures, which contradicts the overall picture in the measurements compiled in Fig. 13. Niemand et al. (2012)'s parameterization extends to temperatures up to  $-12^{\circ}\text{C}$  and compares well with the typical range of measurements on mineral dust.

## 5.1.2 Parameterizations based on atmospheric IN measurements

Phillips et al. (2008) presented an empirical ice nucleation parameterization based on CFDC measurements and coincident aerosol data. A reference IN profile is constructed for the complete range of subzero temperatures and saturation ratios larger than 1. This reference IN concentration is distributed to three types of IN (dust/metallic, black carbon and organic particles) and associated with a reference aerosol concentration. The parameterization is applied to a given aerosol composition and concentration by scaling the reference IN profile with the surface area of dust/metallic, black carbon and organic aerosols.

By comparing Eqs. (9) and (10) in Phillips et al. (2008) to the definition of  $n_s$  in Sect. 4.1, it can be seen that the following terms can be identified with an equivalent INAS density  $\tilde{n}_s$ :

$$25 \quad \tilde{n}_{s,\text{Phillips},X} = H_X(S_i, T) \xi(T) \frac{\alpha_X n_{\text{IN},1,*}}{\Omega_{X,1,*}} \quad (5)$$

[Title Page](#)

[Abstract](#)

[Introduction](#)

[Conclusions](#)

[References](#)

[Tables](#)

[Figures](#)

◀

▶

◀

▶

[Back](#)

[Close](#)

[Full Screen / Esc](#)

[Printer-friendly Version](#)

[Interactive Discussion](#)



Here, the index  $X$  refers to dust/metallic, black carbon and organic aerosols. The variables are listed in Table A1 and in Phillips et al. (2008). In Fig. 17b,  $\tilde{n}_s$  is displayed at water saturation for the three IN types.  $\tilde{n}_{s,\text{Phillips,dust/metallic}}$  has a weaker temperature dependency than  $n_s$  calculated from experiments (Fig. 13), resulting in lower values than observed at  $T < -25^\circ\text{C}$ . The values calculated for  $\tilde{n}_{s,\text{Phillips,soot}}$  are very similar to  $\tilde{n}_{s,\text{Phillips,dust/metallic}}$ . The equivalent INAS density for organic aerosols ( $\tilde{n}_{s,\text{Phillips,organic aerosols}}$ ) is about one order of magnitude lower and disagrees with most observed values for highly ice nucleation active bacteria (Fig. 13) at  $T < -5^\circ\text{C}$ . The agreement is better with fungal spores, pollen and a few estimates of bacteria INAS densities at  $T > -5^\circ\text{C}$ .

A different approach of parameterizing IN concentrations based on CFDC measurements was taken by DeMott et al. (2010), who related IN concentrations to temperature and the number concentration of aerosol particles with diameters larger than  $0.5\text{ }\mu\text{m}$  ( $n_{\text{aer},05}$ ), and found that this relationship could explain a large part of the variability in observed IN concentrations. While the relationship is not strictly proportional to aerosol surface area (nor to aerosol number concentration), we can derive equivalent INAS densities for chosen values of  $n_{\text{aer},05}$  under the assumption of a monodisperse size distribution with diameter  $d$ :

$$\tilde{n}_{s,\text{DeMott}} = \frac{n_{\text{IN}}(T, n_{\text{aer},05})}{\pi d^2 n_{\text{aer},05}} \quad (6)$$

Here,  $n_{\text{IN}}(T, n_{\text{aer},05})$  is parameterized after DeMott et al. (2010, their Eq. 1).  $\tilde{n}_{s,\text{DeMott}}$  is shown in Fig. 17c for  $n_{\text{aer},05} = 1$  to  $100\text{ cm}^{-3}$  and  $d = 0.5$  and  $1\text{ }\mu\text{m}$ . For small aerosol number concentrations,  $\tilde{n}_{s,\text{DeMott}}$  is similar to  $\tilde{n}_{s,\text{Phillips}}$ , but the temperature dependency is steeper for higher aerosol concentrations.  $\tilde{n}_{s,\text{DeMott}}$  is generally lower than observed INAS densities for dust (Fig. 13), which is expected because  $\tilde{n}_{s,\text{DeMott}}$  refers to an average active site density of an aerosol population including inactive particles.

## Laboratory ice nucleation experiments

C. Hoose and O. Möhler

[Title Page](#)

[Abstract](#)

[Introduction](#)

[Conclusions](#)

[References](#)

[Tables](#)

[Figures](#)

◀

▶

◀

▶

[Back](#)

[Close](#)

[Full Screen / Esc](#)

[Printer-friendly Version](#)

[Interactive Discussion](#)



### 5.1.3 Parameterizations employing classical nucleation theory for immersion freezing

In classical nucleation theory (CNT), the nucleation rate coefficient  $j$  is proportional to the aerosol surface area. Different formulations of classical nucleation theory are summarized in Appendix A1. For Fig. 17d, equivalent (or apparent) INAS densities  $\tilde{n}_{s,\text{Zobrist}}$  are obtained by multiplying  $j_{\text{imm}}$  as parameterized by Zobrist et al. (2007) with  $\Delta t = 10 \text{ s}$ , which corresponds to the approximate residence in e.g. a CFDC instrument. The contact angle is set to the fitted values provided by Marcolli et al. (2007) for ATD and by Lüönd et al. (2010) for kaolinite. As also noted in these studies, the temperature dependency of  $\tilde{n}_{s,\text{Zobrist}}$  is much stronger than observed in experiments.

Better fits can be obtained by allowing a distribution of contact angles instead of single values (Marcolli et al., 2007; Lüönd et al., 2010). In this approach, every particle is assigned one value of the contact angle, such that the particles with the smallest contact angles are depleted when the temperature is lowered. To derive an apparent  $\tilde{n}_{s,\theta-\text{pdf}}$ , this depletion has to be taken into account. We proceed by calculating the IN fraction as given by Lüönd et al. (2010) and insert this value into Eq. (1) (for  $f_{\text{IN}} < 0.9$ ):

$$\tilde{n}_{s,\theta-\text{pdf}} = -\frac{1}{A_{\text{aer}}} \ln \left( \int p(\theta) \exp(-A_{\text{aer}} j_{\text{imm}}(\theta) dt) d\theta \right) \quad (7)$$

$p(\theta)$  describes the probability distribution function of the contact angle  $\theta$ . The resulting INAS densities are displayed in Fig. 17e for ATD (Marcolli et al., 2007) and kaolinite (Lüönd et al., 2010). Compared to the CNT-curves with single contact angles for the same materials (Fig. 17d), these apparent INAS densities have a weaker dependency on temperature, and are similar to some of the  $n_s$ -fits displayed in (Fig. 17a). However, the values of low  $\tilde{n}_{s,\theta-\text{pdf}}$  at  $-15$  to  $-20^\circ\text{C}$  are not supported by observations.

[Title Page](#)[Abstract](#)[Introduction](#)[Conclusions](#)[References](#)[Tables](#)[Figures](#)[Back](#)[Close](#)[Full Screen / Esc](#)[Printer-friendly Version](#)[Interactive Discussion](#)

## 5.2 Deposition nucleation parameterizations

For deposition nucleation, the only aerosol-specific parameterizations which cover the full range of possible supersaturations and temperatures, are the empirical formulation by Phillips et al. (2008), or are based on classical nucleation theory. (Fitted INAS densities for deposition nucleation are so far available only for narrow temperature ranges (Wheeler and Bertram, 2012).)

- 5 We will discuss these approaches in the light of the predicted temperature- an supersaturation dependency, expressed by the shape of onset curves in the  $T$ - $S_i$  diagram.

### 5.2.1 Comparison to observed shape of onset curves in $T$ - $S_i$ diagrams

- 10 In Fig. 19, a subset of the data shown in Fig. 2 is connected by lines. Each line represents one experimental setup with constant particle size and/or the same material. Only those data are included for which the nucleation onset supersaturation for a specific temperature is given unambiguously in the original publication (in some cases obtained through averaging over several repetitions of the experiment). These lines  
15 can be interpreted as isolines of a constant INAS density  $n_s$  or a constant nucleation rate coefficient  $j$ . In the following, they are discussed as such isolines and compared to theoretical expectations.

Below water saturation, three different regimes can be distinguished. These are labelled A–C in Fig. 19b. At the lowest investigated temperatures ( $\leq -50^\circ\text{C}$ ), an increase of the  $j$ -isolines or  $n_s$ -isolines with decreasing temperature is frequently observed (regime A), i.e. higher supersaturations are required for the same number of particles to activate. This behaviour is contrary to the common assumption that lower temperatures always facilitate ice nucleation. In an intermediate temperature range, at relative humidities significantly below water saturation, the isolines are approximately horizontal (regime B). This corresponds to a temperature-independent behaviour of deposition nucleation: only ice supersaturation determines the rate of nucleating particles. However, when approaching water saturation, the isolines are frequently bend towards

## Laboratory ice nucleation experiments

C. Hoose and O. Möhler

[Title Page](#)

[Abstract](#)

[Introduction](#)

[Conclusions](#)

[References](#)

[Tables](#)

[Figures](#)

◀

▶

◀

▶

[Back](#)

[Close](#)

[Full Screen / Esc](#)

[Printer-friendly Version](#)

[Interactive Discussion](#)



higher supersaturations, i.e. deposition nucleation seems to be suppressed (regime C). Above water saturation,  $j$  or  $n_s$  is a strong function of temperature (steep lines, regime D), and sets in at higher temperatures than below water saturation. The temperature-dependence of immersion freezing cannot be properly represented as isolines in the  $T$ - $S_i$  diagram because the corresponding data are measured at water saturation. It is expected that immersion freezing of water droplets is temperature-dependent only, i.e. the isolines should be vertical above water saturation, as shown by Schaller and Fukuta (1979). The data above water saturation which are included in Fig. 19, stemming from deposition and condensation nucleation experiments, are not all consistent with this expectation.

## 5.2.2 Deposition nucleation parameterization based on atmospheric CFDC measurements

The isolines of  $\tilde{n}_{s,\text{Phillips},X}(S_i, T)$  (Eq. 5) are displayed in Fig. 20 for dust/metallic, black carbon and organic particles. While the reference IN concentration  $n_{\text{IN},1,*}$  in Eq. (5) mostly depends on  $S_i$ , a strong temperature dependence is introduced by the factor  $H_X(S_i, T)$ . This factor has been introduced to suppress ice nucleation at high temperatures and low supersaturations. The suppression is stronger for black carbon and organic aerosols than for dust/metallic particles. The resulting  $\tilde{n}_s$ -isolines for dust/metallic aerosols agree qualitatively well with the observations, but the  $\tilde{n}_s$ -isolines for black carbon and organic aerosols are distinctly different from typical shape identified in Fig. 19.

## 5.2.3 Deposition nucleation described by classical nucleation theory

As for immersion freezing, different formulations of classical nucleation theory have been used in studies of deposition ice nucleation. These are summarized in Appendix A2. Fig. 21 shows isolines of the nucleation rate coefficient  $j_{\text{dep}}$  for two different contact angles/form factors. The isolines calculated from classical nucleation theory are always quasi-horizontal close to water saturation (Fig. 21). At lower temperatures,

<a href="#">Title Page</a>	
<a href="#">Abstract</a>	<a href="#">Introduction</a>
<a href="#">Conclusions</a>	<a href="#">References</a>
<a href="#">Tables</a>	<a href="#">Figures</a>
<a href="#">◀</a>	<a href="#">▶</a>
<a href="#">◀</a>	<a href="#">▶</a>
<a href="#">Back</a>	<a href="#">Close</a>
<a href="#">Full Screen / Esc</a>	
<a href="#">Printer-friendly Version</a>	
<a href="#">Interactive Discussion</a>	



## Laboratory ice nucleation experiments

C. Hoose and O. Möhler

[Title Page](#)

[Abstract](#)

[Introduction](#)

[Conclusions](#)

[References](#)

[Tables](#)

[Figures](#)

◀

▶

◀

▶

[Back](#)

[Close](#)

[Full Screen / Esc](#)

[Printer-friendly Version](#)

[Interactive Discussion](#)



Fletcher (1958)'s formulation of  $A_{dep}$  does not reproduce the observed nucleation onset curves in regime A, while Chen et al. (2008) and Barahona (2011) tend to agree qualitatively better with the experiments at low temperatures.

For the suppression of deposition nucleation close to water saturation (regime C), classical nucleation theory does not provide any explanation. Fukuta and Schaller (1982) and DeMott (1995) have attempted to cover this range with empirical fits. Other authors derived contact angles for individual data points along the nucleation onset curves, resulting in a strong variation of the contact angle close to water saturation (Welti et al., 2009; Kulkarni and Dobbie, 2010). Physically, the observed behaviour of deposition nucleation might be related to water uptake in subsaturated conditions, which can occur both at the particle surface and within the bulk phase (swelling), depending on the particle composition (Schuttlefield et al., 2007). Mineral dust, which is usually considered to be insoluble, can contain various soluble components (Kelly et al., 2007; Herich et al., 2009).

### 5.3 Time dependence in different parameterizations

In any realization of an INAS density parameterization (Sect. 5.1.1), the resulting IN number at constant  $T$  and  $S_i$  has zero time dependence, i.e. the IN are assumed to activate instantaneously, without measurable time delay. Conversely, all formulations of classical nucleation theory in Sects. 5.1.3 and 5.2.3 have in common that if they are applied to a population of aerosol particles with one value of the contact angle (and activation energy), they predict an increase in IN with observation time at constant  $T$  and  $S_i$ . For small activated fractions, the predicted IN number is proportional to time.

This time dependence is weaker, if not only one value of the contact angle is chosen, but a certain distribution of contact angles (as already discussed in Sect. 5.1.3). In different realizations, this idea was termed “singular hypothesis: contact angle distribution” (Marcolli et al., 2007), “ $\alpha$ -PDF model” (Lüönd et al., 2010), “multi-component stochastic model” (Murray et al., 2011), “soccer ball modell” (Niedermeier et al., 2011b) or “nucleation probability dispersion function” (Barahona, 2011). A detailed discussion

and comparison of these formulations goes beyond the scope of this paper, but they should be compared to experiments with the same aerosol particles at different cooling rates or residence times, such as those shown in Fig. 16.

## 6 Conclusions

- 5 In this compilation of results from six decades of laboratory experiments of heterogeneous ice nucleation, it has become obvious that many fundamental questions in this field are yet unsolved. Observed onset conditions for heterogeneous ice nucleation spread over large ranges of temperature and ice supersaturation, due to differences in methodology and non-standardized reported variables. Normalization by activated fraction and particle surface area (i.e. estimates of the INAS density) leads to some convergence between different methods, but even for materials which are assumed to have a constant composition (e.g. ATD, kaolinite), the agreement is not satisfactory yet. Possible reasons could be impurities in the samples, different methods for the surface area determination, or instrumental biases.
- 15 Among the parameterizations intended for the description of ice nucleation in numerical models, those which are proportional to particle surface area have been discussed in more detail. Some fitted immersion freezing INAS densities, which don't include any a priori assumptions on temperature-dependence, have been shown to be unreliable outside the temperature range they were fitted to. This hinders their application in mesoscale or global models, in which the whole temperature range needs to be covered. Classical nucleation theory, in the different formulations with one contact angle employed for fits to measurements and implementation in models, fails to reproduce various aspects of observed heterogeneous ice nucleation: the temperature dependence for immersion nucleation, temperature and supersaturation dependence for deposition nucleation, and time dependence.
- 25 For future laboratory experiments of heterogeneous ice nucleation, we make the following recommendations:

## Laboratory ice nucleation experiments

C. Hoose and O. Möhler

<a href="#">Title Page</a>	
<a href="#">Abstract</a>	<a href="#">Introduction</a>
<a href="#">Conclusions</a>	<a href="#">References</a>
<a href="#">Tables</a>	<a href="#">Figures</a>
<a href="#">◀</a>	<a href="#">▶</a>
<a href="#">◀</a>	<a href="#">▶</a>
<a href="#">Back</a>	<a href="#">Close</a>
<a href="#">Full Screen / Esc</a>	
<a href="#">Printer-friendly Version</a>	
<a href="#">Interactive Discussion</a>	



## Appendix A

### Different formulations of classical nucleation theory

#### A1 Classical nucleation theory for immersion freezing

The basic form of the nucleation rate coefficient  $j_{\text{imm}}$  for immersion freezing is given by  
5 the following equation (Fletcher, 1962; Zobrist et al., 2007):

$$j_{\text{imm}} = A_{\text{imm}} \exp \left( \frac{-\Delta F_{\text{diff}}(T) - f_{\text{het}} \Delta G_{\text{imm}}}{kT} \right) \quad (\text{A1})$$

$\Delta G_{\text{imm}}$  is the energy for homogeneous germ formation in the immersion mode, given by

$$\Delta G_{\text{imm}} = \frac{16\pi v_{\text{ice}}^2(T) \sigma_{i/w}^3(T)}{3(kT \ln(e_{s,w}(T)/e_{s,i}(T)))^2} \quad (\text{A2})$$

- 10 The temperature-dependent values of  $v_{\text{ice}}$ ,  $\sigma_{i/w}$ ,  $e_{s,i}$  and  $e_{s,w}$  are given in Table A1. The energy of germ formation is lowered by the foreign substrate to the value  $f_{\text{het}} \Delta G_{\text{imm}}(T)$ , where the form factor  $f_{\text{het}}$  can assume values between 0 and 1.  $f_{\text{het}}$  is related to the contact angle  $\theta$  via  $f_{\text{het}} = (2 + \cos \theta)(1 - \cos \theta)^2/4$  if the curvature effect is neglected (Pruppacher and Klett, 1997).
- 15 For the activation energy/energy for diffusion across the liquid-ice boundary  $\Delta F_{\text{diff}}$ , and the prefactor  $A_{\text{imm}}$ , different assumptions have been used. Zobrist et al. (2007) provide a parameterization for  $\Delta F_{\text{diff}}$  which is based on measurements of the diffusivity. For the prefactor a simplified form is used, in which the Zeldovich factor multiplied by the number of water molecules contacting the ice germ is approximated by 1 (Pruppacher

### Laboratory ice nucleation experiments

C. Hoose and O. Möhler

[Title Page](#)

[Abstract](#)

[Introduction](#)

[Conclusions](#)

[References](#)

[Tables](#)

[Figures](#)

◀

▶

◀

▶

[Back](#)

[Close](#)

[Full Screen / Esc](#)

[Printer-friendly Version](#)

[Interactive Discussion](#)



and Klett, 1997, their Eqs. 9–37).

$$\Delta F_{\text{diff, Zobrist}} = \frac{kT^2 E}{(T - T_0)^2} \quad (\text{A3})$$

$$A_{\text{imm, Zobrist}} = n_{1,w} \frac{kT}{h} \quad (\text{A4})$$

The constants  $n_{1,w}$ ,  $k$ ,  $h$  are explained in Table A1. The fitted parameters for  $\Delta F_{\text{diff, Zobrist}}$  are  $E = 892 \text{ K}$  and  $T_0 = 118 \text{ K}$ .

Fornea et al. (2009) use the activation energy for the self-diffusion of water (Pruppacher and Klett, 1997, their Eqs. 3–22), and the same prefactor as Zobrist et al. (2007):

$$\Delta F_{\text{diff, Fornea}} = a_0 \exp(a_1 T_c + a_2 T_c^2 + a_3 T_c^3) \quad (\text{A5})$$

$$A_{\text{imm, Fornea}} = A_{\text{imm, Zobrist}} = n_{1,w} \frac{kT}{h} \quad (\text{A6})$$

with  $a_0 = 4184/(6.022 \times 10^{23}) \times 5.55 \text{ J}$ ,  $a_1 = -8.423 \times 10^{-3}$ ,  $a_2 = 6.384 \times 10^{-4}$  and  $a_3 = 7.891 \times 10^{-6}$ .

Chen et al. (2008) employed  $\Delta F_{\text{diff}}$  as an additional temperature-independent fit parameter, with values ranging from  $9.9$  to  $16 \times 10^{-20} \text{ J}$ . In addition, the surface area of the ice germ and the Zeldovich factor, which describes the depletion of the embryo population due to germ production, are taken into account in the prefactor:

$$A_{\text{imm, Chen}} = n_{1,w} \frac{kT}{h} \times \frac{(kT \ln(e_{s,w}/e_{s,i}))^2}{4V_{\text{ice}} \sigma_{i/w}^2} \sqrt{\frac{4\sigma_{i/w}}{kT}} \sqrt{f_{\text{het}}} \quad (\text{A7})$$

Murray et al. (2011) do not make explicit assumptions about  $\Delta F_{\text{diff}}$  and  $A_{\text{imm}}$ , but implicitly assume that  $A_{\text{imm}} \exp(-\Delta F_{\text{diff}}/(kT))$  varies only weakly with temperature. Similarly,

Laboratory ice  
nucleation  
experiments

C. Hoose and O. Möhler

[Title Page](#)

[Abstract](#)

[Introduction](#)

[Conclusions](#)

[References](#)

[Tables](#)

[Figures](#)

◀

▶

◀

▶

[Back](#)

[Close](#)

[Full Screen / Esc](#)

[Printer-friendly Version](#)

[Interactive Discussion](#)



Niedermeier et al. (2010) used  $A_{\text{imm}} \exp(-\Delta F_{\text{diff}}/(kT))$  as a (temperature-independent) fit parameter.

The implications of these different formulations for  $\Delta F_{\text{diff}}$  (displayed in Fig. 22) will be discussed in the following.

- 5 In Fig. 23, equivalent INAS densities  $\tilde{n}_s$  based on Eq. (A1) are shown. The equivalent INAS densities are obtained by multiplying  $j_{\text{imm}}$  with  $\Delta t = 10\text{s}$ , which corresponds to the approximate residence in e.g. a CFDC instrument. The form factor  $f_{\text{het}}$  is varied from 0.01 to 0.9. The parameterization of  $\Delta F_{\text{diff}}$  has a strong impact on the temperature dependence of  $j_{\text{imm}}$ . With Zobrist et al. (2007)'s and Fornea et al. (2009)'s parameterizations,  $j_{\text{imm}} \cdot \Delta t$  increases much more sharply with decreasing temperatures than measurements (Fig. 13) or fitted parameterizations of  $n_s$  (Fig. 17) indicate. With fitted temperature-independent values of  $\Delta F_{\text{diff}}$  (Chen et al., 2008), the temperature characteristic of  $j_{\text{imm}} \cdot \Delta t$  is more similar to observations (see e.g. the fitted functions in Hoose et al. (2010b)). However, this approach has two disadvantages: First, at low temperatures,  $j_{\text{imm}}$  decreases after reaching a certain maximum, which is not supported by observations. Second, by using  $\Delta F_{\text{diff}}$  as a fit parameter, its physical meaning is ignored.

## A2 Classical nucleation theory for deposition nucleation

Fletcher (1958) gives the nucleation rate per particle by deposition nucleation as

20 
$$j_{\text{dep}} = A_{\text{dep}} \exp\left(-\frac{f_{\text{het}} \Delta G_{\text{dep}}}{kT}\right), \quad (\text{A8})$$

where  $A_{\text{dep}}$  is a kinetic prefactor and the exponential term describes the thermodynamics, including the effect of the ice nucleus on the formation of the ice germ. The energy of homogeneous germ formation from the gas phase,  $\Delta G_{\text{dep}}$ , included in the

[Title Page](#)

[Abstract](#)

[Introduction](#)

[Conclusions](#)

[References](#)

[Tables](#)

[Figures](#)

◀

▶

◀

▶

[Back](#)

[Close](#)

[Full Screen / Esc](#)

[Printer-friendly Version](#)

[Interactive Discussion](#)



exponential term (the thermodynamic factor), can be spelled out in the following way:

$$\Delta G_{\text{dep}} = \frac{16\pi v_{\text{ice}}^2(T)\sigma_{i/v}^3(T)}{3(kT \ln S_i)^2} \quad (\text{A9})$$

The surface tension between ice and vapor,  $\sigma_{i/v}$ , and the volume of a water molecule in ice,  $v_{\text{ice}}$ , are temperature dependent (see Table A1). However, the overall variation with temperature of the thermodynamic factor is much slower than the variation with supersaturation. Between 200 and 270 K, the term in Eq. (A9) varies only by about a factor 3 if the supersaturation is held constant. However, if temperature is held constant and supersaturation is varied between 1.2 and 1.8, it changes by a factor of more than  $10^{10}$ .

According to Fletcher (1958), the kinetic prefactor is approximately constant with the following value:

$$A_{\text{dep, Fletcher}} = 10^{29} \text{ m}^{-2} \text{ s}^{-1} \quad (\text{A10})$$

This constant value has been adopted in recent analyses of ice nucleation experiments (Eastwood et al., 2008; Kulkarni and Dobbie, 2010). With Fletcher (1958)'s formulation, the isolines of  $j_{\text{dep}}$  are near-horizontal in the  $T$ - $S_i$  diagram (Fig. 21a).

In two other recent implementations of classical nucleation theory, the kinetic factor  $A_{\text{dep}}$  is a function of both supersaturation and temperature. Chen et al. (2008) give the following expression :

$$A_{\text{dep, Chen}} = \frac{S_i^2 e_{s,i}^2 v_{\text{ice}}}{m_w k T v_s} \sqrt{\frac{\sigma_{i/v}}{kT}} \sqrt{f_{\text{het}}} \exp\left(\frac{\Delta g_d}{kT}\right) \quad (\text{A11})$$

Chen et al. (2008) use the desorption energy  $\Delta g_d$  as a fit parameter, similar to  $\Delta F_{\text{diff}}$  for immersion freezing. The values derived by Chen et al. (2008) for Asian dust, Saharan dust and ATD range from  $3.3 \times 10^{-20}$  J to  $4.9 \times 10^{-20}$  J.

## Laboratory ice nucleation experiments

C. Hoose and O. Möhler

[Title Page](#)

[Abstract](#)

[Introduction](#)

[Conclusions](#)

[References](#)

[Tables](#)

[Figures](#)

[◀](#)

[▶](#)

[◀](#)

[▶](#)

[Back](#)

[Close](#)

[Full Screen / Esc](#)

[Printer-friendly Version](#)

[Interactive Discussion](#)



Conversely, the expression used by Barahona (2011) differs with respect to the exponent of the form factor  $f_{\text{het}}$  and includes a mass accommodation coefficient  $\alpha_c$ :

$$A_{\text{dep, Barahona}} = \frac{S_i^2 e_{s,i}^2 v_{\text{ice}}}{m_w k T v_s} \sqrt{\frac{\sigma_{i/v}}{kT}} \frac{\alpha_c}{\sqrt{f_{\text{het}}}} \exp\left(\frac{\Delta g_d}{kT}\right) \quad (\text{A12})$$

Barahona (2011) prescribes a desorption energy of  $\Delta g_d = 6.5 \times 10^{-20}$  J for mineral dust and  $\Delta g_d = 4.4 \times 10^{-20}$  J for soot (Seisel et al., 2005).

In Eqs. (A11) and (A12), the saturation vapour pressure over ice ( $e_{s,i}$ ) is strongly temperature dependent and dominates the functional behaviour of  $A_{\text{dep, Chen}}$  and  $A_{\text{dep, Barahona}}$ . Physically, this can be explained with a slow-down of the deposition of water molecules from the vapour phase at lower temperatures. The resulting  $j_{\text{dep}}$  (Fig. 21b, c) exhibits a (small) decrease with decreasing temperatures.

With different assumptions about the prefactor, the contact angles derived from experimental data are also substantially different and not intercomparable (Chen et al., 2008; Hoose et al., 2010b; Eastwood et al., 2008; Fornea et al., 2009; Marcolli et al., 2007; Welti et al., 2009; Kulkarni and Dobbie, 2010).

- 15 **Acknowledgements.** We acknowledge all authors of the numerous original studies which are analysed in this work. Jen-Ping Chen, Paul DeMott, Kristina Höhler, Zamin Kanji, Alexei Kiselev, Daniel Knopf, Thomas Leisner, Ulrike Lohmann, Benjamin Murray, Monika Niemand, Valeria Pinti, Isabelle Steinke, Robert Wagner, Bingbing Wang and Aldona Wiacek are thanked for inspirations, helpful discussions and additional information on published data. The free software g3data was used for the extraction of data from graphs, and its developers are gratefully acknowledged. We acknowledge support by the Deutsche Forschungsgemeinschaft and the Open Access Publishing Fund of the Karlsruhe Institute of Technology. Part of this research was funded by the Helmholtz Association through the President's Initiative and Networking Fund.

## Laboratory ice nucleation experiments

C. Hoose and O. Möhler

[Title Page](#)

[Abstract](#)

[Introduction](#)

[Conclusions](#)

[References](#)

[Tables](#)

[Figures](#)

◀

▶

◀

▶

[Back](#)

[Close](#)

[Full Screen / Esc](#)

[Printer-friendly Version](#)

[Interactive Discussion](#)



## References

### Laboratory ice nucleation experiments

C. Hoose and O. Möhler

- Abbatt, J. P. D., Benz, S., Cziczo, D. J., Kanji, Z., Lohmann, U., and Möhler, O.: Solid ammonium sulfate aerosols as ice nuclei: a pathway for cirrus cloud formation, *Science*, 313, 1770–1773, doi:10.1126/science.1129726, 2006. 12593
- Ahern, H. E., Walsh, K. A., Hill, T. C. J., and Moffett, B. F.: Fluorescent pseudomonads isolated from Hebridean cloud and rain water produce biosurfactants but do not cause ice nucleation, *Biogeosciences*, 4, 115–124, doi:10.5194/bg-4-115-2007, 2007. 12590
- Alpert, P. A., Aller, J. Y., and Knopf, D. A.: Ice nucleation from aqueous NaCl droplets with and without marine diatoms, *Atmos. Chem. Phys.*, 11, 5539–5555, doi:10.5194/acp-11-5539-2011, 2011. 12546
- Archuleta, C. M., DeMott, P. J., and Kreidenweis, S. M.: Ice nucleation by surrogates for atmospheric mineral dust and mineral dust/sulfate particles at cirrus temperatures, *Atmos. Chem. Phys.*, 5, 2617–2634, doi:10.5194/acp-5-2617-2005, 2005. 12584
- Bailey, M. and Hallett, J.: Nucleation effects on the habit of vapour grown ice crystals from –18 to –42 °C, *Q. J. Roy. Meteor. Soc.*, 128, 1461–1483, 2002. 12584
- Barahona, D.: On the ice nucleation spectrum, *Atmos. Chem. Phys.*, 12, 3733–3752, doi:10.5194/acp-12-3733-2012, 2012. 12558, 12565, 12596, 12619
- Baustian, K. J., Wise, M. E., and Tolbert, M. A.: Depositional ice nucleation on solid ammonium sulfate and glutaric acid particles, *Atmos. Chem. Phys.*, 10, 2307–2317, doi:10.5194/acp-10-2307-2010, 2010. 12593, 12594
- Beaver, M. R., Elrod, M. J., Garland, R. M., and Tolbert, M. A.: Ice nucleation in sulfuric acid/organic aerosols: implications for cirrus cloud formation, *Atmos. Chem. Phys.*, 6, 3231–3242, doi:10.5194/acp-6-3231-2006, 2006. 12594
- Bigg, E. K.: The formation of atmospheric ice crystals by the freezing of droplets, *Q. J. Roy. Meteor. Soc.*, 79, 510–519, doi:10.1002/qj.49707934207, 1953. 12552
- Bingemer, H., Klein, H., Ebert, M., Haunold, W., Bundke, U., Herrmann, T., Kandler, K., Müller-Ebert, D., Weinbruch, S., Judt, A., Wéber, A., Nillius, B., Ardon-Dryer, K., Levin, Z., and Curtius, J.: Atmospheric ice nuclei in the Eyjafjallajökull volcanic ash plume, *Atmos. Chem. Phys.*, 12, 857–867, doi:10.5194/acp-12-857-2012, 2012. 12546
- Broadley, S. L., Murray, B. J., Herbert, R. J., Atkinson, J. D., Dobbie, S., Malkin, T. L., Condiffe, E., and Neve, L.: Immersion mode heterogeneous ice nucleation by an illite rich

[Title Page](#)

[Abstract](#)

[Introduction](#)

[Conclusions](#)

[References](#)

[Tables](#)

[Figures](#)



[Back](#)

[Close](#)

[Full Screen / Esc](#)

[Printer-friendly Version](#)

[Interactive Discussion](#)



- powder representative of atmospheric mineral dust, *Atmos. Chem. Phys.*, 12, 287–307, doi:10.5194/acp-12-287-2012, 2012. 12546, 12548, 12551, 12553, 12584, 12609, 12614
- Brunauer, S., Emmett, P. H., and Teller, E.: Adsorption of gases in multimolecular layers, *J. Am. Chem. Soc.*, 60, 309–319, 1938. 12548
- 5 Bundke, U., Nillius, B., Jaenicke, R., Wetter, T., Klein, H., and Bingemer, H.: The fast Ice Nucleus chamber FINCH, *Atmos. Res.*, 90, 180–186, 2008. 12542, 12584
- Chen, J.-P., Hazra, A., and Levin, Z.: Parameterizing ice nucleation rates using contact angle and activation energy derived from laboratory data, *Atmos. Chem. Phys.*, 8, 7431–7449, doi:10.5194/acp-8-7431-2008, 2008. 12558, 12562, 12563, 12564, 12565, 12596, 12619
- 10 Chen, Y., Demott, P. J., Kreidenweis, S. M., Rogers, D. C., and Sherman, D. E.: Ice formation by sulfate and sulfuric acid aerosol particles under upper-tropospheric conditions, *J. Atmos. Sci.*, 57, 3752–3766, 2000. 12593
- Chernoff, D. I. and Bertram, A. K.: Effects of sulfate coatings on the ice nucleation properties of a biological ice nucleus and several types of minerals, *J. Geophys. Res.*, 115, D20205, doi:10.1029/2010JD014254, 2010. 12539, 12542, 12584, 12590, 12595
- 15 Conen, F., Morris, C. E., Leifeld, J., Yakutin, M. V., and Alewell, C.: Biological residues define the ice nucleation properties of soil dust, *Atmos. Chem. Phys.*, 11, 9643–9648, doi:10.5194/acp-11-9643-2011, 2011. 12543, 12584
- Connolly, P. J., Möhler, O., Field, P. R., Saathoff, H., Burgess, R., Choularton, T., and Gallagher, M.: Studies of heterogeneous freezing by three different desert dust samples, *Atmos. Chem. Phys.*, 9, 2805–2824, doi:10.5194/acp-9-2805-2009, 2009. 12545, 12546, 12547, 20  
12553, 12584
- Constantinidou, H. A., Hirano, S. S., Baker, L. S., and Upper, C. D.: Atmospheric dispersal of ice nucleation-active bacteria: the role of rain, *Phytopathology*, 80, 934–937, 1990. 12590
- Crawford, I., Möhler, O., Schnaiter, M., Saathoff, H., Liu, D., McMeeking, G., Linke, C., Flynn, M., Bower, K. N., Connolly, P. J., Gallagher, M. W., and Coe, H.: Studies of propane flame soot acting as heterogeneous ice nuclei in conjunction with single particle soot photometer measurements, *Atmos. Chem. Phys.*, 11, 9549–9561, doi:10.5194/acp-11-9549-2011, 2011. 12538, 12588
- 30 Cziczo, D. J., Froyd, K. D., Gallavardin, S. J., Moehler, O., Benz, S., Saathoff, H., and Murphy, D. M.: Deactivation of ice nuclei due to atmospherically relevant surface coatings, *Environ. Res. Lett.*, 4, 044013, doi:10.1088/1748-9326/4/4/044013, 2009a. 12544, 12584, 12595

[Title Page](#)[Abstract](#)[Introduction](#)[Conclusions](#)[References](#)[Tables](#)[Figures](#)[Back](#)[Close](#)[Full Screen / Esc](#)[Printer-friendly Version](#)[Interactive Discussion](#)

- Cziczo, D. J., Stetzer, O., Worringen, A., Ebert, M., Weinbruch, S., Kamphus, M., Gallavardin, S. J., Curtius, J., Borrmann, S., Froyd, K. D., Mertes, S., Möhler, O., and Lohmann, U.: Inadvertent climate modification due to anthropogenic lead, *Nat. Geosci.*, 2, 333–336, doi:10.1038/ngeo499, 2009b. 12584
- 5 Demirdjian, B., Ferry, D., Suzanne, J., Popovicheva, O. B., Persiantseva, N. M., Kamaev, A. V., Shonija, N. K., and Zubareva, N. A.: Freezing of water adsorbed on hydrophobic and activated soot particles, *Chem. Phys. Lett.*, 480, 247–252, 2009. 12588
- DeMott, P. J.: An exploratory study of ice nucleation by soot aerosols, *J. Appl. Meteorol.*, 29, 1072–1079, 1990. 12538, 12548, 12551, 12588, 12614
- 10 DeMott, P. J.: Quantitative descriptions of ice formation mechanisms of silver iodide-type aerosols, *Atmos. Res.*, 38, 63–99, 1995. 12545, 12558
- DeMott, P. J.: Laboratory studies of cirrus cloud processes, in: *Cirrus*, edited by: Lynch, D. K., Sassen, K., Starr, D. O., and Stephens, G., Oxford University Press, New York, NY, USA, 2002. 12537
- 15 DeMott, P. J., Chen, Y., Kreidenweis, S. M., Rogers, D. C., and Sherman, D. E.: Ice formation by black carbon particles, *Geophys. Res. Lett.*, 26, 2429–2432, 1999. 12588, 12595
- DeMott, P. J., Petters, M. D., Prenni, A. J., Carrico, C. M., Kreidenweis, S. M., Collett Jr., J. L., and Moosmüller, H.: Ice nucleation behavior of biomass combustion particles at cirrus temperatures, *J. Geophys. Res.*, 114, D16205, doi:10.1029/2009JD012036, 2009. 12594
- 20 DeMott, P. J., Prenni, A. J., Liu, X., Kreidenweis, S. M., Petters, M. D., Twohy, C. H., Richardson, M. S., Eidhammer, T., and Rogers, D. C.: Predicting global atmospheric ice nuclei distributions and their impacts on climate, *P. Natl. Acad. Sci. USA*, 107, 11217–11222, 2010. 12554, 12615
- DeMott, P. J., Möhler, O., Stetzer, O., Vali, G., Levin, Z., Petters, M. D., Murakami, M., Leisner, T., Bundke, U., Klein, H., Kanji, Z. A., Cotton, R., Jones, H., Benz, S., Brinkmann, M., Rzesanke, D., Saathoff, H., Nicolet, M., Saito, A., Nillius, B., Bingemer, H., Abbatt, J., Ardon, K., Ganor, E., Georgakopoulos, D. G., and Saunders, C.: Resurgence in ice nuclei measurement research, *B. Am. Meteorol. Soc.*, 92, 1623–1635, doi:10.1175/2011BAMS3119.1, 2011. 12533, 12534, 12537, 12539, 12560
- 25 Després, V. R., Huffman, J. A., Burrows, S. M., Hoose, C., Safatov, A. S., Buryak, G., Fröhlich-Nowoisky, J., Elbert, W., Andreae, M. O., Pöschl, U., and Jaenicke, R.: Primary biological aerosol particles in the atmosphere: a review, *Tellus B*, 64, 15598, doi:10.3402/tellusb.v64i0.15598, 2012. 12539, 12548

**Laboratory ice nucleation experiments**

C. Hoose and O. Möhler

[Title Page](#)[Abstract](#)[Introduction](#)[Conclusions](#)[References](#)[Tables](#)[Figures](#)[Back](#)[Close](#)[Full Screen / Esc](#)[Printer-friendly Version](#)[Interactive Discussion](#)

## Laboratory ice nucleation experiments

C. Hoose and O. Möhler

[Title Page](#)

[Abstract](#)

[Introduction](#)

[Conclusions](#)

[References](#)

[Tables](#)

[Figures](#)

◀

▶

◀

▶

[Back](#)

[Close](#)

[Full Screen / Esc](#)

[Printer-friendly Version](#)

[Interactive Discussion](#)



- Diehl, K. and Mitra, S. K.: A Laboratory study of the effects of a Kerosene-burner exhaust on ice nucleation and the evaporation rate of ice crystals, *Atmos. Environ.*, 32, 3145–3151, 1998. 12538, 12588
- 5 Diehl, K. and Wurzler, S.: Heterogeneous drop freezing in the Immersion mode: model calculations considering soluble and insoluble particles in the drops, *J. Atmos. Sci.*, 61, 2063–2072, 2004. 12552
- Diehl, K., Quick, C., Matthias-Maser, S., Mitra, S. K., and Jaenicke, R.: The ice nucleating ability of pollen. Part I: Laboratory studies in deposition and condensation freezing modes, *Atmos. Res.*, 58, 75–87, 2001. 12590
- 10 Diehl, K., Matthias-Maser, S., Jaenicke, R., and Mitra, S. K.: The ice nucleating ability of pollen. Part II: Laboratory studies in immersion and contact freezing modes., *Atmos. Res.*, 61, 125–133, 2002. 12590
- 15 Diehl, K., Simmel, M., and Wurzler, S.: Numerical sensitivity studies on the impact of aerosol properties and drop freezing modes on the glaciation, microphysics, and dynamics of clouds, *J. Geophys. Res.*, 111, D07202, doi:10.1029/2005JD005884, 2006. 12541
- Dufour, L.: Über das Gefrieren des Wassers und über die Bildung des Hagels, *Bibl. univ. Aer.*, 1861. 12533
- 20 Durant, A. J., Shaw, R. A., Rose, W. I., Mi, Y., and Ernst, G. G. J.: Ice nucleation and overseeding of ice in volcanic clouds, *J. Geophys. Res.*, 113, D09206, doi:10.1029/2007JD009064, 2008. 12540
- Dymarska, M., Murray, B. J., Sun, L., Eastwood, M. L., Knopf, D. A., and Bertram, A. K.: Deposition ice nucleation on soot at temperatures relevant for the lower troposphere, *J. Geophys. Res.*, 111, D04204, doi:10.1029/2005JD006627, 2006. 12538, 12548, 12584, 12588, 12595
- 25 Eastwood, M. L., Cremel, S., Gehrke, C., Girard, E., and Bertram, A. K.: Ice nucleation on mineral dust particles: onset conditions, nucleation rates and contact angles, *J. Geophys. Res.*, 113, D22203, doi:10.1029/2008JD010639, 2008. 12542, 12564, 12565, 12584
- Eastwood, M. L., Cremel, S., Wheeler, M., Murray, B. J., Girard, E., and Bertram, A. K.: Effects of sulfuric acid and ammonium sulfate coatings on the ice nucleation properties of kaolinite particles, *Geophys. Res. Lett.*, 36, L02811, doi:10.1029/2008GL035997, 2009. 12595
- 30 Eidhammer, T., DeMott, P. J., Prenni, A. J., Petters, M. D., Twohy, C. H., Rogers, D. C., Stith, J., Heymsfield, A., Wang, Z., Pratt, K. A., Prather, K. A., Murphy, S. M., Seinfeld, J. H., Subramanian, R., and Kreidenweis, S. M.: Ice initiation by aerosol particles: measured and predicted

ice nuclei concentrations versus measured ice crystal concentrations in an orographic wave cloud, *J. Atmos. Sci.*, 67, 2417–2436, 2010. 12533

Ervens, B., Feingold, G., Sulia, K., and Harrington, J.: The impact of microphysical parameters, ice nucleation mode, and habit growth on the ice/liquid partitioning in mixed-phase Arctic clouds, *J. Geophys. Res.*, 116, D17205, doi:10.1029/2011JD015729, 2011. 12534

Field, P. R., Hogan, R. J., Brown, P. R. A., Illingworth, A. J., Choularton, T. W., Kaye, P. H., Hirst, E., and Greenaway, R.: Simultaneous radar and aircraft observations of mixed-phase cloud at the 100 m scale, *Q. J. Roy. Meteor. Soc.*, 130, 1877–1904, 2004. 12536

Field, P. R., Möhler, O., Connolly, P., Krämer, M., Cotton, R., Heymsfield, A. J., Saathoff, H., and Schnaiter, M.: Some ice nucleation characteristics of Asian and Saharan desert dust, *Atmos. Chem. Phys.*, 6, 2991–3006, doi:10.5194/acp-6-2991-2006, 2006. 12543, 12584

Fletcher, N. H.: Size effect in heterogeneous nucleation, *J. Chem. Phys.*, 29, 572–576, 1958. 12545, 12558, 12563, 12564, 12619

Fletcher, N. H.: Physics of Rain Clouds, Cambridge University Press, 386 pp., 1962. 12561

Fornea, A. P., Brooks, S. D., Dooley, J. B., and Saha, A.: Heterogeneous freezing of ice on atmospheric aerosols containing ash, soot, and soil, *J. Geophys. Res.*, 114, D13201, doi:10.1029/2009JD011958, 2009. 12538, 12562, 12563, 12565, 12588

Friedman, B., Kulkarni, G., Beránek, J., Zelenyuk, A., Thornton, J., and Cziczo, D.: Ice nucleation and droplet formation by bare and coated soot particles, *J. Geophys. Res.*, 116, D17203, doi:10.1029/2011JD015999, 2011. 12538, 12584, 12588

Fukuta, N.: Ice nucleation by metaldehyde, *Nature*, 199, 475–476, doi:10.1038/199475a0, 1963. 12540

Fukuta, N. and Schaller, R. C.: Ice nucleation by aerosol particles: theory of condensation-freezing nucleation, *J. Atmos. Sci.*, 39, 648–655, 1982. 12558

Georgii, H. W. and Kleinjung, E.: Relations between the chemical composition of atmospheric aerosol particles and the concentration of natural ice nuclei, *J. Rech. Atmos.*, 3, 145–156, 1967. 12533

Gorbunov, B., Baklanov, A., Kakutkina, N., Windsor, H. L., and Toumi, R.: Ice nucleation on soot particles, *J. Aerosol Sci.*, 32, 199–215, 2001. 12538, 12548, 12588

Gross, D. C., Cody, Y. S., Proebsting Jr., E. L., Rademaker, G. K., and Spotts, R. A.: Distribution, population dynamics, and characteristics of ice nucleation-active bacteria in deciduous fruit tree orchards, *Appl. Environ. Microbiol.*, 46, 1370–1379, 1983. 12590

## Laboratory ice nucleation experiments

C. Hoose and O. Möhler

[Title Page](#)

[Abstract](#)

[Introduction](#)

[Conclusions](#)

[References](#)

[Tables](#)

[Figures](#)

◀

▶

◀

▶

[Back](#)

[Close](#)

[Full Screen / Esc](#)

[Printer-friendly Version](#)

[Interactive Discussion](#)



## Laboratory ice nucleation experiments

C. Hoose and O. Möhler

[Title Page](#)

[Abstract](#)

[Introduction](#)

[Conclusions](#)

[References](#)

[Tables](#)

[Figures](#)

◀

▶

◀

▶

[Back](#)

[Close](#)

[Full Screen / Esc](#)

[Printer-friendly Version](#)

[Interactive Discussion](#)



Grützun, V., Knoth, O., and Simmel, M.: Simulation of the influence of aerosol particle characteristics on clouds and precipitation with LM-SPECS: model description and first results, *Atmos. Res.*, 90, 233–242, 2008. 12533

5 Haag, W., Kärcher, B., Ström, J., Minikin, A., Lohmann, U., Ovarlez, J., and Stohl, A.: Freezing thresholds and cirrus cloud formation mechanisms inferred from in situ measurements of relative humidity, *Atmos. Chem. Phys.*, 3, 1791–1806, doi:10.5194/acp-3-1791-2003, 2003. 12536

Hendricks, J., Kärcher, B., and Lohmann, U.: Effects of ice nuclei on cirrus clouds in a global climate model, *J. Geophys. Res.*, 116, D18206, doi:10.1029/2010JD015302, 2011. 12534

10 Herich, H., Tritscher, T., Wiacek, A., Gysel, M., Weingartner, E., Lohmann, U., Baltensperger, U., and Cziczo, D. J.: Water uptake of clay and desert dust aerosol particles at sub- and supersaturated water vapor conditions, *Phys. Chem. Chem. Phys.*, 11, 7804–7809, doi:10.1039/b901585j, 2009. 12542, 12558

15 Hirano, S. S. and Upper, C. D.: Ecology of ice nucleation-active bacteria, in: *Biological Ice Nucleation and its Applications*, edited by: Lee, R. E., Warren, G. J., and Gusta, L. V., The American Phytopathological Society, St. Paul, Minnesota, US, 41–61, 1995. 12539

Hirano, S. S., Baker, L., and Upper, C. D.: Ice nucleation temperature of individual leaves in relation to population sizes of ice nucleation active bacteria and frost injury, *Plant Physiol.*, 77, 259–265, 1985. 12590

20 Hoffer, T. E.: A laboratory investigation of droplet freezing, *J. Meteorol.*, 18, 766–778, 1961. 12541, 12542, 12584, 12604, 12605

Hoose, C., Lohmann, U., Erdin, R., and Tegen, I.: Global influence of dust mineralogical composition on heterogeneous ice nucleation in mixed-phase clouds, *Environ. Res. Lett.*, 3, 025003, doi:10.1088/1748-9326/3/2/025003, 2008. 12541

25 Hoose, C., Kristjánsson, J. E., and Burrows, S. M.: How important is biological ice nucleation in clouds on a global scale?, *Environ. Res. Lett.*, 5, 024009, doi:10.1088/1748-9326/5/2/024009, 2010a. 12533

Hoose, C., Kristjánsson, J. E., Chen, J.-P., and Hazra, A.: A classical-theory-based parameterization of heterogeneous ice nucleation by mineral dust, soot and biological particles in a global climate model, *J. Atmos. Sci.*, 67, 2483–2503, doi:10.1175/2010JAS3425.1, 2010b. 12533, 12534, 12563, 12565

30 Hoyle, C. R., Pinti, V., Welti, A., Zobrist, B., Marcolli, C., Luo, B., Höskuldsson, Á., Mattsson, H. B., Stetzer, O., Thorsteinsson, T., Larsen, G., and Peter, T.: Ice nucleation properties

## Laboratory ice nucleation experiments

C. Hoose and O. Möhler

[Title Page](#)

[Abstract](#)

[Introduction](#)

[Conclusions](#)

[References](#)

[Tables](#)

[Figures](#)

[◀](#)

[▶](#)

[◀](#)

[▶](#)

[Back](#)

[Close](#)

[Full Screen / Esc](#)

[Printer-friendly Version](#)

[Interactive Discussion](#)



of volcanic ash from Eyjafjallajökull, *Atmos. Chem. Phys.*, 11, 9911–9926, doi:10.5194/acp-11-9911-2011, 2011. 12540, 12551, 12584

Hung, H., Malinowski, A., and Martin, S. T.: Kinetics of heterogeneous ice nucleation on the surfaces of mineral dust cores inserted into aqueous ammonium sulfate particles, *J. Phys. Chem. A*, 107, 1296–1306, 2003. 12584, 12595

Iannone, R., Chernoff, D. I., Pringle, A., Martin, S. T., and Bertram, A. K.: The ice nucleation ability of one of the most abundant types of fungal spores found in the atmosphere, *Atmos. Chem. Phys.*, 11, 1191–1201, doi:10.5194/acp-11-1191-2011, 2011. 12590

Iraci, L. T., Phebus, B. D., Stone, B. M., and Colaprete, A.: Water ice cloud formation on Mars is more difficult than presumed: Laboratory studies of ice nucleation on surrogate materials, *Icarus*, 210, 985–991, doi:10.1016/j.icarus.2010.07.020, available at: <http://www.sciencedirect.com/science/article/pii/S0019103510002927>, 2010. 12585

Isono, K. and Ibeke, Y.: On the ice-nucleating ability of rock-forming minerals and soil particles, *J. Meteorol. Soc. Jpn.*, 38, 213–230, 1960. 12542, 12585

Isono, K., Komabayashi, M., and Ono, A.: The nature and the origin of ice nuclei in the atmosphere, *J. Meteorol. Soc. Jpn.*, 37, 195–199, 1959a. 12533, 12543, 12585

Isono, K., Komabayashi, M., and Ono, A.: Volcanoes as a source of atmospheric ice nuclei, *Nature*, 31, 317–318, 1959b. 12585

Jayaweera, K. and Flanagan, P.: Investigations on biogenic ice nuclei in the Arctic atmosphere., *Geophys. Res. Lett.*, 9, 94–97, 1982. 12549

Jones, H. M., Flynn, M. J., DeMott, P. J., and Möhler, O.: Manchester Ice Nucleus Counter (MINC) measurements from the 2007 International workshop on Comparing Ice nucleation Measuring Systems (ICIS-2007), *Atmos. Chem. Phys.*, 11, 53–65, doi:10.5194/acp-11-53-2011, 2011. 12585, 12606

Junge, K. and Swanson, B. D.: High-resolution ice nucleation spectra of sea-ice bacteria: implications for cloud formation and life in frozen environments, *Biogeosciences*, 5, 865–873, doi:10.5194/bg-5-865-2008, 2008. 12590

Kanitz, T., Seifert, P., Ansmann, A., Engelmann, R., Althausen, D., Casiccia, C., and Rohrher, E. G.: Contrasting the impact of aerosols at northern and southern midlatitudes on heterogeneous ice formation, *Geophys. Res. Lett.*, 38, L17802, doi:10.1029/2011GL048532, 2011. 12536

## Laboratory ice nucleation experiments

C. Hoose and O. Möhler

[Title Page](#)

[Abstract](#)

[Introduction](#)

[Conclusions](#)

[References](#)

[Tables](#)

[Figures](#)

◀

▶

◀

▶

[Back](#)

[Close](#)

[Full Screen / Esc](#)

[Printer-friendly Version](#)

[Interactive Discussion](#)



## Laboratory ice nucleation experiments

C. Hoose and O. Möhler

[Title Page](#)

[Abstract](#)

[Introduction](#)

[Conclusions](#)

[References](#)

[Tables](#)

[Figures](#)

◀

▶

◀

▶

[Back](#)

[Close](#)

[Full Screen / Esc](#)

[Printer-friendly Version](#)

[Interactive Discussion](#)



- Ladino, L., Stetzer, O., Lüönd, F., Welti, A., and Lohmann, U.: Contact freezing experiments of kaolinite particles with cloud droplets, *J. Geophys. Res.*, 116, D22202, doi:10.1029/2011JD015727, 2011. 12586
- 5 Langer, G.: Analysis of results from second international ice nucleus workshop with emphasis on expansion chambers, NCAR counters, and membrane filters, *J. Appl. Meteorol.*, 12, 991–999, doi:10.1175/1520-0450(1973)012<0991:AORFSI>2.0.CO;2, 1973. 12534
- Levin, Z. and Yankofsky, S. A.: Contact versus immersion freezing of freely suspended droplets by bacterial ice nuclei, *J. Clim. Appl. Meteorol.*, 22, 1964–1966, 1983. 12591
- 10 Lindemann, J., Constantinidou, H. A., Barchet, W. R., and Uppen, C. D.: Plants as sources of airborne bacteria, including ice nucleation-active bacteria, *Appl. Environ. Microb.*, 44, 1059–1063, 1982. 12591
- Lindow, S. E., Lahue, E., Govindarajan, A. G., Panopoulos, N. J., and Gies, D.: Localization of ice nucleation activity and the *iceC* gene product in *Pseudomonas syringae* and *Escherichia coli*, *Mol. Plant Microbe In.*, 2, 262–272, 1989. 12591
- 15 Liu, X. and Penner, J. E.: Ice nucleation parameterization for global models, *Meteorol. Z.*, 14, 499–514, 2005. 12533, 12534
- Lohmann, U. and Diehl, K.: Sensitivity studies of the importance of dust ice nuclei for the indirect aerosol effect on stratiform mixed-phase clouds, *J. Atmos. Sci.*, 63, 968–982, 2006. 12533, 12534, 12541
- 20 Lüönd, F., Stetzer, O., Welti, A., and Lohmann, U.: Experimental study on the ice nucleation ability of size selected kaolinite particles in the immersion mode, *J. Geophys. Res.*, 115, D14201, doi:10.1029/2009JD012959, 2010. 12547, 12553, 12555, 12558, 12586, 12616
- Maki, L. R. and Willoughby, K. J.: Bacteria as biogenic sources of freezing nuclei, *J. Appl. Meteorol.*, 17, 1049–1053, 1978. 12591
- 25 Maki, L. R., Galyan, E. L., Chang-Chien, M.-M., and Caldwell, D. R.: Ice nucleation induced by *Pseudomonas syringae*, *Appl. Microbiol.*, 28, 456–459, 1974. 12591
- Mangold, A., Wagner, R., Saathoff, H., Schurath, U., Gieseemann, C., Ebert, V., Krämer, M., and Möhler, O.: Experimental investigation of ice nucleation by different types of aerosols in the aerosol chamber AIDA: implications to microphysics of cirrus clouds, *Meteorol. Z.*, 14, 485–497, 2005. 12586, 12593
- 30 Marcolli, C., Gedamke, S., Peter, T., and Zobrist, B.: Efficiency of immersion mode ice nucleation on surrogates of mineral dust, *Atmos. Chem. Phys.*, 7, 5081–5091, doi:10.5194/acp-7-5081-2007, 2007. 12543, 12555, 12558, 12565, 12586, 12616

**Laboratory ice nucleation experiments**

C. Hoose and O. Möhler

[Title Page](#)[Abstract](#)[Introduction](#)[Conclusions](#)[References](#)[Tables](#)[Figures](#)[◀](#)[▶](#)[◀](#)[▶](#)[Back](#)[Close](#)[Full Screen / Esc](#)[Printer-friendly Version](#)[Interactive Discussion](#)

## Laboratory ice nucleation experiments

C. Hoose and O. Möhler

[Title Page](#)

[Abstract](#)

[Introduction](#)

[Conclusions](#)

[References](#)

[Tables](#)

[Figures](#)

◀

▶

◀

▶

[Back](#)

[Close](#)

[Full Screen / Esc](#)

[Printer-friendly Version](#)

[Interactive Discussion](#)



## Laboratory ice nucleation experiments

C. Hoose and O. Möhler

[Title Page](#)

[Abstract](#)

[Introduction](#)

[Conclusions](#)

[References](#)

[Tables](#)

[Figures](#)

[◀](#)

[▶](#)

[◀](#)

[▶](#)

[Back](#)

[Close](#)

[Full Screen / Esc](#)

[Printer-friendly Version](#)

[Interactive Discussion](#)



Obata, H., Muryoi, N., Kawahara, H., Yamade, K., and Nishikawa, J.: Identification of a novel ice-nucleating bacterium of Antarctic origin and its ice nucleation properties, *Cryobiology*, 38, 131–139, 1999. 12592

Peter, T., Marcolli, C., Spichtinger, P., Corti, T., Baker, M., and Koop, T.: When dry air is too humid, *Science*, 314, 1399–1402, doi:10.1126/science.1135199, 2006. 12536

5 Petters, M. D., Parsons, M. T., Prenni, A. J., DeMott, P. J., Kreidenweis, S. M., Carriço, C. M., Sullivan, A. P., McMeeking, G. R., Levin, E., Wold, C. E., Collett Jr., J. L., and Moosmüller, H.: Ice nuclei emissions from biomass burning, *J. Geophys. Res.*, 114, L06808, doi:10.1029/2008JD011532, 2009. 12540, 12594

10 Phillips, V. T. J., DeMott, P. J., and Andronache, C.: An empirical parameterization of heterogeneous ice nucleation for multiple chemical species of aerosol, *J. Atmos. Sci.*, 65, 2757–2783, 2008. 12553, 12554, 12556, 12596, 12615, 12618

15 Phillips, V. T. J., Andronache, C., Christner, B., Morris, C. E., Sands, D. C., Bansemer, A., Lauer, A., McNaughton, C., and Seman, C.: Potential impacts from biological aerosols on ensembles of continental clouds simulated numerically, *Biogeosciences*, 6, 987–1014, doi:10.5194/bg-6-987-2009, 2009. 12533

Pinti, V., Marcolli, C., Zobrist, B., Hoyle, C. R., and Peter, T.: Ice nucleation efficiency of clay minerals in the immersion mode, *Atmos. Chem. Phys. Discuss.*, 12, 3213–3261, doi:10.5194/acpd-12-3213-2012, 2012. 12542, 12546, 12547, 12548, 12587, 12604, 12605, 20 12609

Pitter, R. L. and Pruppacher, H. R.: A wind tunnel investigation of freezing of small water drops falling at terminal velocity in air, *Q. J. Roy. Meteor. Soc.*, 99, 540–550, 1973. 12541, 12587, 12604

25 Popovicheva, O., Kireeva, E., Persiantseva, N., Khokhlova, T., Shonija, N., Tishkova, V., and Demirdjian, B.: Effect of soot on immersion freezing of water and possible atmospheric implications, *Atmos. Res.*, 90, 326–337, 2008. 12538, 12589

Pouleur, S., Richard, C., Martin, J.-G., and Antoun, H.: Ice nucleation activity in *Fusarium acuminatum* and *Fusarium avenaceum*, *Appl. Environ. Microb.*, 58, 2960–2964, 1992. 12592

30 Prenni, A. J., DeMott, P. J., Kreidenweis, S. M., Sherman, D. E., Russell, L. M., and Ming, Y.: The effects of low molecular weight dicarboxylic acids on cloud formation, *J. Phys. Chem. A*, 105, 11240–11248, doi:10.1021/jp012427d, 2001. 12540, 12594

Prenni, A. J., Petters, M. D., Faulhaber, A., Carriço, C. M., Ziemann, P. J., Kreidenweis, S. M., and DeMott, P. J.: Heterogeneous ice nucleation measurements of secondary

## Laboratory ice nucleation experiments

C. Hoose and O. Möhler

[Title Page](#)

[Abstract](#)

[Introduction](#)

[Conclusions](#)

[References](#)

[Tables](#)

[Figures](#)

◀

▶

◀

▶

[Back](#)

[Close](#)

[Full Screen / Esc](#)

[Printer-friendly Version](#)

[Interactive Discussion](#)



## Laboratory ice nucleation experiments

C. Hoose and O. Möhler

[Title Page](#)

[Abstract](#)

[Introduction](#)

[Conclusions](#)

[References](#)

[Tables](#)

[Figures](#)

◀

▶

◀

▶

[Back](#)

[Close](#)

[Full Screen / Esc](#)

[Printer-friendly Version](#)

[Interactive Discussion](#)



- Schuttlefield, J. D., Cox, D., and Grassian, V. H.: An investigation of water uptake on clays minerals using ATR-FTIR spectroscopy coupled with quartz crystal microbalance measurements, *J. Geophys. Res.*, 112, D20201, doi:10.1029/2007JD008973, 2007. 12558
- Seifert, P., Ansmann, A., Mattis, I., Wandinger, U., Tesche, M., Engelmann, R., Müller, D., Pérez, C., and Haustein, K.: Saharan dust and heterogeneous ice formation: Eleven years of cloud observations at a central European EARLINET site, *J. Geophys. Res.*, 115, D12204, doi:10.1029/2009JD013222, 2010. 12536
- Seisel, S., Pashkova, A., Lian, Y., and Zellner, R.: Water uptake on mineral dust and soot: A fundamental view of the hydrophilicity of atmospheric particles?, *Faraday Discuss.*, 130, 437–451, doi:10.1039/b417449f, 2005. 12565
- Shilling, J. E., Fortin, T. J., and Tolbert, M. A.: Depositional ice nucleation on crystalline organic and inorganic solids, *J. Geophys. Res.*, 111, D05207, doi:10.1029/2005JD006664, 2006. 12540, 12593, 12594
- Spichtinger, P. and Gierens, K. M.: Modelling of cirrus clouds – Part 2: Competition of different nucleation mechanisms, *Atmos. Chem. Phys.*, 9, 2319–2334, doi:10.5194/acp-9-2319-2009, 2009. 12536
- Steinke, I., Möhler, O., Kiselev, A., Niemand, M., Saathoff, H., Schnaiter, M., Skrotzki, J., Hoose, C., and Leisner, T.: Ice nucleation properties of fine ash particles from the Eyjafjallajökull eruption in April 2010, *Atmos. Chem. Phys.*, 11, 12945–12958, doi:10.5194/acp-11-12945-2011, 2011. 12540, 12546, 12553
- Storelvmo, T., Kristjánsson, J. E., and Lohmann, U.: Aerosol influence on mixed-phase clouds in CAM-Oslo, *J. Atmos. Sci.*, 65, 3214–3230, 2008. 12541
- Storelvmo, T., Hoose, C., and Eriksson, P.: Global modeling of mixed-phase clouds: The albedo and lifetime effects of aerosols, *J. Geophys. Res.*, 116, D03205, doi:10.1029/2010JD014724, 2011. 12533
- Sullivan, R. C., Miñambres, L., DeMott, P. J., Prenni, A. J., Carrico, C. M., Levin, E. J. T., and Kreidenweis, S. M.: Chemical processing does not always impair heterogeneous ice nucleation of mineral dust particles, *Geophys. Res. Lett.*, 37, L24805, doi:10.1029/2010GL045540, 2010a. 12544, 12587, 12595
- Sullivan, R. C., Petters, M. D., DeMott, P. J., Kreidenweis, S. M., Wex, H., Niedermeier, D., Hartmann, S., Clauss, T., Stratmann, F., Reitz, P., Schneider, J., and Sierau, B.: Irreversible loss of ice nucleation active sites in mineral dust particles caused by sulphuric acid condensation, *Atmos. Chem. Phys.*, 10, 11471–11487, doi:10.5194/acp-10-11471-2010, 2010b. 12595

<a href="#">Title Page</a>	
<a href="#">Abstract</a>	<a href="#">Introduction</a>
<a href="#">Conclusions</a>	<a href="#">References</a>
<a href="#">Tables</a>	<a href="#">Figures</a>
<a href="#"></a>	<a href="#"></a>
<a href="#"></a>	<a href="#"></a>
<a href="#">Back</a>	<a href="#">Close</a>
<a href="#">Full Screen / Esc</a>	
<a href="#">Printer-friendly Version</a>	
<a href="#">Interactive Discussion</a>	



## Laboratory ice nucleation experiments

C. Hoose and O. Möhler

[Title Page](#)

[Abstract](#)

[Introduction](#)

[Conclusions](#)

[References](#)

[Tables](#)

[Figures](#)

◀

▶

◀

▶

[Back](#)

[Close](#)

[Full Screen / Esc](#)

[Printer-friendly Version](#)

[Interactive Discussion](#)



## Laboratory ice nucleation experiments

C. Hoose and O. Möhler

- Wheeler, M. J. and Bertram, A. K.: Deposition nucleation on mineral dust particles: a case against classical nucleation theory with the assumption of a single contact angle, *Atmos. Chem. Phys.*, 12, 1189–1201, doi:10.5194/acp-12-1189-2012, 2012. 12556, 12587
- 5 Wise, M. E., Baustian, K. J., and Tolbert, M. A.: Laboratory studies of ice formation pathways from ammonium sulfate particles, *Atmos. Chem. Phys.*, 9, 1639–1646, doi:10.5194/acp-9-1639-2009, 2009. 12593
- Wise, M. E., Baustian, K. J., and Tolbert, M. A.: Internally mixed sulfate and organic particles as potential ice nuclei in the tropical tropopause region, *P. Natl. Acad. Sci. USA*, 107, 6693–6698, 2010. 12593, 12594
- 10 Wise, M. E., Baustian, K. J., Koop, T., Freedman, M. A., Jensen, E. J., and Tolbert, M. A.: Depositional ice nucleation onto crystalline hydrated NaCl particles: a new mechanism for ice formation in the troposphere, *Atmos. Chem. Phys.*, 12, 1121–1134, doi:10.5194/acp-12-1121-2012, 2012. 12540
- Wood, S. E., Baker, M. B., and Swanson, B. D.: Instrument for studies of homogeneous and heterogeneous ice nucleation in free-falling supercooled water droplets, *Rev. Sci. Instrum.*, 73, 3988–3996, 2002. 12592
- 15 Worland, M. R. and Block, W.: Ice-nucleating bacteria from the guts of two sub-Antarctic beetles *Hydromedion sparsutum* and *Perimylops antarcticus* (Perimylopidae), *Cryobiology*, 38, 60–67, 1999. 12592
- Yankovsky, S. A., Levin, Z., Bertold, T., and Sanderman, N.: Some basic characteristics of bacterial freezing nuclei, *J. Appl. Meteorol.*, 20, 1013–1019, 1981. 12592
- 20 Young, K. C.: A numerical simulation of wintertime, orographic precipitation: Part I. Description of model microphysics and numerical techniques, *J. Atmos. Sci.*, 31, 1735–1748, 1974. 12533
- Zimmermann, F., Weinbruch, S., Schütz, L., Hofmann, H., Ebert, M., Kandler, K., and Worringer, A.: Ice nucleation properties of the most abundant mineral dust phases, *J. Geophys. Res.*, 113, D23204, doi:10.1029/2008JD010655, 2008. 12541, 12542, 12546, 12547, 12587, 12604, 12605
- 25 Zobrist, B., Marcolli, C., Koop, T., Luo, B. P., Murphy, D. M., Lohmann, U., Zardini, A. A., Krieger, U. K., Corti, T., Cziczo, D. J., Fueglistaler, S., Hudson, P. K., Thomson, D. S., and Peter, T.: Oxalic acid as a heterogeneous ice nucleus in the upper troposphere and its indirect aerosol effect, *Atmos. Chem. Phys.*, 6, 3115–3129, doi:10.5194/acp-6-3115-2006, 2006. 12540, 12594

- Zobrist, B., Koop, T., Luo, B. P., Marcolli, C., and Peter, T.: Heterogeneous ice nucleation rate coefficient of water droplets coated by a nonadecanol monolayer, *J. Phys. Chem. C*, 111, 2149–2155, doi:10.1021/jp066080w, 2007. 12555, 12561, 12562, 12563, 12596, 12616
- 5 Zobrist, B., Marcolli, C., Peter, T., and Koop, T.: Heterogeneous ice nucleation in aqueous solutions: the role of water activity, *J. Phys. Chem. A*, 112, 3965–3975, doi:10.1021/jp7112208, 2008. 12595
- Zuberi, B., Bertram, A. K., Koop, T., Molina, L. T., and Molina, M. J.: Heterogeneous freezing of aqueous particles induced by crystallized  $(\text{NH}_4)_2\text{SO}_4$ , ice, and letovicite, *J. Phys. Chem. A*, 105, 6458–6464, 2001. 12593
- 10 Zuberi, B., Bertram, A. K., Cassa, C. A., Molina, L. T., and Molina, M. J.: Heterogeneous nucleation of ice in  $(\text{NH}_4)_2\text{SO}_4-\text{H}_2\text{O}$  particles with mineral dust immersions, *Geophys. Res. Lett.*, 29, 1504, doi:10.1029/2001GL014289, 2002. 12541, 12595, 12604

## Laboratory ice nucleation experiments

C. Hoose and O. Möhler

[Title Page](#)

[Abstract](#)

[Introduction](#)

[Conclusions](#)

[References](#)

[Tables](#)

[Figures](#)

◀

▶

◀

▶

[Back](#)

[Close](#)

[Full Screen / Esc](#)

[Printer-friendly Version](#)

[Interactive Discussion](#)



Reference	material	type of instrument	name of instrument or institution	nucleation mode	size	activated fraction	residence time/cooling rate
Archuleta et al. (2005)	Asian dust	CFDC-C	CSU	deposition and condensation	50, 100 and 200 nm	1 %	10 to 13 s
Bailey and Hallett (2002)	kaolinite	TGDC/CECC	DRI	deposition and condensation	5 to 10 $\mu\text{m}$ and smaller	$\approx 0.1 \%$	$200 \text{s K}^{-1}$
Broadley et al. (2012)	illite	CS	ULeeds	immersion	specific surface area given	0–100 %	$6 \text{ to } 75 \text{s K}^{-1}$
Bundke et al. (2008)	ATD, kaolinite	CFMC	FINCH	deposition and condensation	n. a.	relative to maximum value	4.5 s
Bundke et al. (2008)	kaolinite, illite	ISDC	FRIDGE	deposition and condensation	n. a.	relative to maximum value	$\approx 90 \text{s}$
Connolly et al. (2009)	ATD, Asian dust, Saharan dust	CECC	AIDA	deposition and immersion	mode diameters of 0.3 to 0.5 $\mu\text{m}$	INAS density	20 to 60 $\text{s K}^{-1}$
Chernoff and Bertram (2010)	kaolinite, illite, montmorillonite, quartz	CS-FDC	UBC	deposition and condensation	mean diameters 5.8 to 10.3 $\mu\text{m}$	0.1 to 1 %	$600 \text{s K}^{-1}$
Conen et al. (2011)	montmorillonite and 3 soil dusts from Europe and Asia	DFA	UBasel	immersion	< 15 $\mu\text{m}$	n. a. (IN per dust mass given)	$180 \text{s K}^{-1}$
Cziczo et al. (2009a)	ATD and illite	CECC	AIDA	deposition and immersion	< 1 $\mu\text{m}$	1 %	corresponding to a vertical velocity of about 0.1 to 2 $\text{ms}^{-1}$
Cziczo et al. (2009b)	kaolinite, undoped and doped with lead	CFDC-P	ZINC	deposition	200 nm	n. a.	10 to 30 s
Dymarska et al. (2006)	kaolinite	CS-FDC	UBC	deposition and condensation	majority between 1 and 20 $\mu\text{m}$	$\approx 0.1 \text{ to } 0.5 \%$	$600 \text{s K}^{-1}$
Eastwood et al. (2008)	kaolinite, montmorillonite, quartz, calcite, muscovite	CS-FDC	UBC	deposition and condensation	mostly 1 to 20 $\mu\text{m}$ , mean sizes 7.7 to 14.2 $\mu\text{m}$	0.1 to 1 %	10 s (1 to 20 s)
Field et al. (2006)	Asian and Saharan dust	CECC	AIDA	deposition and condensation	mode diameter: 0.4 $\mu\text{m}$	0.5 % and 8 %	20 to 60 $\text{s K}^{-1}$
Friedman et al. (2011)	kaolinite	CFDC-P	PNNL-CIC	deposition and condensation	100, 200 and 400 nm	1 %	12 s
Hoffer (1961)	kaolinite, montmorillonite, illite, halloysite	EDF	UChicago	immersion	n. a.	n. a.	$60 \text{s K}^{-1}$
Hoyle et al. (2011)	ATD	CFDC-P	IMCA/ZINC	immersion	800 nm	spectra	12 s
Hung et al. (2003)	hematite and corundum	AFT	Harvard	immersion	50–250 nm	1.e-6	60 s



**Table 1.** Continued.

Reference	material	type of instrument	name of instrument or institution	nucleation mode	size	activated fraction	residence time/cooling rate
Iraci et al. (2010)	ATD and clay sample collected in Sedona (Arizona)	CS-SDC	NASA Ames	deposition	ATD volume mean: 5 µm, ATD number median: 1.2 µm, Sedona clay number median: 1.4 µm	n. a.	n. a.
Isono et al. (1959a)	quartz, loess	CC	Bigg IN counter, UTokyo	n. a.	1 to 10 µm	$10^{-6}$ to $10^{-3}$	n. a.
Isono et al. (1959b)	quartz	CC	Bigg IN counter, UTokyo	n. a.	n. a.	n. a.	n. a.
Isono and Ibeke (1960)	Japanese sand, Chinese loess, kaolinite, quartz and fifteen other minerals	CC	Bigg IN counter, UTokyo	n. a.	< 30 µm, most particles < 5 µm	$10^{-6}$ to $10^{-3}$	n. a.
Jones et al. (2011)	ATD, Saharan dust	CFDC-C	CSU and MINC	deposition/condensation	mostly < 1 µm	spectra; 0.01 %	≈ 10 s
Kanji and Abbatt (2006)	Saharan dust, montmorillonite, silica, alumina	CS-FDC	UToronto	deposition and condensation	0.5 to 5 µm	≈ $10^{-4}$	6 s per 1 % change in RH <sub>i</sub>
Kanji et al. (2008)	ATD, Saharan dust, kaolinite, montmorillonite, silica	CS-FDC	UToronto	deposition and condensation	ATD: 0–5 µm, silica: 1.5 µm, others n. a., surface area determined	≥ $10^{-5}$	6 s per 1 % change in RH <sub>i</sub>
Kanji and Abbatt (2010)	ATD	CFDC-P	UToronto	deposition and condensation	40, 100, 240 nm	0.1%, 1%, INAS densities	9–11 s
Kanji et al. (2011)	ATD, Saharan, Canary Island and Israel dust	CFDC-P	UToronto	deposition and condensation	size ranges between 0.02 and 3 µm, number modes between 0.15 and 0.3 µm	0.1 %	9–11 s
Knopf and Koop (2006)	ATD	CS-SDC	ETHZ	deposition and condensation	0.7–10 µm	5 %	3–30 s per 1 % change in RH <sub>i</sub>
Knopf et al. (2010)	kaolinite	CS-FDC	Stony Brook U	deposition	mean size 4.1–5.0 µm	0.02–0.8 %	600 s K <sup>-1</sup>
Koehler et al. (2007)	Owens lake dust	CFDC-C	CSU	deposition and condensation	100, 200, 300 and 400 nm	1 % (aircraft unit), 5 % (laboratory unit)	4 s (aircraft unit) and 11 s (laboratory unit)
Koehler et al. (2010)	ATD, Saharan and Canary Island dust	CFDC-C	CSU	deposition and condensation	200, 300 and 400 nm	1 % (ATD), 5 % (others)	4 s (aircraft unit) and 11 s (laboratory unit)

## Laboratory ice nucleation experiments

C. Hoose and O. Möhler

[Title Page](#)

[Abstract](#)

[Introduction](#)

[Conclusions](#)

[References](#)

[Tables](#)

[Figures](#)



[Full Screen / Esc](#)

[Printer-friendly Version](#)

[Interactive Discussion](#)



**Table 1.** Continued.

Reference	material	type of instrument	name of instrument or institution	nucleation mode	size	activated fraction	residence time/cooling rate
Koop and Zobrist (2009)	ATD	DSC	UBielefeld/ETHZ	immersion	median diameter: 0.35 µm	n. a.	6 s K <sup>-1</sup>
Kulkarni et al. (2009)	Saharan dust (Nigeria)	TGDC	ULeeds	deposition	< 38 µm	≈ 1/8	60 s
Kulkarni and Dobbie (2010)	Spain, Dakar and Nigeria dust	TGDC	ULeeds	deposition and condensation	< 38 µm	≈ 1/10	≈ 40 to 550 s
Kulkarni et al. (2012)	ATD and kaolinite	CFDC-P	PNNL-CIC	deposition	100, 300, 400 and 500 nm	10 <sup>-4</sup> to 10 <sup>-1</sup>	n. a.
Ladino et al. (2011)	kaolinite	FDNC	CLINCH	contact	400 and 800 nm	spectra	n. a.
Lüönd et al. (2010)	kaolinite	CFDC-P	IMCA	immersion	200, 400 and 800 nm	0–100 % (spectra)	14 s
Mangold et al. (2005)	ATD	CECC	AIDA	deposition	0.1 to 1.5 µm, count median diameter ≈ 0.5 µm	n. a. for onset, maximum value: 97 %	20 to 45 s K <sup>-1</sup>
Marcolli et al. (2007)	ATD	DSC	ETHZ	immersion	fine ATD: nominal 0–3 µm, coarse ATD: nominal 0–7 µm, size distributions measured	n. a.	60 s K <sup>-1</sup>
Mason and Maybank (1958)	kaolinite, montmorillonite, and 28 more	DMCC	Imperial College	deposition, condensation and contact?	ground material, submicron and supermicron	roughly 0.01%	120 s
Mason (1960)	kaolinite, montmorillonite, illite and seven more	DMCC	Imperial College	deposition, condensation and contact?	ground material, large submicron number fraction	roughly 0.01 %	120 s
Möhler et al. (2006)	ATD, Asian and Saharan dust	CECC	AIDA	deposition and condensation	median: 350–400 nm, specific surface area given	onset, 8 %	≥ 15 s K <sup>-1</sup> , dS <sub>d</sub> /dt available
Murray et al. (2010a)	kaolinite, montmorillonite	CS	ULeeds	immersion	specific surface area given	0–100 %	6 s K <sup>-1</sup>
Murray et al. (2011)	kaolinite	CS	ULeeds	immersion	specific surface area given	0–100 %	6 to 75 s K <sup>-1</sup>
Niedermeier et al. (2010)	ATD	LFT	LACIS	immersion	300 nm, INAS density given	(spectra)	1.6 s
Niedermeier et al. (2011a)	ATD	LFT	LACIS	immersion	300 nm	(spectra)	n. a.
Niemand et al. (2012)	ATD, Asian, Saharan, Canary Island and Israel dust	CECC	AIDA	immersion	number median $d = 0.2\text{--}1 \mu\text{m}$		

## Laboratory ice nucleation experiments

C. Hoose and O. Möhler

[Title Page](#)

[Abstract](#)

[Introduction](#)

[Conclusions](#)

[References](#)

[Tables](#)

[Figures](#)



[Full Screen / Esc](#)

[Printer-friendly Version](#)

[Interactive Discussion](#)



**Table 1.** Continued.

Reference	material	type of instrument	name of instrument or institution	nucleation mode	size	activated fraction	residence time/cooling rate
Pinti et al. (2012)	kaolinite, montmorillonite, illite and Saharan dust	DSC	ETHZ	immersion	number mode 0.29–0.45 µm	n. a.	n. a.
Pitter and Pruppacher (1973)	kaolinite, montmorillonite	VWT	UCLA	immersion and contact	$d = 0.1\text{--}30\,\mu\text{m}$ , mode between 1 and 2 µm	n. a.	n. a.
Pruppacher and Saenger (1955)	clay, olivine, tremolite, quartz, diatomite, and others	CC	ETHZ	unknown	0.5–2 µm	n.a.	≈ 5 to 30 s
Roberts and Hallett (1968)	kaolinite, montmorillonite, calcite, gypsum, biotite mica	CS-SDC	Imperial College	condensation	0.5 to 3 µm	0.01 to 100 % (spectra)	n. a.
Salam et al. (2006)	kaolinite, montmorillonite	CFDC-C	UDalhousie	deposition and condensation	< 0.5 to ≈ 5 µm	n. a.	20 to 30 s
Schaefer (1949)	various soil, loam and clay samples	CC	General Electrics	n. a.	n. a.	n. a.	n. a.
Schaller and Fukuta (1979)	kaolinite, local soil	wedge-shaped TGDC	UDenver	deposition and condensation	n. a.	1.3 %	60 s
Sullivan et al. (2010a)	ATD	CFDC-C	CSU	deposition and condensation	200 nm	spectra	n. a.
Svensson et al. (2009)	kaolinite	EDBC	UGothenburg	contact	0.2–5 µm	0–1	n. a.
Wang and Knopf (2011)	kaolinite	CS-FDC	Stony Brook U	deposition	mean size 2.3–4.3 µm	0.01–0.3 %	60 s per 2.3 % to 1.5 % change in RH <sub>i</sub> , 12 s between subsequent observations
Welti et al. (2009)	ATD, kaolinite, montmorillonite, illite	CFDC-P	ZINC	deposition and condensation	100, 200, 400 and 800 nm	1 %	12 s
Wheeler and Bertram (2012)	kaolinite, illite	CS-FDC	UBC	deposition	average diameters: kaolinite 8 µm, illite 11 µm	1 %	600 s K <sup>-1</sup> , 60 s per 1 % change in RH <sub>i</sub>
Zimmermann et al. (2008)	kaolinite, montmorillonite, illite and 6 more	ESEM	UDarmstadt	deposition (and condensation)	1–100 µm	≈ 1 % and 2–3 %	n. a.

## Laboratory ice nucleation experiments

C. Hoose and O. Möhler

[Title Page](#)

[Abstract](#)

[Introduction](#)

[Conclusions](#)

[References](#)

[Tables](#)

[Figures](#)

◀

▶

◀

▶

[Back](#)

[Close](#)

[Full Screen / Esc](#)

[Printer-friendly Version](#)

[Interactive Discussion](#)



**Table 2.** Laboratory experiments with soot particles.

Reference	material	type of instrument	name of instrument or institution	nucleation mode	size	activated fraction	residence time
Crawford et al. (2011)	CAST and mini-CAST propane soot with different OC content	CECC	AIDA	deposition	modal diameter $0.3\text{ }\mu\text{m}$	0.1 and 1 %	$24 \text{ to } 86\text{ s K}^{-1}$
Demirdjian et al. (2009)	aviation kerosene flame soot	CS	CINaM	deposition	bulk sample	n. a.	n. a.
DeMott (1990)	acetylene burner soot	CECC	CSU	immersion	0.08 and $0.12\text{ }\mu\text{m}$	0.1 to 3 %	$30\text{ s K}^{-1}$ , $60\text{ s K}^{-1}$
DeMott et al. (1999)	Degussa lamp black soot	CFDC-C	CSU	deposition	number mean $d = 240\text{ nm}$ , $\sigma = 1.6$	1, 10, 100 %	11–15 s
Diehl and Mitra (1998)	kerosine burner exhaust	VWT	UMainz	immersion and contact	initially 0.1 to $0.12\text{ }\mu\text{m}$ , aggregates up to $1\text{ }\mu\text{m}$	n. a.	n. a.
Dymarska et al. (2006)	n-hexane soot, lamp black, furnace black, channel black	CS-FDC	UBC	deposition/condensation	1 to $20\text{ }\mu\text{m}$	n. a.	$600\text{ s K}^{-1}$ , images every 10 s; one experiment: 8 h at constant $S_{ice}$ and $T$
Fornea et al. (2009)	carbon lamp black	CS	TAMU	contact	250 to $300\text{ }\mu\text{m}$	0 to 1	$60\text{ s K}^{-1}$
Friedman et al. (2011)	CAST propane soot with low OC content, uncoated and coated	CFDC-P	PNNL-CIC	deposition/condensation	100, 200, 400 nm	1 %, spectra (ice/droplet discrimination not possible)	12 s
Gorbunov et al. (2001)	soot produced from a thermal decomposition aerosol generator and a benzene/toluene combustion generator	DMCC	Urban Pollution Research Centre, London	deposition/condensation/contact?	mean diameter $0.02 \text{ to } 2\text{ }\mu\text{m}$	$10^{-8} \text{ to } 50\text{ %}$	20 min
Kanji and Abbatt (2006)	n-hexane soot	CS-FDC	UToronto	deposition	$0.5\text{--}5\text{ }\mu\text{m}$	$10^{-5}$	$40\text{--}60\text{ s K}^{-1}$ , 6 s per 1 % change in $RH_i$
Kanji et al. (2011)	graphite spark generator soot	CFDC-C and CECC	UToronto, CSU, AIDA	deposition/condensation	0.02 to $0.45\text{ }\mu\text{m}$ , number mode= $0.15\text{ }\mu\text{m}$	0.1 %	9 s (UT-CFDC), 4–5 s (CSU-CFDC), $30\text{--}60\text{ s K}^{-1}$ (AIDA)

## Laboratory ice nucleation experiments

C. Hoose and O. Möhler

[Title Page](#)

[Abstract](#)

[Introduction](#)

[Conclusions](#)

[References](#)

[Tables](#)

[Figures](#)



[Back](#)

[Close](#)

[Full Screen / Esc](#)

[Printer-friendly Version](#)

[Interactive Discussion](#)



**Table 2.** Continued.

Reference	material	type of instrument	name of instrument or institution	nucleation mode	size	activated fraction	residence time
Kireeva et al. (2009)	lamp black, furnace black, and more soot types from different combustion sources, some modified with organic substances	CS	UMoscow	immersion	n. a.	n. a. (numerous particles per droplet)	$40\text{ s K}^{-1}$
Koehler et al. (2009)	soot	CFDC-C	CSU	deposition/condensation	100, 200 and 250 nm	spectra, $\approx 10^{-4}\text{--}10^{-2}$ before homogeneous freezing	11 s
Möhler et al. (2005b)	CAST soot with different OC content	CECC	AIDA	deposition	CS16 soot: mean $d = 220\text{ nm}$ , CS40 soot: mean $d = 110\text{ nm}$	n. a. for CS16, < 1% for CS40	15 to $600\text{ s K}^{-1}$
Möhler et al. (2005a)	graphite spark generator soot	CECC	AIDA	deposition	count median diameters: 70 to 140 nm	$\leq 0.3\%$	17 to $100\text{ s K}^{-1}$
Popovicheva et al. (2008)	graphite spark generator soot lamp black, furnace black, channel black, and soot from different combustion sources	CS	UMoscow	immersion	0.01 to $0.25\text{ }\mu\text{m}$ , depending on soot type	n. a. (numerous particles per droplet)	$40\text{ s K}^{-1}$
Suzanne et al. (2003)	kerosene soot	CS	CINaM	deposition	bulk sample	n. a.	n. a.
Tishkova et al. (2011)	aircraft engine combustor soot	CS	CINaM	deposition	bulk sample	n. a.	n. a.

## Laboratory ice nucleation experiments

C. Hoose and O. Möhler

[Title Page](#)

[Abstract](#)

[Introduction](#)

[Conclusions](#)

[References](#)

[Tables](#)

[Figures](#)

◀

▶

◀

▶

[Back](#)

[Close](#)

[Full Screen / Esc](#)

[Printer-friendly Version](#)

[Interactive Discussion](#)



**Table 3.** Laboratory experiments with bioaerosols.

Reference	material	type of instrument	name of instrument or institution	nucleation mode	size	activated fraction	residence time/cooling rate
Ahern et al. (2007)	<i>Pseudomonas</i> isolates from cloud- and rainwater	DSC	UEastLondon	immersion	n. a.	n. a.	$60\text{ s K}^{-1}$
Chernoff and Bertram (2010)	Snowmax™	CS-FDC	UBC	deposition and condensation	mean diameters: 5.8 and 15.9 $\mu\text{m}$ (two different nebulizers)	0.1 to 1 %	$600\text{ s K}^{-1}$
Constantinidou et al. (1990)	<i>Pseudomonas syringae</i> isolated from air and rain-water	DFA	UWisconsin	immersion	n. a.	n. a.	n. a.
Diehl et al. (2001)	Pine, birch, oak and grass pollens	CS-FDC and ISDC	UMainz	deposition and condensation	20–70 $\mu\text{m}$	0–1 (spectra)	several minutes for deposition nucleation; < 1 min for condensation nucleation
Diehl et al. (2002)	Pine, birch, oak and grass pollens	VWT	UMainz	immersion and contact	25–70 $\mu\text{m}$	n. a.	n. a.
Gross et al. (1983)	<i>Pseudomonas syringae</i> , different strains	DFA	Washington State U	immersion	n. a.	$10^{-7}$ to 0.0043	120 s
Hirano et al. (1985)	ice nucleation active bacteria on oat leaves	FA	UWisconsin	immersion	n. a.	$10^{-7}$ to 0.008	n. a.
Iannone et al. (2011)	<i>Cladosporium</i> spores	CS-FDC	UBC	immersion	average diameter: 3.2 $\mu\text{m}$	0.002 to 1	$12\text{ s K}^{-1}$
Jayaweera and Flanagan (1982)	<i>Pseudomonas</i> species, unidentified microbacteria, <i>Penicillium digitatum</i> , <i>Cladosporium herbarum</i> , <i>Penicillium notatum</i> , <i>Penicillium frequentes</i> and <i>Rhizopus stolonifera</i> spores isolated from air	DFA	UAlaska	immersion	bacterial cells: average length 0.2–1.1 $\mu\text{m}$	1 % for spores, 5–10 % for bacteria	n. a.
Junge and Swanson (2008)	Arctic and Antarctic sea-ice bacterial isolates	FDNC	UWashington	immersion	n. a.	n. a.	n. a.

## Laboratory ice nucleation experiments

C. Hoose and O. Möhler

[Title Page](#)

[Abstract](#)

[Introduction](#)

[Conclusions](#)

[References](#)

[Tables](#)

[Figures](#)

◀

▶

◀

▶

[Back](#)

[Close](#)

[Full Screen / Esc](#)

[Printer-friendly Version](#)

[Interactive Discussion](#)



**Table 3.** Continued.

Reference	material	type of instrument	name of instrument or institution	nucleation mode	size	activated fraction	residence time/cooling rate
Kanji et al. (2011)	<i>Pseudomonas syringae</i> Snomax™ and	CFDC-P	UToronto	deposition and condensation	size ranges between 0.04 and 2 µm, number modes at 0.1 and 0.7 µm	0.1 %	9–11 s
Koop and Zobrist (2009)	Snomax™, insects and larvae	DSC	UBielefeld/ETHZ	immersion	n. a.	n. a.	$6\text{ s K}^{-1}$
Levin and Yankofsky (1983)	M1 bacteria	VWT	UCLA	immersion and contact	n. a.	n. a.	$\leq 240\text{ s}$
Lindemann et al. (1982)	<i>Pseudomonas syringae</i> and <i>Erwinia herbicola</i> isolated from air	FA	UWisconsin	immersion	n. a.	n. a.	n. a.
Lindow et al. (1989)	<i>Pseudomonas syringae</i> strain 31R1	DFA		immersion	n. a.	$10^{-8}$	n. a.
Maki et al. (1974)	<i>Pseudomonas syringae</i>	DFA	freezing nucleus spectrometer	immersion	n. a.	$10^{-8}$ to 0.01	n. a.
Maki and Willoughby (1978)	<i>Pseudomonas fluorescens</i> isolated from leaves, lake/stream water and/or snow	DFA and DMCC	UWyoming and CSU	immersion	$1\text{ }\mu\text{m} \times 3\text{--}5\text{ }\mu\text{m}$	2 % to 94 %	n. a.
Möhler et al. (2008b)	<i>Pseudomonas syringae</i> , <i>Pseudomonas viridisflava</i> , <i>Erwinia herbicola</i> and Snomax™	CECC	AIDA	immersion and condensation	median diameter of bacterial cells: 0.6–0.8 µm	0.07 % to 23 %	immersion freezing: a few seconds to a few minutes; condensation freezing: $\approx 80\text{ s K}^{-1}$
Morris et al. (2008)	<i>Pseudomonas syringae</i> isolated from rain, snow, alpine streams, lakes and wild plants	DFA	INRA	immersion	n. a.	$10^{-7}$	n. a.
Mortazavi et al. (2008)	<i>Microbacterium</i> , <i>Xanthomonas</i> , <i>Bacillus</i> , <i>Acinetobacter</i> , <i>Luteimonas</i> , <i>Stenotrophomonas</i> and unspecified bacteria isolated from snow	DFA	McGill U	immersion	n. a.	n. a.	$60\text{ s K}^{-1}$

## Laboratory ice nucleation experiments

C. Hoose and O. Möhler

[Title Page](#)

[Abstract](#)

[Introduction](#)

[Conclusions](#)

[References](#)

[Tables](#)

[Figures](#)

◀

▶

◀

▶

[Back](#)

[Close](#)

[Full Screen / Esc](#)

[Printer-friendly Version](#)

[Interactive Discussion](#)



## Laboratory ice nucleation experiments

C. Hoose and O. Möhler

**Table 3.** Continued.

Reference	material	type of instrument	name of instrument or institution	nucleation mode	size	activated fraction	residence time/cooling rate
Obata et al. (1999)	<i>Pseudomonas antarctica</i>	FA	Kansai U	immersion	n. a.	$10^{-7}$ to 0.2	$60\text{s K}^{-1}$
Pouleur et al. (1992)	<i>Fusarium avanaceum</i> , <i>Fusarium acuminatum</i>	DFA	ULaval Québec	immersion	n. a.	n. a.	$200\text{s K}^{-1}$
Pummer et al. (2012)	15 different pollen species, Snomax™	EDF	TU Wien	immersion	13–65 µm	n. a.	$30\text{--}60\text{s K}^{-1}$
Sands et al. (1982)	<i>Pseudomonas syringae</i> isolated from rain and hail	n. a.	Montana State U	immersion	n. a.	n. a.	n. a.
Vali et al. (1976)	<i>Pseudomonas syringae</i> , leaf litter	DFA		immersion	length of bacterial cell: 2 µm	$2 \times 10^{-6}\text{--}5 \times 10^{-5}$	n. a.
von Blohn et al. (2005)	tree and grass pollens	VWT	UMainz	immersion	26–28 µm	n. a.	n. a.
Ward and DeMott (1989)	Snomax™	IMCC and CECC	CSU	condensation and immersion	n. a.		$\approx 180\text{--}300\text{s in IMCC, } 60\text{s K}^{-1}$ in CECC
Wood et al. (2002)	Snomax™	FDNC	UWashington	immersion	< 0.2 µm (filtrate)	n. a.	n. a.
Worland and Block (1999)	<i>Pseudomonas</i> species isolated from the guts of beetles	DFA	British Antarctic Survey	immersion	n. a.	$10^{-6}$	n. a.
Yankofsky et al. (1981)	M1 bacteria	DFA	Tel Aviv U	immersion	$d \geq 0.4\mu\text{m}$	$10^{-6}$ to 0.01	n. a.

- [Title Page](#)
- [Abstract](#) | [Introduction](#)
- [Conclusions](#) | [References](#)
- [Tables](#) | [Figures](#)
- [◀](#) | [▶](#)
- [◀](#) | [▶](#)
- [Back](#) | [Close](#)
- [Full Screen / Esc](#)
- [Printer-friendly Version](#)
- [Interactive Discussion](#)



**Table 4.** Laboratory experiments with ammonium sulfate particles.

Reference	material	type of instrument	name of instrument or institution	nucleation mode	size	activated fraction	residence time
Abbatt et al. (2006)	solid ammonium sulfate	CECC, CS-FDC	AIDA, UToronto	deposition/ condensation	AIDA: diameters $\geq 40\text{--}400\text{ nm}$ , CS-FDC: typically $8\text{ }\mu\text{m}$	AIDA: 0.1 to 1 %, CS-FDC: $10^{-5}$	AIDA: n. a., CS-FDC: 6 s per 1 % change in $\text{RH}_i$
Baustian et al. (2010)	solid ammonium sulfate	CS-FDC	CIRES	deposition/ condensation	0.5 to $10\text{ }\mu\text{m}$ , mean: $2.1\text{ }\mu\text{m}$	$\approx 0.1\%$	n.a.
Chen et al. (2000)	solid and liquid ammonium sulfate and letovicite	CFDC-C	CSU	homogeneous, no heterogeneous nucleation observed	0.05 and $0.2\text{ }\mu\text{m}$	0.1, 1 and 10 %	12 s
Mangold et al. (2005)	ammonium sulfate particles, majority in liquid phase, but possibly some effloresced particles present	CECC	AIDA	deposition/ condensation	number median $d: 0.2\text{ to }0.3\text{ }\mu\text{m}$	n. a.	$20\text{ to }25\text{ s K}^{-1}$
Shilling et al. (2006)	solid ammonium sulfate	CS-SDC	CIRES	deposition/ condensation/ immersion	$1\text{--}10\text{ }\mu\text{m}$	$\geq 10^{-5}$	$\approx 600\text{ s}$
Wise et al. (2009)	solid ammonium sulfate	CS-FDC	CIRES	deposition/ condensation	n. a.	n. a.	n. a.
Wise et al. (2010)	solid ammonium sulfate with and without coatings of palmitic acid	CS-FDC	CIRES	deposition	$1\text{--}10\text{ }\mu\text{m}$ with typical values around $5\text{ }\mu\text{m}$	n. a.	n. a.
Zuberi et al. (2001)	solid ammonium sulfate and letovicite	CS and DSC	MIT	immersion freezing of concentrated aqueous solution droplets	droplet sizes: 5 to $55\text{ }\mu\text{m}$ , containing numerous microcrystals	n. a.	$60\text{ s K}^{-1}$

## Laboratory ice nucleation experiments

C. Hoose and O. Möhler

[Title Page](#)

[Abstract](#)

[Introduction](#)

[Conclusions](#)

[References](#)

[Tables](#)

[Figures](#)



[Back](#)

[Close](#)

[Full Screen / Esc](#)

[Printer-friendly Version](#)

[Interactive Discussion](#)



**Table 5.** Laboratory experiments with organic acids, humic-like substances and biomass burning particles.

Reference	material	type of instrument	name of instrument or institution	nucleation mode	size	activated fraction	residence time
Baustian et al. (2010)	solid glutaric acid	CS-FDC	CIRES	deposition/condensation	0.5–10 µm, mean: 2.4 µm	≈ 0.1 %	n. a.
Beaver et al. (2006)	aldehydes and ketones	LFT	CIRES	immersion freezing in sulfuric acid droplets	< 1 µm	n. a.	n. a.
DeMott et al. (2009)	biomass burning particles	CFDC-C	CSU	deposition and homogeneous	100 nm	10 <sup>-5</sup> –10 <sup>-1</sup>	15 s
Kanji et al. (2008)	leonardite, oxalic acid dihydrate, sodium humic salt, octyl-silica	CS-FDC	UToronto	deposition and condensation	size n. a., surface area determined	≥ 10 <sup>-5</sup>	6 s per 1 % change in RH <sub>i</sub>
Murray et al. (2010b)	citric acid, glassy organic acids	CECC	AIDA	unknown		10 <sup>-4</sup> –3.5 × 10 <sup>-3</sup>	≈ 36 s K <sup>-1</sup>
Prenni et al. (2001)		CFDC-C	CSU	deposition and condensation	50 and 100 nm	1 and 10 %	n. a.
Prenni et al. (2009)	secondary organic aerosol generated from ozonolysis of alkenes	CFDC-C	CSU	condensation	mode: 80–200 nm	no ice nucleation detected	n. a.
Petters et al. (2009)	biomass burning	CFDC-C	CSU	condensation	mode: 80–200 nm	10 <sup>-4</sup> –10 <sup>-2</sup>	4–5 s
Shilling et al. (2006)	maleic acid	CS-SDC	CIRES	deposition	1–10 µm	≥ 10 <sup>-5</sup>	≈ 600 s
Wagner et al. (2010)	oxalic acid dihydrate and sodium oxalate	CECC	AIDA	deposition and condensation	0.03–0.8 µm	0.1–22 %	≈ 30–100 s K <sup>-1</sup>
Wagner et al. (2011)	oxalic acid	CECC	AIDA	immersion	≥ 0.27 µm	≤ 0.18	≈ 40 s K <sup>-1</sup>
Wang and Knopf (2011)	Suwannee river standard fulvic acid (SRFA)	CS-FDC	Stony Brook U	deposition	mean: 2.0–2.4 µm	0.02 to 0.13 %	60 s per 1.5 % to 2.3 % change in RH <sub>i</sub>
Wang and Knopf (2011)	Leonardite standard humic acid	CS-FDC	Stony Brook U	deposition	mean: 1.7–3.3 µm	0.01 to 0.1 %	60 s per 1.5 % to 2.3 % change in RH <sub>i</sub>
Wise et al. (2010)	palmitic acid	CS-FDC	CIRES	deposition	1–10 µm with typical values around 5 µm	n. a.	n. a.
Zobrist et al. (2006)	phthalic, adipic, fumaric, succinic and oxalic acid	DSC	ETHZ	immersion	n. a.	n. a.	6 s K <sup>-1</sup>

## Laboratory ice nucleation experiments

C. Hoose and O. Möhler

[Title Page](#)

[Abstract](#)

[Introduction](#)

[Conclusions](#)

[References](#)

[Tables](#)

[Figures](#)



[Full Screen / Esc](#)

[Printer-friendly Version](#)

[Interactive Discussion](#)



# Laboratory ice nucleation experiments

C. Hoose and O. Möhler

Reference	material	type of instrument	name of instrument or institution	nucleation mode	coating/surface treatment
Chernoff and Bertram (2010)	illite, montmorillonite, quartz, Snomax™	CS-FDC	UBC	deposition	H <sub>2</sub> SO <sub>4</sub> and NH <sub>4</sub> HSO <sub>4</sub>
Cziczo et al. (2009a)	ATD	CECC	AIDA	deposition	ammonium sulfate, sulfuric acid
Eastwood et al. (2009)	kaolinite	CS-FDC	UBC	deposition	H <sub>2</sub> SO <sub>4</sub> and (NH <sub>4</sub> ) <sub>2</sub> SO <sub>4</sub>
Hung et al. (2003)	hematite and corundum	AFT	Harvard	immersion	aqueous ammonium sulfate
Knopf and Koop (2006)	ATD	CS-FDC	ETHZ	deposition	sulfuric acid
Koop and Zobrist (2009)	ATD and Snomax™	DSC	UBielefeld/ETHZ	immersion	ammonium sulfate, sulfuric acid, glucose, polyethylene glycol
Koehler et al. (2010)	ATD	CFDC-C	CSU	deposition and condensation	SOA
Möhler et al. (2008a)	ATD and illite	CECC	AIDA	deposition	SOA
Niedermeier et al. (2010)	ATD	LFT	LACIS	immersion	ammonium sulfate, sulfuric acid and succinic acid
Niedermeier et al. (2011a)	ATD	LFT	LACIS	immersion	sulfuric acid and sulfuric acid + ammonia
Reitz et al. (2011)	ATD	LFT	LACIS	immersion	sulfuric acid and sulfuric acid + ammonia
Salam et al. (2007)	montmorillonite	CFDC-C	UDalhousie	deposition	ammonia gas exposure
Sullivan et al. (2010b)	ATD	C-CFDC	CSU	deposition and condensation	sulfuric acid and sulfuric acid + ammonia
Sullivan et al. (2010a)	ATD	C-CFDC	CSU	deposition and condensation	nitric acid gas exposure
Zobrist et al. (2008)	ATD	DSC	ETHZ	immersion	ammonium sulfate
Zuberi et al. (2002)	kaolinite and montmorillonite	CS	MIT	immersion	aqueous ammonium sulfate
DeMott et al. (1999)	soot	CFDC-C	CSU	deposition	sulfuric acid
Möhler et al. (2005a)	soot	CECC	AIDA	deposition	sulfuric acid
Dymarska et al. (2006)	lamp black soot	CS-FDC	UBC	deposition	ozone
Wang and Knopf (2011)	humic-like substances	CS-FDC	Stony Brook U	deposition	ozone

# Laboratory ice nucleation experiments

C. Hoose and O. Möhler

symbol	description
$a_0, a_1, a_2, a_3$ [various]	constants in Eq. (A5)
$A_{\text{aer}}$ [ $\text{m}^2$ ]	aerosol surface area
$A_{\text{dep}}$ [ $\text{m}^{-2} \text{s}^{-1}$ ]	kinetic prefactor for deposition nucleation
$A_{\text{imm}}$ [ $\text{m}^{-2} \text{s}^{-1}$ ]	kinetic prefactor for immersion freezing
$e$ [Pa]	water vapor pressure
$E$ [K]	constant (892 K) (Zobrist et al., 2007)
$e_{\text{s,i}}$ [Pa]	saturation vapor pressure over ice (Murphy and Koop, 2005)
$e_{\text{s,w}}$ [Pa]	saturation vapor pressure over water (Murphy and Koop, 2005)
$f_{\text{het}}$ [\#]	form factor
$f_{\text{IN}}$ [\#]	active fraction
$\Delta F_{\text{diff}}$ [J]	energy for diffusion across the liquid-ice boundary
$\Delta g_d$ [J]	desorption energy
$\Delta G_{\text{dep}}$ [J]	energy for homogeneous germ formation in the deposition mode
$\Delta G_{\text{imm}}$ [J]	energy for homogeneous germ formation in the immersion mode
$h$ [Js]	Planck constant ( $6.63 \times 10^{-34}$ Js)
$H_X$ [\#]	prefactor ranging from 0–1 (Phillips et al., 2008)
$j_{\text{het}}$ [ $\text{m}^{-2} \text{s}^{-1}$ ]	heterogeneous nucleation rate coefficient
$j_{\text{dep}}$ [ $\text{m}^{-2} \text{s}^{-1}$ ]	deposition nucleation rate coefficient
$j_{\text{imm}}$ [ $\text{m}^{-2} \text{s}^{-1}$ ]	immersion freezing rate coefficient
$k$ [JK $^{-1}$ ]	Boltzmann constant ( $1.38 \times 10^{-23}$ JK $^{-1}$ )
$m_w$ [kg]	mass of a water molecule ( $2.99 \times 10^{-26}$ kg)
$n_{1,\text{w}}$ [ $\text{m}^{-2}$ ]	number of single molecules in contact with unit area of the substrate (in liquid water) ( $10^{19}$ m $^{-2}$ , Chen et al., 2008)
$n_{\text{IN},1,*}$ [ $\text{m}^{-3}$ ]	reference IN spectrum (Phillips et al., 2008)
$n_s$ [ $\text{m}^{-2}$ ]	INAS density
$S_i$ [\#]	saturation ratio with respect to ice
$\Delta t$ [s]	time interval
$T$ [K]	temperature
$T_0$ [K]	constant (118 K) (Zobrist et al., 2007)
$T_c$ [ $^{\circ}\text{C}$ ]	temperature in $^{\circ}\text{C}$
$V_{\text{ice}}$ [ $\text{m}^3$ ]	volume of a water molecule in ice (= $m_w/\rho_0$ )
$X$	index: $X = \text{dust/metallic, black carbon and organic aerosols}$ (Phillips et al., 2008)
$\alpha_c$ [\#]	mass accommodation coefficient (Barahona, 2011)
$\alpha_X$ [\#]	fractional contribution of aerosol $X$ to the background IN spectrum $n_{\text{IN},1,*}$ (Phillips et al., 2008)
$\theta$ [ $^{\circ}$ ]	contact angle
$v_s$ [ $\text{s}^{-1}$ ]	frequency of vibration of water vapor molecule adsorbed on solid substrate, $10^{13}$ s $^{-1}$ (Pruppacher and Klett, 1997, p. 299)
$\xi$ [\#]	temperature-dependent function ranging from 0–1 (Phillips et al., 2008)
$\rho_i$ [kg m $^{-3}$ ]	density of ice (= $916.7 - 0.175T_c - 5 \cdot 10^{-4}T_c^2$ (Pruppacher and Klett, 1997, Eq. (3–2)))
$\sigma_{\text{lv}}$ [J m $^{-2}$ ]	surface tension between ice and vapor (= $\sigma_{\text{iww}} + \sigma_{\text{vw}} = (76.1 - 0.155 * T_c + 28.5 + 0.25 * T_c) \times 10^{-3}$ (Pruppacher and Klett, 1997, Eqs. (5–46), (5–47a) and (5–12)))
$\sigma_{\text{iw}}$ [J m $^{-2}$ ]	surface tension between ice and water (= $(28 + 0.257_c) \times 10^{-3}$ (Pruppacher and Klett, 1997, Eqs. (5–47a)))
$\Omega_{X,1,*}$ [ $\text{m}^2 \text{kg}^{-1}$ ]	aerosol surface area mixing ratio of species $X$ in the reference scenario (Phillips et al., 2008)



## Laboratory ice nucleation experiments

C. Hoose and O. Möhler

[Title Page](#)

[Abstract](#)

[Introduction](#)

[Conclusions](#)

[References](#)

[Tables](#)

[Figures](#)



[Full Screen / Esc](#)

[Printer-friendly Version](#)

[Interactive Discussion](#)



Instrument types	
AFT	aerosol flow tube
CC	cold chamber
CECC	controlled expansion cloud chamber
CFDC	continuous flow diffusion chamber
CFDC-C	CFDC with cylindrical plates
CFDC-P	CFDC with parallel plates
CFMC	continuous flow mixing chamber
CS	cold stage
CS-FDC	cold stage in flow diffusion cell
CS-SDC	cold stage in static diffusion cell
DFA	droplet freezing assay
DMCC	dynamic mixing cloud chamber
DSC	differential scanning calorimeter
EDBC	electrodynamic balance cell
EDF	emulsified droplet freezing
ESEM	environmental scanning electron microscope
FA	freezing assay
FDNC	falling droplet nucleation chamber
ISDC	isothermal static diffusion chamber
LFT	laminar flow tube
VWT	vertical wind tunnel
Other abbreviations	
AD	Asian dust
ATD	Arizona test dust
CCN	Cloud condensation nuclei
CID	Canary Island dust
CNT	Classical nucleation theory
IN	ice nuclei
INA	ice nucleation active
INAS	ice nucleation active (surface) site
pdf	probability distribution function
SD	Saharan dust
SOA	secondary organic aerosol

**Table A2.** Continued.

Instrument names and institutions	
AIDA	Aerosol Interaction and Dynamics in the Atmosphere
CC	Cold chamber
CFDC	Continuous flow diffusion chamber
CINaM	Centre Interdisciplinaire de Nanoscience de Marseille
CIRES	Cooperative Institute for Research in Environmental Sciences, University of Colorado
CLINCH	Collision Ice Nucleation Chamber
CSU	Colorado State University
DRI	Desert Research Institute
ESEM	Environmental scanning electron microscope
ETHZ	ETH (Eidgenössische Technische Hochschule) Zurich
FINCH	Fast Ice Nucleus Chamber
FRIDGE	FRankfurt Ice Nuclei Deposition FreezinG Experiment
IMCA	Immersion mode cooling chamber
INRA	Institut National de la Recherche Agronomique
LACIS	Leipzig Aerosol Cloud Interaction Simulator
MINC	Manchester Ice Nucleus Counter
PNNL	Pacific Northwest National Laboratory
PNNL-CIC	PNNL Compact Ice Chamber
UBC	University of British Columbia, Vancouver
U	University (of)
ZINC	Zurich Ice Nucleation Chamber

## Laboratory ice nucleation experiments

C. Hoose and O. Möhler

[Title Page](#)[Abstract](#)[Introduction](#)[Conclusions](#)[References](#)[Tables](#)[Figures](#)[◀](#)[▶](#)[◀](#)[▶](#)[Back](#)[Close](#)[Full Screen / Esc](#)[Printer-friendly Version](#)[Interactive Discussion](#)

# Laboratory ice nucleation experiments

C. Hoose and O. Möhler

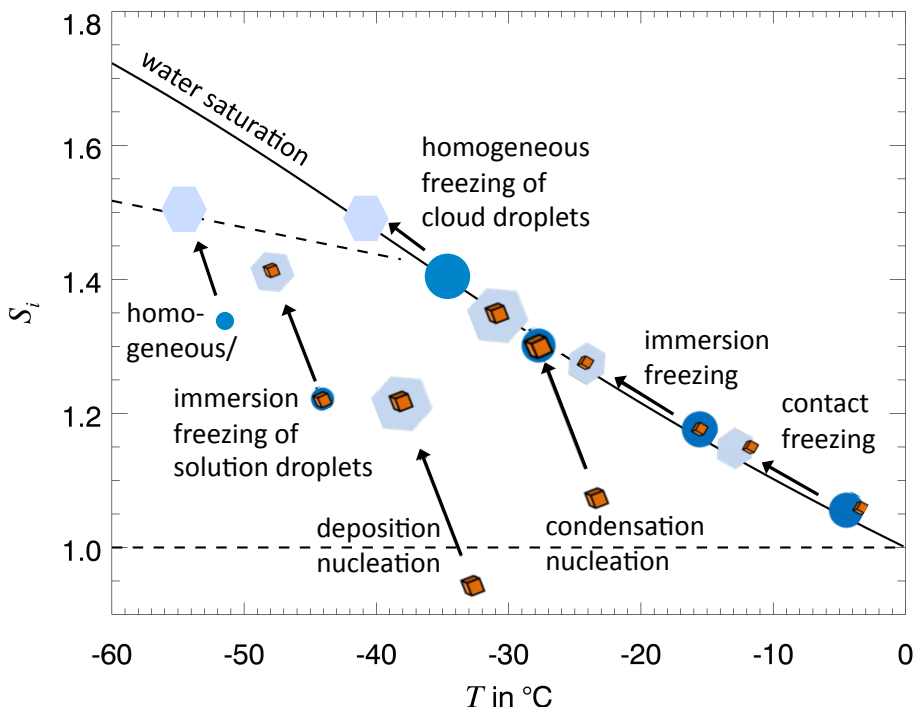


**Fig. 1.** Schematic representation of the different nucleation modes.

## Laboratory ice nucleation experiments

C. Hoose and O. Möhler

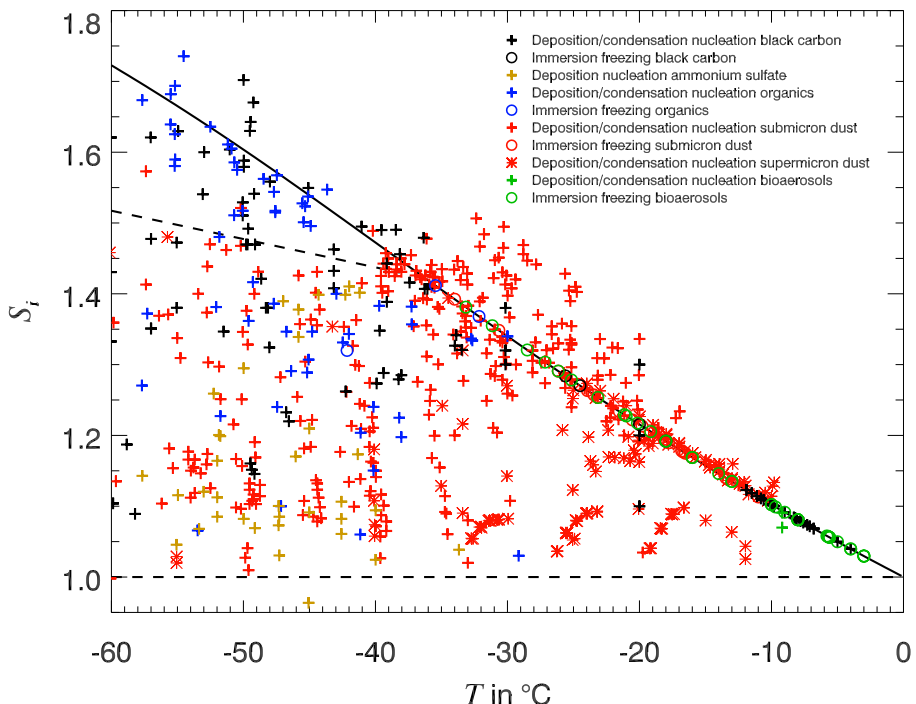


**Fig. 2.** Overview of ice nucleation onset temperatures and saturation ratios. Data sources are listed in the following figures.

## Laboratory ice nucleation experiments

C. Hoose and O. Möhler

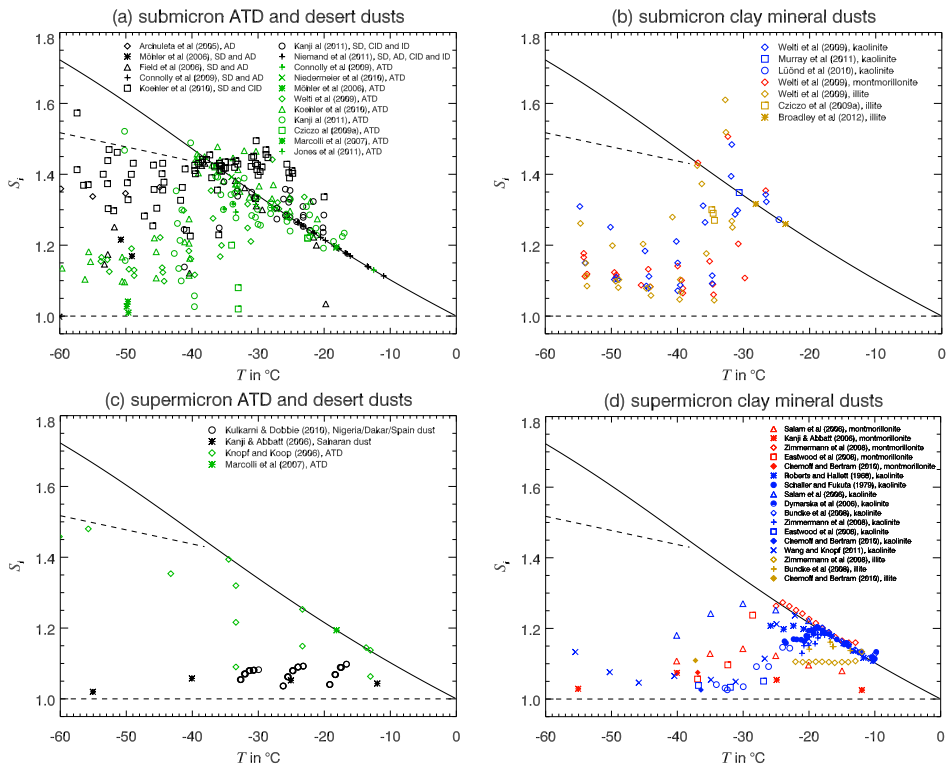


**Fig. 3.** Ice nucleation onset temperatures and saturation ratios for mineral dust particles.

## Laboratory ice nucleation experiments

C. Hoose and O. Möhler

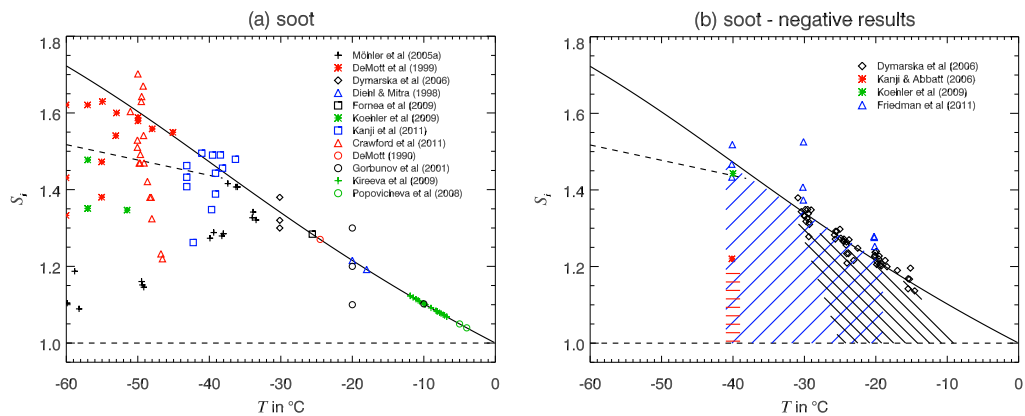


**Fig. 4.** **(a)** Ice nucleation onset temperatures and saturation ratios for soot. **(b)** Conditions under which ice nucleation on soot particles was *not* found or could not be distinguished from nucleation on the substrate. The dashed areas indicate the range of conditions which have been probed during the experimental trajectories to the indicated points.

- [Title Page](#)
- [Abstract](#) [Introduction](#)
- [Conclusions](#) [References](#)
- [Tables](#) [Figures](#)
- [◀](#) [▶](#)
- [◀](#) [▶](#)
- [Back](#) [Close](#)
- [Full Screen / Esc](#)
- [Printer-friendly Version](#)
- [Interactive Discussion](#)

# Laboratory ice nucleation experiments

C. Hoose and O. Möhler

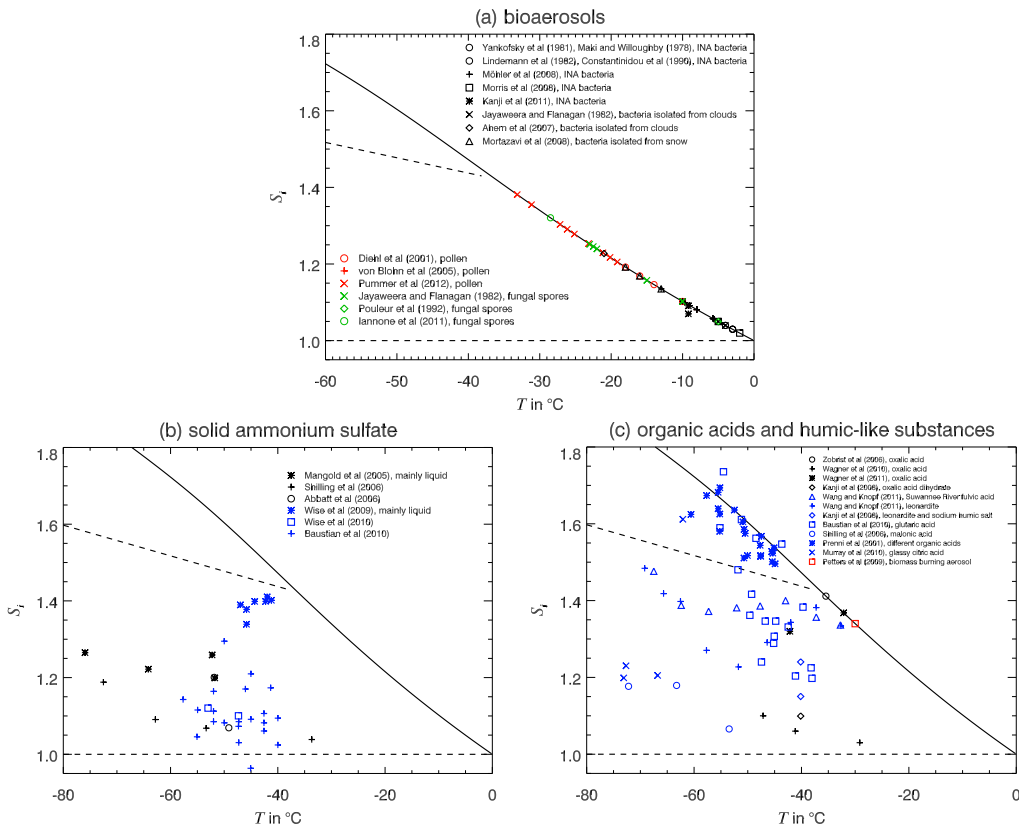


**Fig. 5.** Ice nucleation onset temperatures and saturation ratios for **(a)** bioaerosols, **(b)** ammonium sulfate and **(c)** organic aerosols. Note the different temperature ranges.

## Laboratory ice nucleation experiments

C. Hoose and O. Möhler

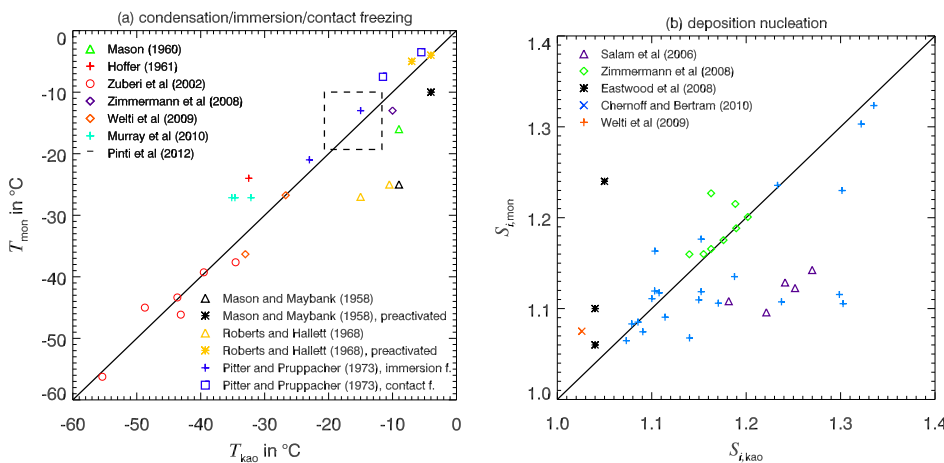


**Fig. 6.** (a) Freezing temperatures (onset or median) for kaolinite and montmorillonite under comparable experimental conditions. Includes immersion freezing experiments (Hoffer, 1961; Pitter and Pruppacher, 1973; Murray et al., 2010a) and presumed condensation freezing experiments at water-supersaturated conditions (Zimmermann et al., 2008; Welti et al., 2009). The data by Welti et al. (2009) for 100 and 800 nm-sized particles are interpolated to  $\approx 5\%$  supersaturation over water. For the mixing-cloud chamber experiments by Mason and Maybank (1958) and Mason (1960), the nucleation mode is uncertain. Zuberi et al. (2002) measured immersion nucleation in aqueous ammonium sulfate droplets, data are shown for the same weight percentages of kaolinite and montmorillonite. Pinti et al. (2012) show results for several different kaolinites and montmorillonites, as indicated by the dashed lines. (b) Saturation ratios at deposition nucleation onset for kaolinite and montmorillonite under comparable experimental conditions and temperature (for Welti et al. (2009), the data have been interpolated to the same temperatures). In Zimmermann et al. (2008)'s study, ice nucleation on montmorillonite was observed only at or slightly above water saturation, but no liquid water was seen. All other data in (b) are for deposition nucleation experiments, below water saturation.

<a href="#">Title Page</a>	<a href="#">Abstract</a>	<a href="#">Introduction</a>
<a href="#">Conclusions</a>	<a href="#">References</a>	
<a href="#">Tables</a>	<a href="#">Figures</a>	
<a href="#">◀</a>	<a href="#">▶</a>	
<a href="#">◀</a>	<a href="#">▶</a>	
<a href="#">Back</a>	<a href="#">Close</a>	
<a href="#">Full Screen / Esc</a>		
<a href="#">Printer-friendly Version</a>		
<a href="#">Interactive Discussion</a>		

## Laboratory ice nucleation experiments

C. Hoose and O. Möhler

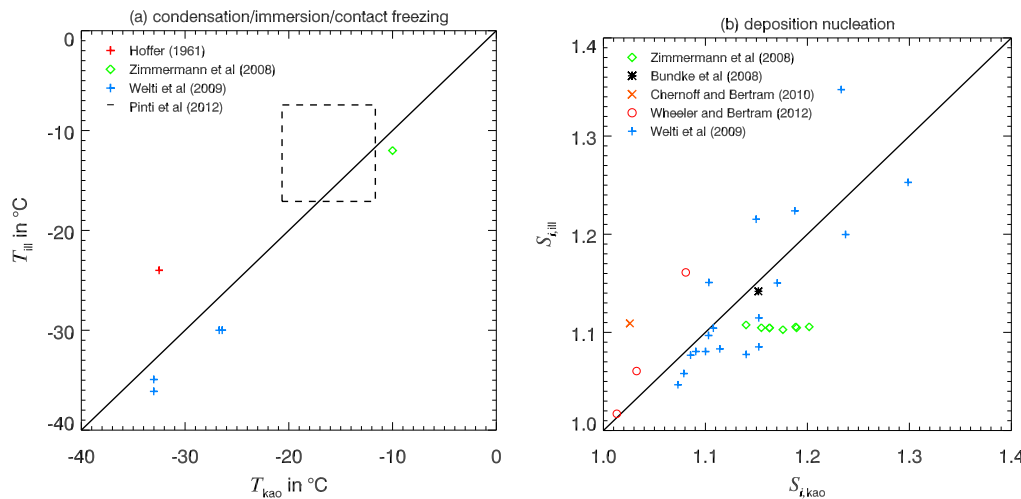


**Fig. 7.** **(a)** Freezing temperatures (onset or median) for kaolinite and illite under comparable experimental conditions. Includes immersion freezing experiments (Hoffer, 1961) and presumed condensation freezing experiments at water-supersaturated conditions (Zimmermann et al., 2008; Welti et al., 2009). The data by Welti et al. (2009) for 100 and 800 nm-sized particles are interpolated to  $\approx 5\%$  supersaturation over water. Pinti et al. (2012) show results for several different kaolinites and illites, as indicated by the dashed lines. **(b)** Saturation ratios at nucleation onset for kaolinite and illite under comparable experimental conditions and temperature.

- [Title Page](#)
- [Abstract](#) | [Introduction](#)
- [Conclusions](#) | [References](#)
- [Tables](#) | [Figures](#)
- [◀](#) | [▶](#)
- [◀](#) | [▶](#)
- [Back](#) | [Close](#)
- [Full Screen / Esc](#)
- [Printer-friendly Version](#)
- [Interactive Discussion](#)



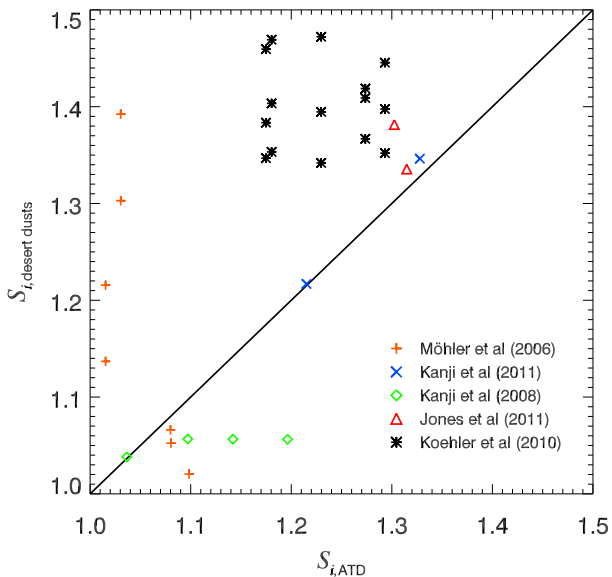


**Fig. 8.** Saturation ratios at nucleation onset for Arizona test dust and natural desert dusts (Saharan, Asian, Canary Island and Owens Lake dust) under comparable experimental conditions and interpolated to the same temperatures, respectively. The data by Koehler et al. (2010) are for dry dispersed particles of 200 nm size. The data by Kanji et al. (2011) are for UT-CFDC measurements sampled from the aerosol preparation and characterization chamber for ATD and Canary Island dust, which have similar size distributions. The data by Kanji et al. (2008) are interpolated to the same total particle surface areas. The data by Jones et al. (2011) are from the CSU-CFDC instrument and for water-subsaturated conditions.

12606

## Laboratory ice nucleation experiments

C. Hoose and O. Möhler

- + Möhler et al (2008), ATD+SOA, T<=210K
- # Möhler et al (2008), illite+SOA, T<=210K
- Koehler et al (2010), ATD+SOA
- ▲ Eastwood et al (2009), kaolinite + (NH4)2SO4
- Eastwood et al (2009), kaolinite + H2SO4
- Cziczo et al (2009a), illite + (NH4)2SO4 or H2SO4
- Cziczo et al (2009a), ATD + (NH4)2SO4 or H2SO4
- ▲ Knopf and Koop (2006), ATD + H2SO4, 220-260K
- ◆ Sullivan et al (2010a), ATD + HNO3, 243K
- ◆ Sullivan et al (2010b), ATD + H2SO4, 243K
- ◇ Chemoff and Bertram (2010), minerals + H2SO4

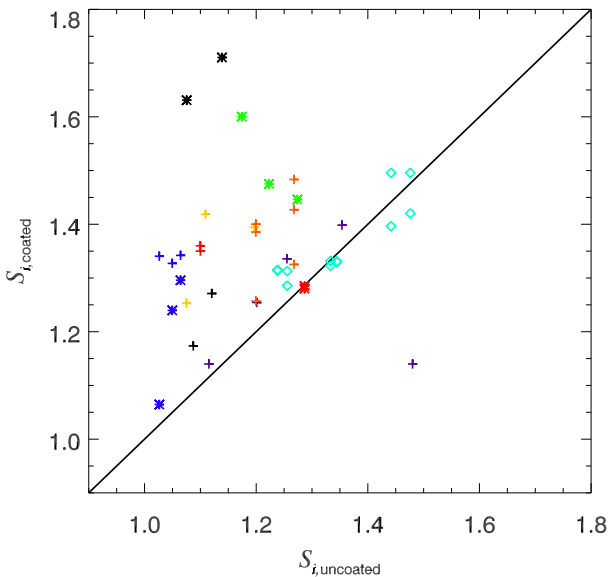


**Fig. 9.** Effect of different coatings on supersaturation required to activate a specific fraction of IN in experiments at similar temperatures.

[Title Page](#)[Abstract](#)[Introduction](#)[Conclusions](#)[References](#)[Tables](#)[Figures](#)[Back](#)[Close](#)[Full Screen / Esc](#)[Printer-friendly Version](#)[Interactive Discussion](#)

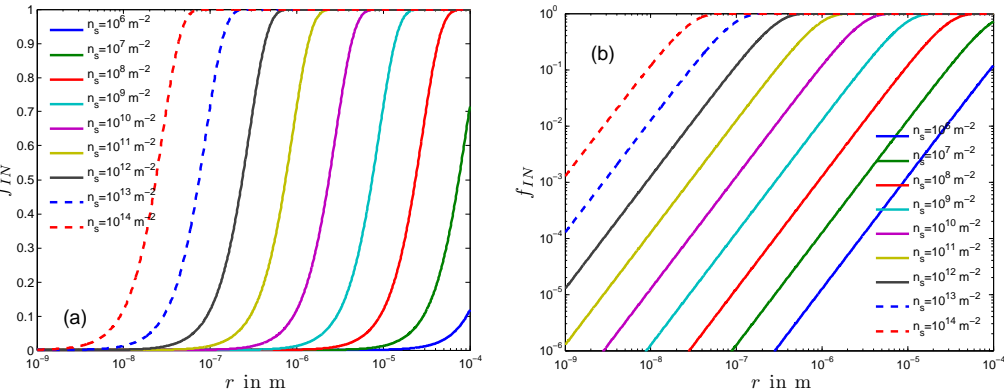


**Fig. 10.** Activated fraction as a function of aerosol radius for values of different INAS densities. (b) is identical to (a) except that the y-axis is spaced logarithmically.

## Laboratory ice nucleation experiments

C. Hoose and O. Möhler

[Title Page](#)

[Abstract](#)

[Introduction](#)

[Conclusions](#)

[References](#)

[Tables](#)

[Figures](#)

◀

▶

◀

▶

[Back](#)

[Close](#)

[Full Screen / Esc](#)

[Printer-friendly Version](#)

[Interactive Discussion](#)



## Laboratory ice nucleation experiments

C. Hoose and O. Möhler

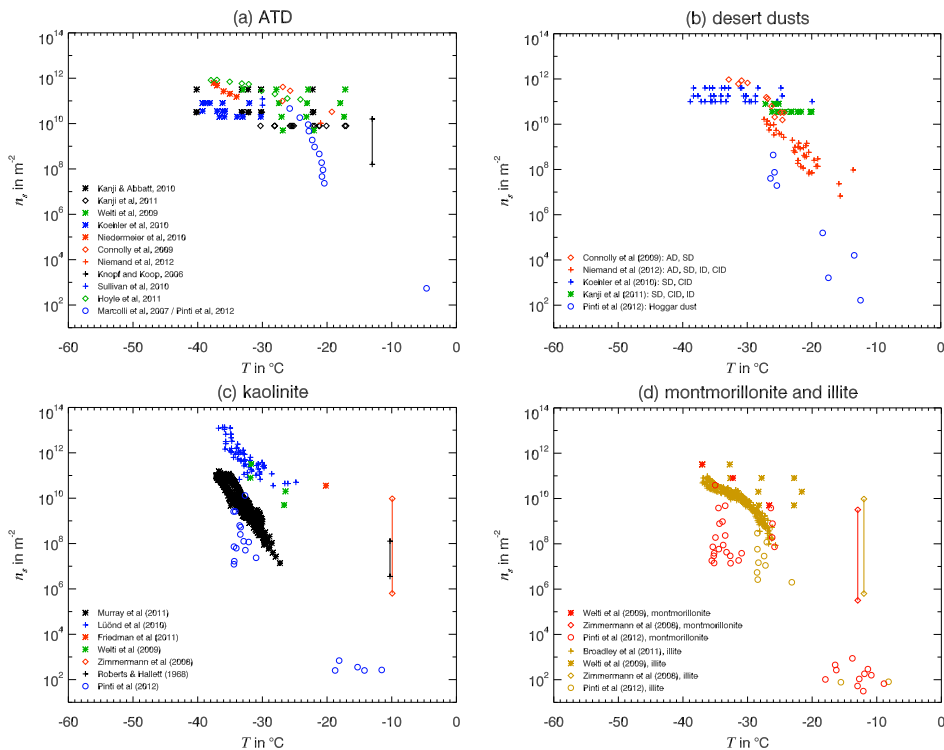


**Fig. 11.** INAS densities for ATD, natural desert dusts and different clay minerals for immersion freezing, including deposition/condensation freezing experiments at or above water saturation. The INAS densities are derived either by assuming spherical particles or with BET surface areas (Murray et al., 2011; Broadley et al., 2012; Pinti et al., 2012).

## Laboratory ice nucleation experiments

C. Hoose and O. Möhler

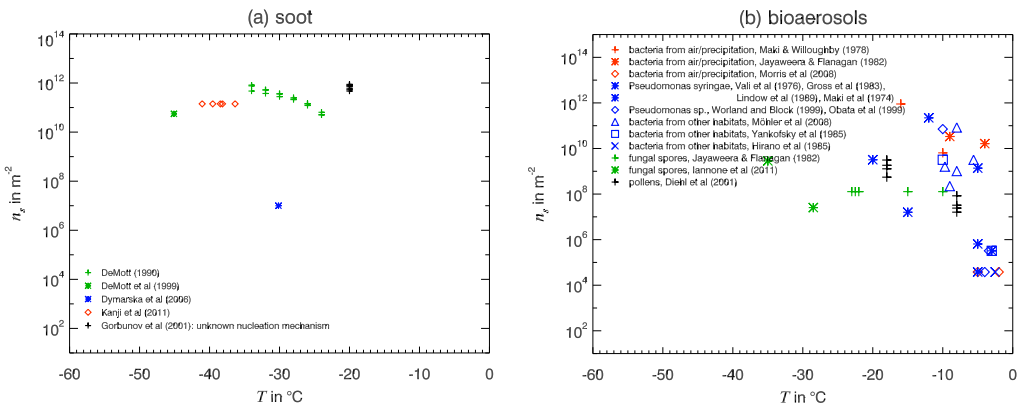


**Fig. 12.** INAS densities for soot and bioaerosols for immersion freezing, including deposition/condensation freezing experiments at or above water saturation.

<a href="#">Title Page</a>	<a href="#">Abstract</a>	<a href="#">Introduction</a>
<a href="#">Conclusions</a>	<a href="#">References</a>	
<a href="#">Tables</a>	<a href="#">Figures</a>	
<a href="#"></a>	<a href="#"></a>	
<a href="#"></a>	<a href="#"></a>	<a href="#">Close</a>
<a href="#">Full Screen / Esc</a>		
<a href="#">Printer-friendly Version</a>		
<a href="#">Interactive Discussion</a>		

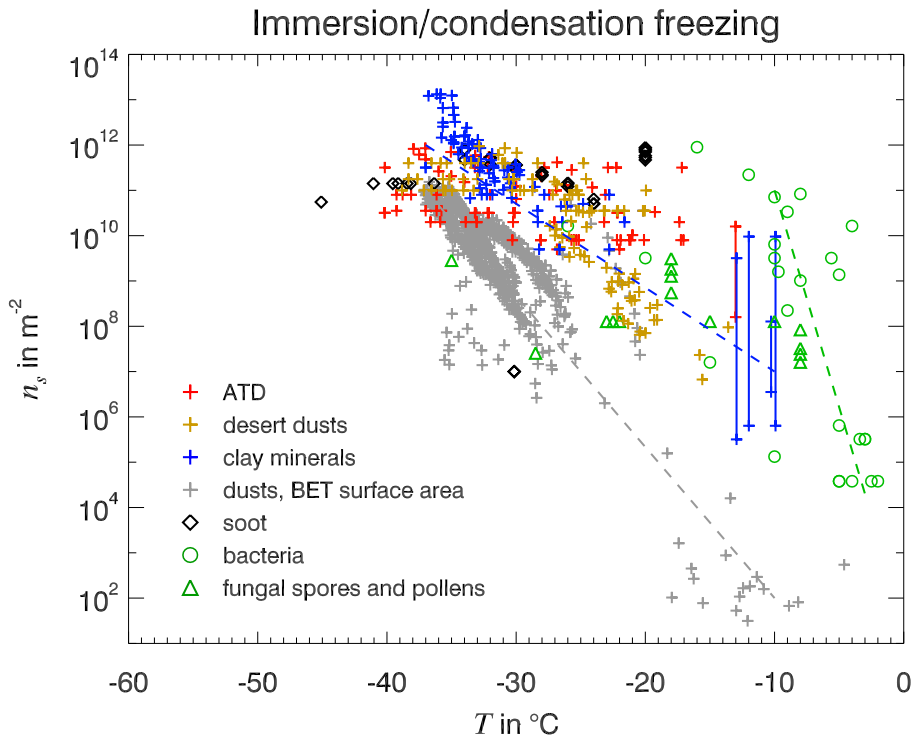


**Fig. 13.** INAS densities for ATD, kaolinite, natural desert dusts, soot and bioaerosols for immersion freezing, including deposition/condensation freezing experiments at or above water saturation. The data sources are the same as in Figs. 11 and 12. The lines are inserted to guide the eye. The blue line refers to both ATD, desert dusts and clay minerals. The green line refers to highly INA biological aerosols.

# Laboratory ice nucleation experiments

C. Hoose and O. Möhler

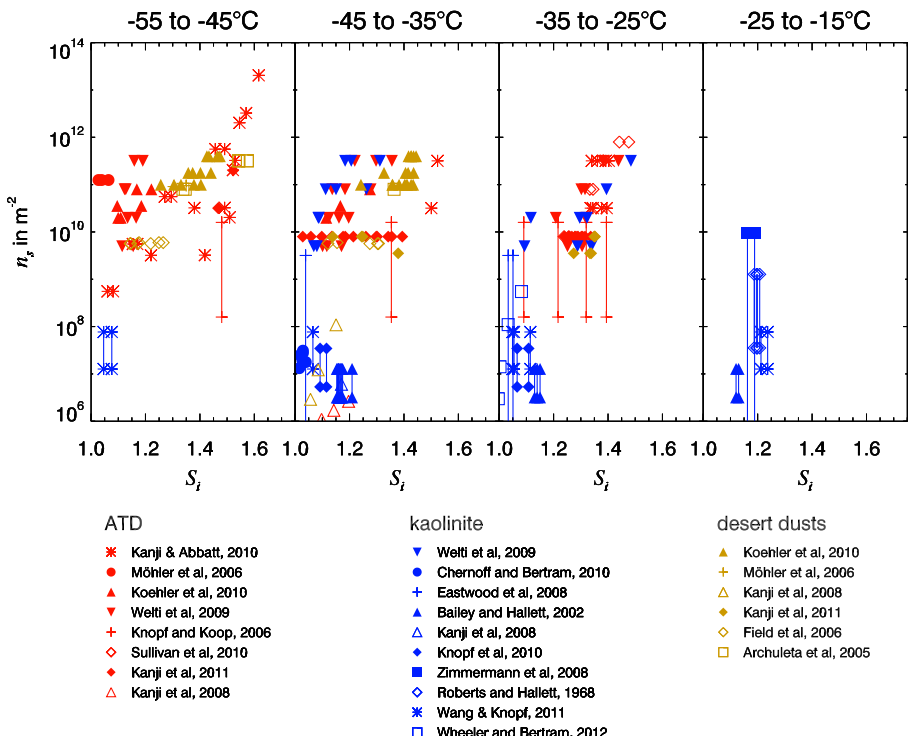


**Fig. 14.** INAS densities for ATD, kaolinite and desert dusts for deposition nucleation.

## Laboratory ice nucleation experiments

C. Hoose and O. Möhler

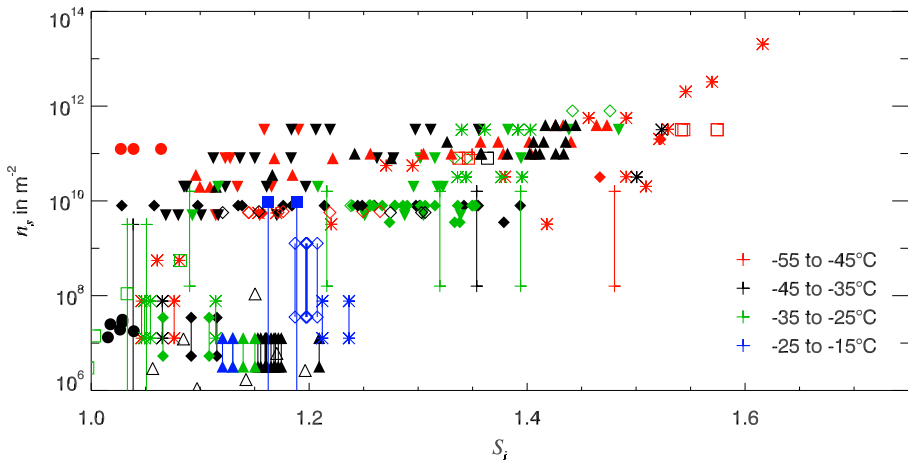


**Fig. 15.** INAS densities for ATD, kaolinite and desert dusts for deposition nucleation, binned into temperature intervals. The symbols and data sources are the same as in Fig. 14.

<a href="#">Title Page</a>	
<a href="#">Abstract</a>	<a href="#">Introduction</a>
<a href="#">Conclusions</a>	<a href="#">References</a>
<a href="#">Tables</a>	<a href="#">Figures</a>
<a href="#">◀</a>	<a href="#">▶</a>
<a href="#">◀</a>	<a href="#">▶</a>
<a href="#">Back</a>	<a href="#">Close</a>
<a href="#">Full Screen / Esc</a>	
<a href="#">Printer-friendly Version</a>	
<a href="#">Interactive Discussion</a>	

## Laboratory ice nucleation experiments

C. Hoose and O. Möhler

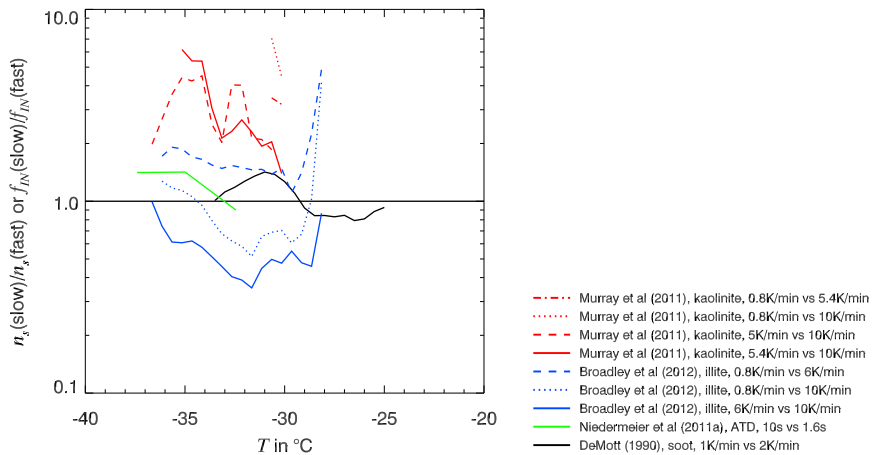


**Fig. 16.** Ratio of INAS densities or ice fractions in experiments with different cooling rates or residence times, but the same aerosol. The data from Murray et al. (2011), their Fig. 6a, and Broadley et al. (2012), their Fig. 6b, are binned into intervals of 0.5 K and compared for overlapping temperature ranges. For Broadley et al. (2012), the experiments with cooling rates of  $7.5 \text{ K min}^{-1}$ ,  $5 \text{ K min}^{-1}$  and  $1 \text{ K min}^{-1}$  are not included here because of the large spread in the data. The data shown from Niedermeier et al. (2011b) represent the three data points for which experiments with a nucleation time of 10 s were conducted (their Fig. 1). For soot, two experiments with  $0.08 \mu\text{m}$  particles are compared (DeMott, 1990, his Fig. 5).

<a href="#">Title Page</a>	<a href="#">Abstract</a>	<a href="#">Introduction</a>
<a href="#">Conclusions</a>	<a href="#">References</a>	
<a href="#">Tables</a>	<a href="#">Figures</a>	
<a href="#"></a>	<a href="#"></a>	
<a href="#"></a>	<a href="#"></a>	<a href="#">Close</a>
<a href="#">Full Screen / Esc</a>		
<a href="#">Printer-friendly Version</a>		
<a href="#">Interactive Discussion</a>		



## Laboratory ice nucleation experiments

C. Hoose and O. Möhler

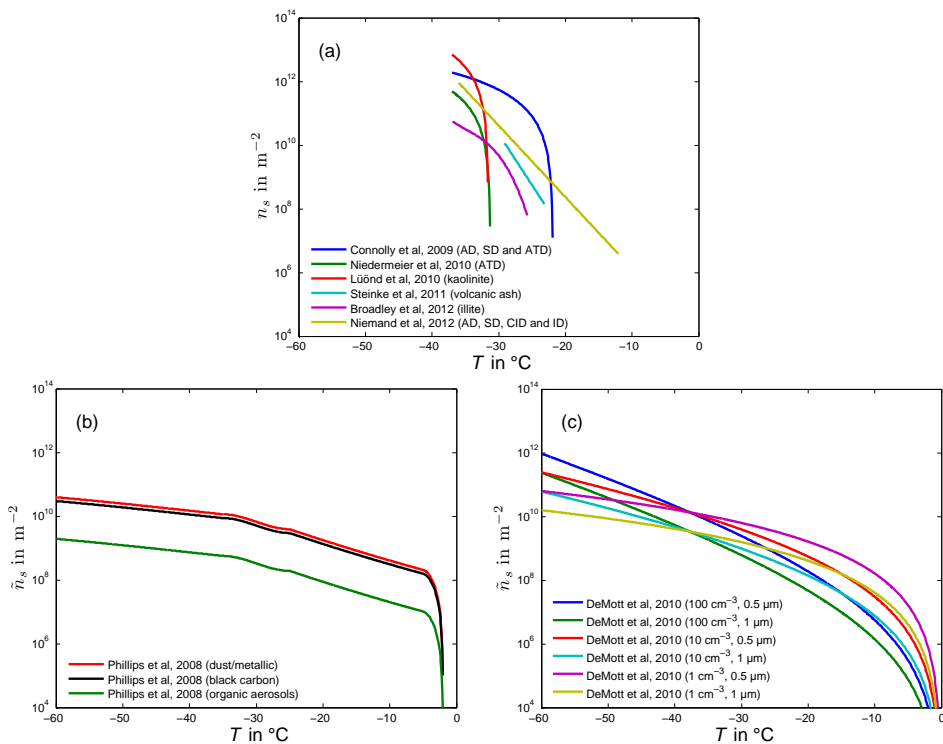


**Fig. 17.** **(a)** Parameterizations of  $n_s$  for immersion freezing. **(b)** Equivalent  $\tilde{n}_s$  from Phillips et al. (2008) evaluated at water saturation. **(c)** Equivalent  $\tilde{n}_s$  derived from DeMott et al. (2010) for different concentrations and monodisperse particles.

[Title Page](#)

[Abstract](#)

[Introduction](#)

[Conclusions](#)

[References](#)

[Tables](#)

[Figures](#)



[Back](#)

[Close](#)

[Full Screen / Esc](#)

[Printer-friendly Version](#)

[Interactive Discussion](#)

## Laboratory ice nucleation experiments

C. Hoose and O. Möhler

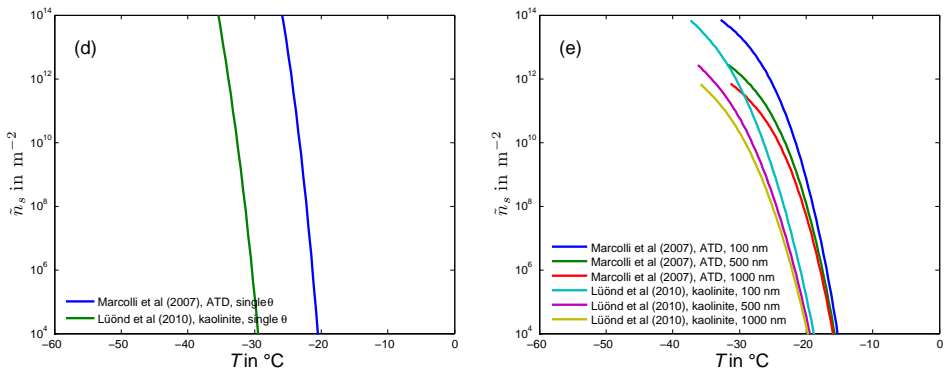


**Fig. 18.** (d) Apparent  $\tilde{n}_s$  from CNT (as formulated by Zobrist et al. (2007)) with single contact angles, fitted by Marcolli et al. (2007) and Lüönd et al. (2010). (e) Apparent  $\tilde{n}_s$  from CNT with a distribution of contact angles, with parameters fitted by Marcolli et al. (2007) and Lüönd et al. (2010), for different particle sizes.

- [Title Page](#)
- [Abstract](#) | [Introduction](#)
- [Conclusions](#) | [References](#)
- [Tables](#) | [Figures](#)
- [◀](#) | [▶](#)
- [◀](#) | [▶](#)
- [Back](#) | [Close](#)
- [Full Screen / Esc](#)
- [Printer-friendly Version](#)
- [Interactive Discussion](#)



## Laboratory ice nucleation experiments

C. Hoose and O. Möhler

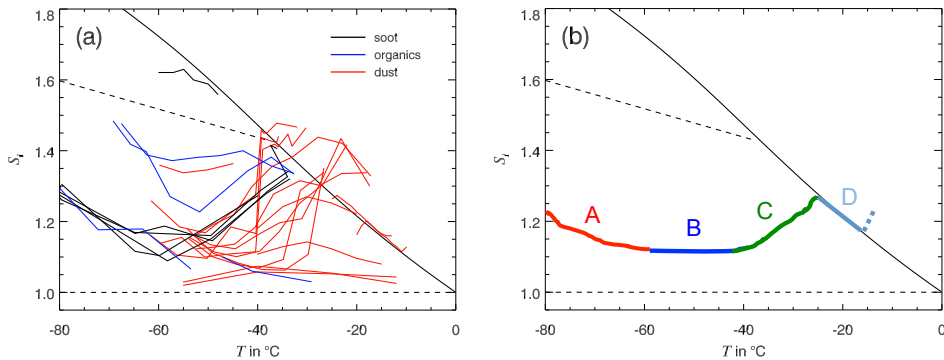


**Fig. 19.** Isolines of constant nucleation rate coefficients or INAS densities. **(a)** Selected data from Fig. 2. Each line connects data from one instrument, for one particle type and a constant activated fraction. **(b)** idealized curve with regimes A to D as discussed in the text.

<a href="#">Title Page</a>	<a href="#">Abstract</a>	<a href="#">Introduction</a>
<a href="#">Conclusions</a>	<a href="#">References</a>	
<a href="#">Tables</a>	<a href="#">Figures</a>	
<a href="#">◀◀</a>	<a href="#">▶▶</a>	
<a href="#">◀</a>	<a href="#">▶</a>	
<a href="#">Back</a>	<a href="#">Close</a>	
<a href="#">Full Screen / Esc</a>		
<a href="#">Printer-friendly Version</a>		
<a href="#">Interactive Discussion</a>		



# Laboratory ice nucleation experiments

C. Hoose and O. Möhler

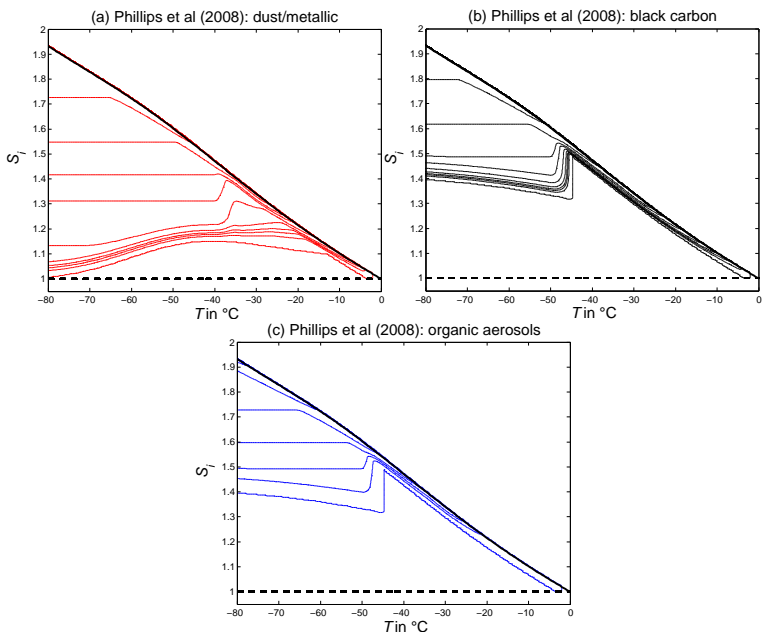


**Fig. 20.** Equivalent INAS densities for deposition and condensation nucleation as parameterized by Phillips et al. (2008): **(a)** dust/metallic aerosols, **(b)** black carbon, and **(c)** organic aerosols. The isolines correspond to (from bottom to top)  $\bar{n}_s(S_i, T) = 1, 1 \times 10^8, 2 \times 10^8, 3 \times 10^8, 5 \times 10^8, 1 \times 10^9, 2 \times 10^9, 3 \times 10^9, 5 \times 10^9$ , and  $1 \times 10^{10} \text{ m}^{-2}$ . In **(b)**, the highest visible isoline is  $5 \times 10^9 \text{ m}^{-2}$ , and in **(c)**,  $1 \times 10^9 \text{ m}^{-2}$ .

12618

# Laboratory ice nucleation experiments

C. Hoose and O. Möhler

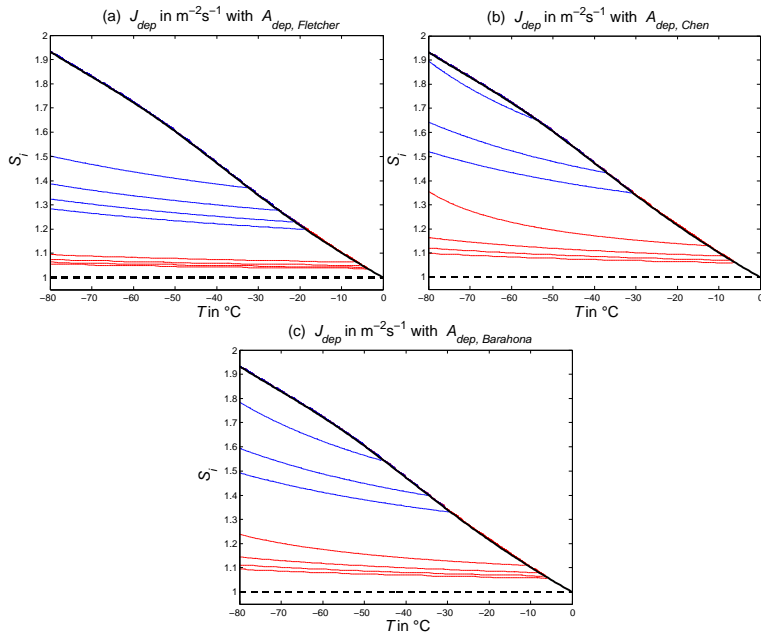


**Fig. 21.** Deposition nucleation rates calculated from classical nucleation theory, with different formulations of the kinetic factor  $A_{\text{dep}}$ : **(a)** Fletcher (1958), **(b)** Chen et al. (2008), and **(c)** Barahona (2011). The red lines are valid for  $f_{\text{het}} = 0.0005$ , and the blue lines for  $f_{\text{het}} = 0.01$ . From bottom to top, the isolines correspond to  $j_{\text{dep}} = 1, 1 \times 10^6, 1 \times 10^{12}$ , and (beyond the plotting range for the blue lines in **b** and **c**)  $1 \times 10^{18} \text{ m}^{-2} \text{ s}^{-1}$ . In **(b)** and **(c)**, a desorption energy  $\Delta g_d$  of  $6.5 \times 10^{-20} \text{ J}$  was used.

12619

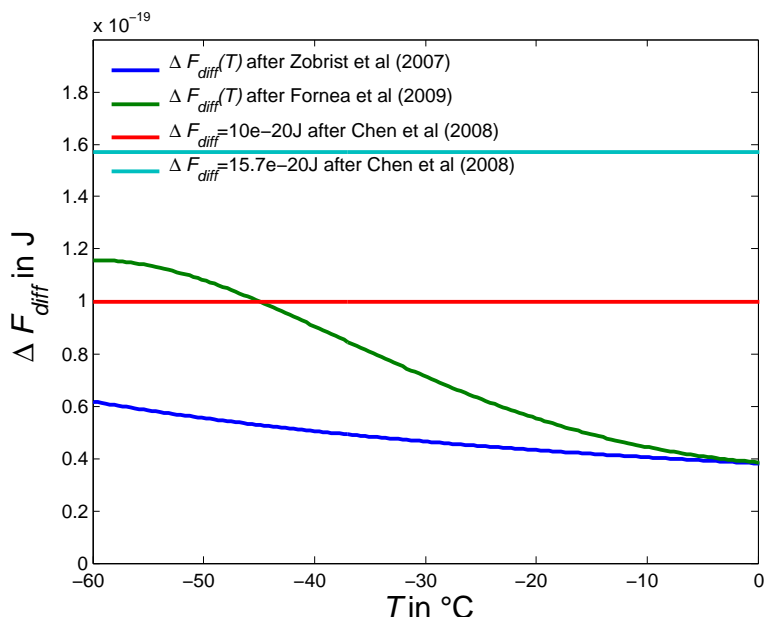


**Fig. 22.** Energy for diffusion across the liquid-ice boundary  $\Delta F_{\text{diff}}$  as used in different immersion freezing formulations of classical nucleation theory.

Title Page	
Abstract	Introduction
Inclusions	References
Tables	Figures
◀	▶
◀	▶
Back	Close
Full Screen / Esc	
Printer-friendly Version	
Interactive Discussion	

## Laboratory ice nucleation experiments

C. Hoose and O. Möhler

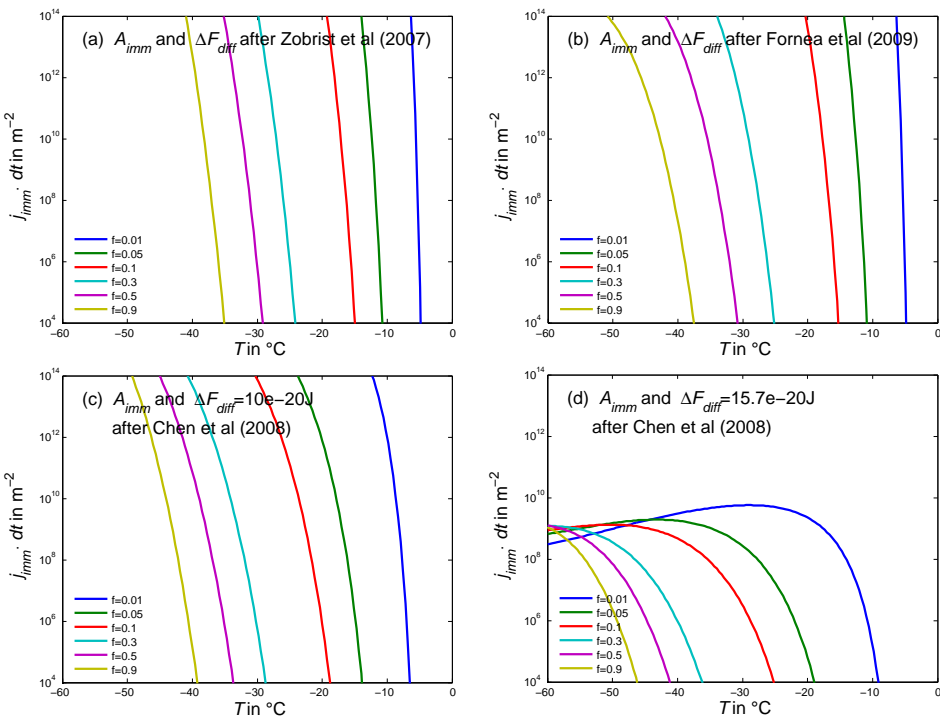


**Fig. 23.** Equivalent INAS densities calculated obtained from various formulations of classical nucleation theory by multiplying immersion freezing rate coefficients with an exemplary time step of 10 s, shown for different form factors  $f$ .